N.T.

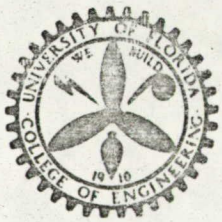

ENGINEERING AND INDUSTRIAL EXPERIMENT STATION

College of Engineering

University of Florida

Gainesville

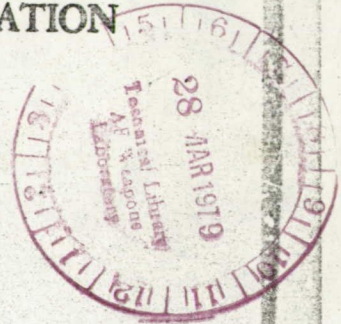

A STUDY OF GAS SOLUBILITIES AND TRANSPORT PROPERTIES IN FUEL CELL ELECTROLYTES

Research Grant NGR 10-005-022

Sixth Semi-Annual Report

Period Covered: March 1, 1968 - August 31, 1968

Prepared For

National Aeronautics and Space Administration
Washington, D. C.

February 25, 1969

Robert D. Walker, Jr.
Principal Investigator

ENGINEERING AND INDUSTRIAL EXPERIMENT STATION

College of Engineering
University of Florida
Gainesville, Florida

Table of Contents

List of Tables

List of Figures

1. Summary

This report summarizes the work of the past three years and includes the following areas: Solubility of hydrogen and oxygen in KOH and LiOH solutions, diffusivity of oxygen and hydrogen in KOH solutions, mutual diffusivity in KOH solutions, and densities and vapor pressures of both KOH and LiOH solutions.

The solubility of hydrogen and oxygen has been measured over the temperature range 25-100°C and the KOH concentration range zero to saturation. The solubilities of several other roughly spherical molecules have been measured to test a theoretical model. The solubilities of all of these gas decreased substantially with increasing temperature, and they decreased sharply with increasing KOH concentration at all temperatures. At KOH concentrations greater than 30 wt. per cent the solubility of all of the gases studied was found to be essentially independent of temperature. Solubilities at KOH concentrations above 50 wt. per cent are generally about one per cent of the solubility in water.

There was good agreement between experimentally measured solubilities and those predicted from a cavity model theory except for SF_6 and $C(CH_3)_4$; whereas electrostatic and modified Debye failed to predict solubilities suitably at high KOH concentrations.

The solubility of hydrogen, oxygen, helium, and argon has been measured in LiOH solutions over the general temperature range 25-100°C and from zero to saturation in LiOH (about 10 weight per cent). The solubility was found

to decrease with both temperature and LiOH concentration, as with KOH solutions. However, the solubility of oxygen and hydrogen at a given LiOH concentration is substantially less than the solubility in a KOH solution of that concentration. The solubility of these gases in LiOH solutions was quite satisfactorily predicted by the cavity model theory.

The diffusivity of hydrogen and oxygen in KOH solutions has been measured over the same ranges of temperature and KOH concentration as the solubility using a stagnant microelectrode technique. The diffusivity decreases sharply with increase in KOH concentration, while it increases equally sharply with temperature with the result that temperature and concentration effects very roughly cancel each other. The experimental data are correlated well up to 35 wt. per cent KOH by a modified Eyring theory, but deviate significantly at higher concentrations.

Mutual diffusion coefficients have been measured at four different temperatures and at KOH concentrations from zero to near saturation. The isothermal concentration dependence of the mutual diffusion coefficient is complex but is reasonably well-described by a simple activation theory up to KOH concentrations of about 35 wt. per cent.

The vapor pressure of water over LiOH solutions has been measured over the temperature range 25-100°C and the LiOH concentration range zero to saturation using a dew point method. These results correlate well with previously published vapor pressures at 25°C and from 100 to 350°C.

The density of KOH solutions was measured by the hydrostatic weighing

method of Kohlrausch using a silver plummet over the temperature range 60-161°C and the KOH concentration range zero to 77.1 wt. per cent. The density increased substantially with increasing KOH concentration and decreased slightly with increasing temperature.

2. INTRODUCTION

This investigation was undertaken with two principal objects in mind. The first objective was to measure the solubility and diffusivity of hydrogen and oxygen in alkaline fuel cell electrolytes over a considerable range of temperatures and alkali concentrations. Secondly, it was desired to develop theories which could be used for the prediction of thermodynamic and transport properties of the dissolved gases in these systems, and which could be used for correlation of experimental data. In considerable measure these objectives have been achieved.

The solubility of hydrogen and oxygen in KOH solutions has been measured over a temperature range of 25-100°C and a KOH concentration range of zero to saturation, and the diffusivity of these gases in KOH solutions has been measured over similar ranges of temperature and KOH concentration. The solubility of oxygen and hydrogen in LiOH solutions has been measured over a temperature range of 0-100°C and over the LiOH concentration range of zero to saturation. No diffusivity data have been obtained for LiOH solutions.

This report summarizes the results of this investigation for the past three years both as regards experimental, as well as theoretical work. In connection with the experimental measurement of solubility and diffusivity, it has been necessary to make certain other measurements as, for example, densities and vapor pressures, and these measurements are also summarized in this report.

In the area of theory, the "cavity model" has been applied to the solution process in alkaline fuel cell electrolytes with promising results Both the theory and its application are summarized here, and experimental solubilities are compared with predicted solubilities with generally excellent results. A modification of absolute reaction rate theory has been used to correlate diffusivity data.

Much additional work remains to be done, and it is the purpose of the extension of the original investigation to continue developments along several lines. First, additional solubility and diffusivity work is required. Likewise, additional work on a theory of solubility seems desirable, and development of an adequate theory of diffusivity as well as measurements of diffusivity in LiOH solutions are needed.

In the course of development of the theory for the cavity model for solubility of gases in electrolytic solutions it became clear that the partial molal volume is an important parameter. Unfortunately, however, very few partial molal volume data are available, and this work is required for extension of the theory. It is, therefore, being undertaken.

3.0 SOLUBILITY OF GASES IN LiOH AND KOH SOLUTIONS - J. Jolly and S K. Shoor

3.1 Classical Thermodynamics of Solutions

A brief survey is made of classical thermodynamics in this section. Discussion of the phase equilibrium relations which are applicable to gas-electrolyte systems is included and thermodynamic relations are derived to calculate partial molal heats of solution, entropy of solution and energy of solution.

In the following discussion subscripts 1, 2 and 3 have been used to denote solute gas, water and electrolyte, respectively. Consider a nonideal liquid solution in contact with a vapor phase. For any component i

$$f_i^G = f_i^L \qquad (3.1\text{-}1)$$

where superscripts G and L refer to the gas and liquid phase and f_i is the fugacity of component i. For the gas phase we can write

$$f_i^G = \phi_i \, p_i \qquad (3.1\text{-}2)$$

where ϕ_i is the fugacity coefficient of component i and p_i is its partial pressure. The fugacity in the liquid phase is given by

$$f_i^L = x_i \, \gamma_i \, f_i^S \qquad (3.1\text{-}3)$$

where f_i^S is the standard state fugacity. It is convenient to choose the following standard states for the gas-liquid equilibrium:

1) The standard state chosen for the solute gas is the pure solute in a hypothetical liquid state which is defined by reference to the behavior of this component at infinite dilution in pure water, that is

$$\lim_{\substack{x_1 \to 0 \\ x_3 = 0}} \gamma_1 \to 1 \qquad (3.1\text{-}4)$$

Henry's Law for pure water is

$$\lim_{\substack{x_1 \to 0 \\ x_3 = 0}} f_1^{\circ} = K_1^{\circ} x_1^{\circ} \qquad (3.1\text{-}5)$$

where K_1° is Henry's Law constant for the gas in pure water.

2) For water the standard state is pure liquid at the same temperature and pressure as the mixture (pure liquid standard state)

$$\lim_{x_2 \to 1} \gamma_2 \to 1$$

From Equations 3.1-3, 4 and 5 we see that

$$f_1^L = K_1^{\circ} \gamma_1 x_1 \qquad (3.1\text{-}6)$$

where γ_1 and x_1 are the activity coefficient and mole fraction of gas in the electrolyte solution. Because the pressure involved is only about one atmosphere, the gas phase behaves essentially ideally and the fugacity can be replaced by the partial pressure, so that

$$f_1^G \doteq p_1^G = (P - p_2) = K_1^{\circ} \gamma_1 x_1 \qquad (3.1\text{-}7)$$

where P is the total pressure, and p_2 is the vapor pressure of the electrolyte solution. Similarly, for water we can write

$$P - p_2^{\circ} = x_1^{\circ} K_1^{\circ} \qquad (3.1\text{-}8)$$

For the systems studied here the solubilities are low enough that Henry's Law should be a good approximation. This law may therefore be used to

calculate solubilities for a partial pressure of one atmosphere of solute gas, and these are designated $x_1(1)$ and $x_1^c(1)$. From Equations 3.1-7 and 8 it is clear that

$$K_1^c \gamma_1 = \frac{1}{x_1(1)} \tag{3.1-9}$$

and

$$\gamma_1 = \frac{x_1^c(1)}{x_1(1)} \tag{3.1-10}$$

A knowledge of the solute activity coefficient as a function of temperature can be used to calculate partial molal heats and entropies of solution. The effect of temperature on fugacity is given by

$$\left(\frac{\partial \ln f_2}{\partial T} \right)_{P,n_j} = - \frac{(\bar{H}_1 - h_1^G)}{RT^2} \tag{3.1-11}$$

so that from Equation 3.1-7

$$\left(\frac{\partial \ln(\gamma_1 K_1^0)}{\partial T} \right)_{P,n_j} = - \frac{(\bar{H}_1^L - h_1^G)}{RT^2} = - \frac{\Delta \bar{H}_1}{RT^2} \tag{3.1-12}$$

Moreover,

$$\Delta \bar{S}_1 = \frac{\Delta \bar{H}_1}{T} \tag{3.1-13}$$

and

$$\Delta \bar{E}_1 = \Delta \bar{H}_1 + RT \tag{3.1-14}$$

where $\Delta \bar{S}_1$, $\Delta \bar{H}_1$ and $\Delta \bar{E}_1$ are the partial molal entropy, enthalpy, and energy changes of solution when one mole of gas in the ideal state dissolves in the electrolyte solution.

3.2 Theories of Gas Solubility

3.2.1 Electrostatic Theories

The effect of salts on solutions of nonelectrolytes is a very complex phenomenon. There have been a number of qualitative and quantitative theories of the salt effect, all with common underlying aspects but emphasizing different approaches to the problem. A comprehensive review of electrostatic theories has been made by Long and McDevit (1). Conway (2) has further reviewed and summarized the recent important improvements made in these theories.

All of these theories assume the solvent to be a continuous dielectric medium containing ions and solute molecules. Only departures from ideality which arise from electrostatic interactions involving the ionic charges are considered. No explicit account is taken of molecular interaction between ion and solvent, and nonelectrolyte and solvent. It is difficult to test the theoretical equations quantitatively because they involve parameters which are not readily available. Qualitatively, the theories fail to explain salting effects satisfactorily even in dilute solutions. As the theories have been reviewed (3) at length recently only a brief discussion will be given here.

The earliest and most important electrostatic theory of salt effects was that of Debye and McAulay (4). It relates salt effects to the influence of the nonelectrolyte on the dielectric constant of the solvent. The solvent molecules are treated as a continuous dielectric medium whose dielectric constant is uniform throughout the solution. Further, it is assumed that there is a continuous charge density function around a given ion due to the ionic atmosphere. The amount of work

necessary to discharge the ions in a pure solvent of dielectric constant, ϵ, containing the nonelectrolyte is calculated. This quantity yields the electrostatic contribution to the chemical potential of the neutral salt, and the expression for the activity coefficient of solute is

$$\log_{10}\gamma_1 = K_s C_s \qquad (3.2\text{-}1)$$

where C_s is the molar concentration of salt and K_s is the salting coefficient given by

$$K_s = \frac{\bar{\beta} N_o}{2.303 \times 1000 kT\epsilon_o} \sum_j \frac{\nu_j e_j^2}{a_j} \qquad (3.2\text{-}2)$$

where N_o is Avagadro's number, ϵ_o is the dielectric constant of water, ν_j is the number of ions of type j per mole of electrolyte, and e_j and a_j are ionic charge and diameter. The term $\bar{\beta}$ is related to the dielectric constant D of the nonelectrolyte solution by

$$D = \epsilon_o(1-\bar{\beta}n) \qquad (3.2\text{-}3)$$

where n is the number of molecules of nonelectrolyte solute per cm^3 of solution. The term $\bar{\beta}$ is not usually available and is difficult to estimate.

Debye later developed a more exact theory to obtain an expression for the concentration of nonelectrolyte molecules in the presence of a spherical ion in which he calculated the free energy for the real solution by taking into account the energy of the electric field surrounding the ion. Kirkwood (5) has calculated the mutual electrostatic energy of a spherical ion and a neutral molecule represented as a cavity (in the surrounding dielectric) and containing an arbitrary distribution of charges.

Conway, Desnoyers, and Smith (6) recently proposed a new theory in which the calculation of the salting-out behavior is carried out over two regions; (1) in the primary hydration shell where a high degree of solvent dielectric saturation prevails, and (2) beyond the primary region where weaker polarization occurs and Kirkwood's theory of dielectrics can be applied. Each ion of type i is supposed to have a hydration shell of radius $r_h^{(i)}$ containing n_1 water molecules, in which the dielectric constant is assumed very small. Outside of this shell the dielectric constant is assumed to have the value ϵ_o for pure water. The resulting equation is

$$\frac{S_1^\circ - S_1}{S_1^\circ C_s} = \frac{18(n_3+n_4)}{1000d - C_s M_s} + \frac{e^2(\bar{V}_1\epsilon_o - \frac{9}{2}P_2)}{2000kT\epsilon_o^2}\left[\frac{1}{r_h^{(3)}} + \frac{1}{r_h^{(4)}} - \frac{2}{R}\right] \qquad (3.2\text{-}4)$$

where S_1, S_1° are solubilities in electrolyte and pure water, respectively. n_3 and n_4 are hydration numbers for the two ions, $r_h^{(3)}$ and $r_h^{(4)}$ are the corresponding radii of the primary hydration shells, d is density of solution, M_s the molecular weight of electrolyte, e is electronic charge, P_2 is total molar polarization of solute, and R is a radius corresponding to the volume available per ion in the solution.

3.2.2 Scaled Particle Theory

Pierotti (7) has recently proposed a theory of gas solubility in non-polar solvents and in water which is based on the scaled-particle theory of Reiss, Frisch, Helfand, and Lebowitz (8). The theory predicts solubilities within a factor of two of experiment for a wide variety of solutes and solvents, and gives a good representation of the effects of temperature and pressure. In this approach it is not necessary to propose any special models for the structure of the solvent (e.g.

hydrogen-bonding, "iceberg" models, etc.). However, the theory provides no information concerning the solution density, which must be available from experiment. As pointed out by Pierotti (9), it is the use of experimental densities that allows the theory to avoid such structural concepts.

The solvent medium may be regarded as the electrolyte solution itself, and thus consists of a mixture of several species. It is assumed that the system contains m components, one of which is the solute gas (component 1), whereas the remaining (m-1) components comprise the solvent species and may include water molecules, ions of different types, undissociated electrolyte, etc.

Assuming that the total potential energy is the sum of pair potentials, the following equation can be obtained for the partial molecular Gibbs free energy of the solute gas in the liquid phase (10)

$$\mu_1^L = kT \ln \rho \Lambda_1^3 + \sum_{j=1}^{m} \rho_j \int_0^{\infty} dr \int_{\xi} \frac{\partial U_{ij}(r,\xi)}{\partial \xi} g_{ij}(r,\xi)\, 4\pi r^2 d\xi \qquad (3.2\text{-}5)$$

where

$$\Lambda_1 = \left(\frac{h^2}{2\pi mkT} \right)^{\frac{1}{2}}$$

and ρ_j is number density of component j, U_{ij} is the pair potential between a solute gas molecule and a solvent molecule of species j at a distance r, and g_{ij} is the radial distribution function for 1-j pairs. The term ξ is a coupling parameter (11) which allows the solute molecule to be coupled with the solvent. The lower and upper integration limits of ξ in Equation 3.2-5 correspond to complete uncoupling and complete coupling of the solute molecule and the solvent, respectively. The real molecules are assumed to possess hard cores of diameters a_1, a_2 ... an so that the pair potential

is of the form

$$U_{ij}(r,\xi) = U^{h}_{ij}(r,\xi_h) + U^{s}_{ij}(r,\xi_s) \qquad (3.2\text{-}6)$$

where U^{h}_{ij} and U^{s}_{ij} are the hard core or soft potential interaction, respectively, given by

$$\left.\begin{aligned} U^{h}_{ij}(r) &= \infty \qquad r \leq a_{ij} = \frac{a_i + a_j}{2} \\ U^{h}_{ij}(r) &= 0 \\ U^{s}_{ij}(r,\xi_s) &= \xi_s U_{ij}(r) \end{aligned}\right\} \quad r > a_{ij} \qquad (3.2\text{-}7)$$

In charging up the hard core contribution the coupling parameter ξ_h varies from 0 to a_{ij}, and in charging the soft potential contribution ξ_s varies from 0 to 1. When the two coupling parameters are zero the solute molecule is decoupled from the system. If the two coupling processes are imagined to take place separately, Equation 3.2-5 becomes

$$\mu^{L}_1 = kT\ln\rho_1 \Lambda^3_1 + \bar{g}^{h}_1 + \bar{g}^{s}_1 \qquad (3.2\text{-}8)$$

where

$$\bar{g}^{h}_1 = \sum_{j=1}^{m} \rho_j \int_{\xi_h=0}^{\xi_h=a_{ij}} d\xi_h \int_{r=0}^{\infty} \frac{\partial U^{h}_{ij}}{\partial \xi_h}(r,\xi_h)\, g_{ij}(r,\xi_m,\xi_s=0)\, 4\pi r^2 dr \qquad (3.2\text{-}9)$$

and

$$\bar{g}^{s}_1 = \sum_{j=1}^{m} \rho_j \int_{\xi_s=0}^{\xi_s=1} d\xi_s \int_{r=a_{ij}}^{\infty} U^{s}_{ij}(r) g_{ij}(r,\xi_h=a_{ij},\xi_s)\, 4\pi r^2 dr \qquad (3.2\text{-}10)$$

For a vapor and liquid phase in equilibrium,

$$\mu^{G}_1 = \mu^{L}_1 \qquad (3.2\text{-}11)$$

and the chemical potential of the solute gas phase is given by

$$\mu^{G}_1 = kT \ln\left(\frac{\Lambda^3_1}{kT}\right) + kT \ln f^{G}_1 \qquad (3.2\text{-}12)$$

where f_1^G is the gas-phase fugacity of the solute.

Putting Equation 3.2-8 into Equations 3.2-11 and 12 and rearranging results in

$$\ln \left(\frac{f_1^G}{\rho_1} \right) = \frac{\bar{g}_1^h}{kT} + \frac{\bar{g}_1^s}{kT} + \ln kT \qquad (3.2\text{-}13)$$

The mole fraction (solubility) of the solute gas in the solution is

$$x_1 = \frac{\rho_1}{\sum_j \rho_j} \qquad (3.2\text{-}14)$$

so that Equation 3.2-13 may be written as, after combination with Equation 3.1-7,

$$\ln \left(\frac{f_1^G}{x_1} \right) = \ln(\gamma_1 K_1^o) = \frac{\bar{g}_1^h}{kT} + \frac{\bar{g}_1^s}{kT} + \ln(kT \sum \rho_j) \qquad (3.2\text{-}15)$$

At low pressures the fugacity in Equation 3.2-15 may be replaced by partial pressure, and the last term on the right-hand side of this equation may be calculated if the density is known. It remains to evaluate the terms $\bar{g}_1^h$ and $\bar{g}_1^s$

Evaluation of $\bar{g}_1^h$ This term represents the free energy of introducing a hard sphere of diameter a_1 into the solvent (electrolyte solution). Alternatively, it may be thought of as the work required to make a cavity (hence the term cavity model which is sometimes applied to this theory) of this size in the solvent (12). Lebowitz et al. (13) have shown that this cavity work is given by

$$\frac{\bar{g}_1^h}{kT} = -\ln(1-\zeta_3) + \left[\frac{6\zeta_2}{1-\zeta_3} \right] \frac{a_1}{2} + \left[\frac{12\zeta_1}{1-\zeta_3} + \frac{18\zeta_2^2}{(1-\zeta_3)^2} \right] \left(\frac{a_1}{2} \right)^2 + \frac{4}{3}\pi \frac{P}{kT} \left(\frac{a_1}{2} \right)^3 \qquad (3.2\text{-}16)$$

where

$$\zeta_k = \frac{1}{6}\pi \sum_{j=1}^{m} \rho_j (a_j)^k$$

and P is pressure.

Evaluation of $\overline{g}_1^s$ The term due to the soft part of the potential may be thought of as the free energy needed to introduce the solute molecule into the cavity, or may be written

$$\overline{g}_1^s = \overline{e}_1^s + P\overline{V}_1^s - T\overline{S}_1^s \qquad (3.2\text{-}17)$$

where $\overline{e}_1^s$, $\overline{V}_1^s$, $\overline{S}_1^s$ are partial internal energy, volume, and entropy. Following Pierotti (7), it is here assumed that the terms $P\overline{V}_1^s$ and $T\overline{S}_1^s$ are much smaller than the internal energy known to be small at low pressures; the approximation concerning $\overline{S}_1^s$ may lead to errors for some solutes. With these assumptions

$$\overline{g}_1^s \doteq \overline{e}_1^s = \sum_{j=1}^{m} \int_{r=a_{ij}}^{\infty} U_{ij}(r) g_{ij}(r) \rho_j 4\pi r^2 dr \qquad (3.2\text{-}18)$$

The radial distribution function is not readily evaluated. As an approximation we assume the solvent particles to be uniformly distributed about the solute molecule so that

$$g_{ij}(r) = 1 \qquad r > a_{ij}$$

Equation 3.2-18 becomes

$$\overline{g}_1^s = \sum_{j=1}^{m} \rho_j \int_{a_{ij}}^{\infty} U_{ij}(r) 4\pi r^2 dr \qquad (3.2\text{-}19)$$

The nonpolar part of the pair interaction between a solute molecule and a solvent molecule of type j is assumed to be given by the Lennard-Jones

(6-12) potential

$$U_{ij}^{np} = 4\epsilon_{ij}\left[\left(\frac{\sigma_{ij}}{r}\right)^{12} - \left(\frac{\sigma_{ij}}{r}\right)^{6}\right] \qquad (3.2\text{-}20)$$

where the mixture potential parameters σ_{ij} and ϵ_{ij} are related to the pure component parameters by the approximate mixing rules

$$\sigma_{ij} = \frac{1}{2}(\sigma_i + \sigma_j) \qquad \epsilon_{ij} = (\epsilon_i\epsilon_j)^{1/2} \qquad (3.2\text{-}21)$$

It is now assumed that the electrolyte is completely dissociated, and the only species present in solution are solute molecules (1), water molecules (2), and positive and negative ions (3 and 4). In addition, the solute molecule is assumed nonpolar. The treatment for polar solutes, or an electrolyte solution containing additional species (e.g. undissociated electrolyte, various water structures, etc.) is an obvious extension of what follows. After averaging the interaction between the permanent dipole of the water molecule and the solute induced dipole over all orientations, and neglecting terms due to higher multiple moments, the solute-water pair potential is given by

$$U_{12} = U_{12}^{np} - \frac{\mu_2^2\alpha_1}{r^6} \qquad (3.2\text{-}22)$$

where U_{12}^{np} is given by Equation 3.2-20, μ_2 is the dipole moment of a water molecule, and α_1 is the solute polarizability.

The total ion-induced dipole interaction of a solute molecule with all of the surrounding ion may be written

$$U^{(c,ind\mu)} = -\int_0^{\underline{E}} \underline{\mu}_1^{(ind)} \cdot d\underline{E}^1 = -\frac{1}{2}\alpha_1 E^2 \qquad (3.2\text{-}23)$$

where $\underline{\mu}_1^{(ind)}$ is the induced dipole for the solute, and E is the electric field at the position of the solute molecule that is produced by all of the surrounding ions. The field E depends upon the distribution of ions

about the neutral molecule. If, as above, the distribution is assumed uniform there is on the average a spherically symmetrical charge distribution about the solute molecule. For such a distribution the field, and hence also the ion-induced dipole interaction of Equation 3.2-23, is zero (14). For the real solution it is clear that the solute molecule will experience a small fluctuating field E^+ due to the surrounding ions, and since this term is squared in Equation 3.2-23, there will be a finite ion-induced dipole interaction whose time-average is not zero. This contribution is assumed small, however, and it is neglected here. Its inclusion would make the calculated $\bar{g}_1^s$ value more negative. The only ion-solute interactions included in Equation 3.2-19 are therefore non-polar contributions.

Substituting the above expressions for U_{ij} into Equation 3.1-19 gives

$$\bar{g}_1^s \doteq -16\pi \sum_{j=1}^{m} \rho_j \int_{a_{1j}}^{\infty} \epsilon_{ij} \left[\frac{\sigma_{1j}^6}{r^4} - \frac{\sigma_{1j}^{12}}{r^{10}} \right] dr - 4\pi\rho_2 \int_{a_{12}}^{\infty} \frac{\mu_2^2 \alpha_1}{r^4} dr \qquad (3.2\text{-}24)$$

On performing the integrations and following Pierotti (8) (11) in taking $a_{1j} = \sigma_{1j}$

$$\bar{g}_1^s \doteq -\frac{32\pi}{9} \sum_{j=1}^{4} \rho_j \epsilon_{1j} \sigma_{1j}^3 - \frac{4\pi\rho_2 \mu_2^2 \alpha_1}{3\sigma_{12}} \qquad (3.2\text{-}25)$$

Insertion of the values of $\bar{g}_1^h$ or $\bar{g}_1^s$ in Equation 3.2-15 gives the required result.

3.3 Experimental Procedures

Several previous studies of the solubility of oxygen and hydrogen in KOH solution have been reported (15 - 18). Substantial differences exist between the results of different workers, particularly at temperatures much above 25°C. No previous studies of solubilities in KOH solutions seem to have been made for the other gases reported here, namely, helium, argon, methane, sulfur hexafluoride or neopentane. An extensive literature survey also failed to reveal any gas solubility data for lithium hydroxide solution. Manometric and volumetric methods of determining gas solubilities are not well-suited to concentrations as low as these (19), and therefore the concentration of dissolved gas was determined by gas chromatographic analysis.

3.3.1 Materials

Minimum purities for the gases used were as follows: helium and argon 99.99%, hydrogen 99.9%, oxygen 99.6%, neopentane and methane 99.0%, and sulfur hexafluoride 98.0%. KOH or LiOH solutions were prepared from especially distilled (all glass-teflon still) and degassed water. The method of degassing was similar to that employed by Clever et al. (20). KOH pellets used for preparing aqueous solutions were Baker analyzed reagent grade and contained a maximum of 1% K_2CO_3. Purified crystalline LiOH (purity 99.5%) was used to prepare solutions. To minimize CO_2 absorption, bottles containing KOH or LiOH solutions were fitted with absorption bulbs containing Ascarite. The concentration of KOH and LiOH was determined by titrating a known volume of solution with standard HCl using methyl orange as the indicator. Concentration was checked both at the beginning and at the end of each experiment to ascertain that there was no change in concentration during the experiment.

3.3.2 Saturation of Solutions with Gases

Saturated solutions of the gas in the electrolyte were prepared by bubbling the gas through a set of presaturators containing the same solution as that being studied and then through the saturating vessel. This apparatus is shown schematically in Figure 3.3-1. The presaturators were required to saturate the gas with water vapor so as to not change the concentration of the solution under test. Attainment of equilibrium is of prime importance for equilibrium solubility determinations and this was checked by withdrawing samples after different intervals of saturation time and analyzing the dissolved gas. The equilibrium solubility was taken and the value measured when at least 3 samples withdrawn at different times gave the same result within the limits of experimental error. This process was repeated at different gas flow rates and it was found that gas flow rate did not affect the measured solubility value. Supersaturation was guarded against by the following procedure. A sample of the solution through which solute gas was bubbling was removed and analyzed. Bubbling of the gas was then stopped and the solution maintained under an atmosphere of the solute gas. Samples of the solution were analyzed periodically, and the results compared with the original values. No measurable super-saturation effect was observed in these experiments.

Samples were withdrawn from the saturating vessel by means of a gas tight Hamilton syringe. The samples were withdrawn very slowly so that at no stage of the sampling process was the flask or syringe placed under significant reduced pressure. Several samples were taken and rejected before final sampling was made. As a check on the procedure

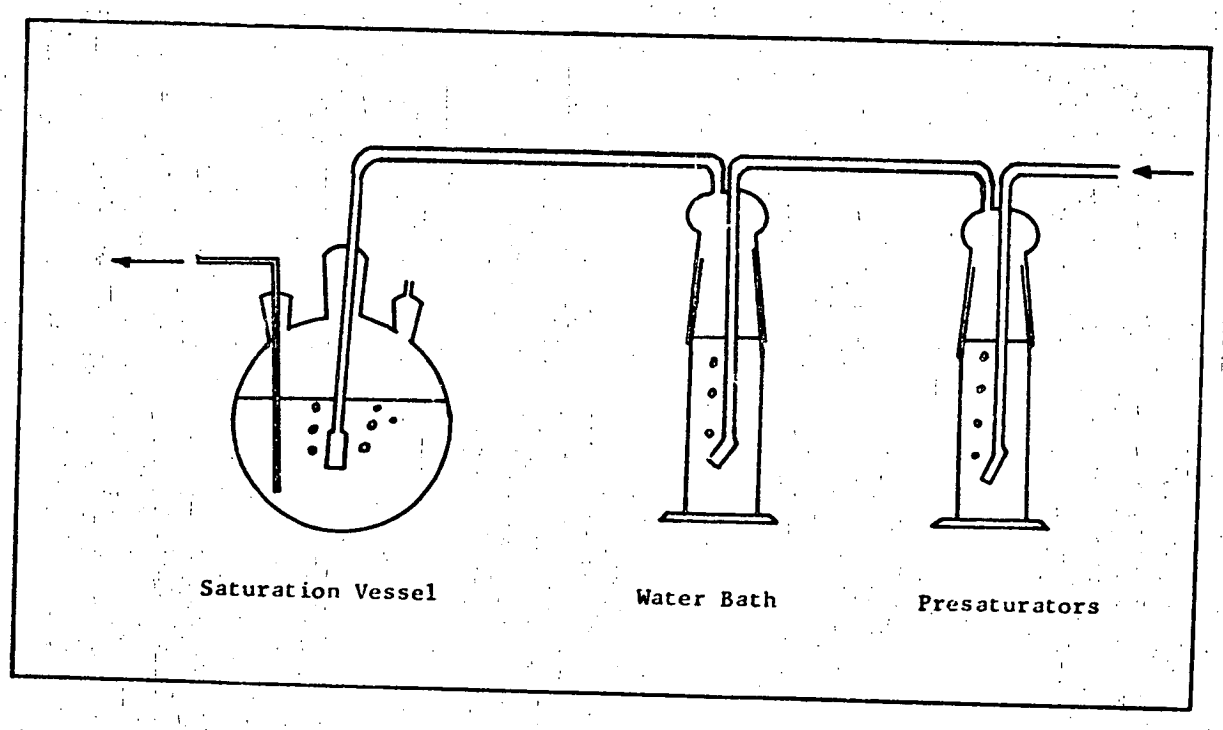

Figure 3.3-1. Apparatus Set-up for Gas Solubility

of sampling and degassing, blank samples consisting of electrolyte saturated with carrier gas were injected into the chromatograph. No peak for the solute gas or air was obtained, indicating that negligible contamination with atmospheric or other gases occurs.

For experiments at a temperature of 80°C or below, two presaturators containing the electrolyte solution were used. For experiments at 100°C additional presaturators were necessary. To check that the solute gas stream containing the sample was fully saturated with water vapor, samples of exit gas were analyzed for water vapor. In addition, the concentration of electrolyte in the solution contained in the saturation flask was checked at the end of the experiment.

The whole assembly, consisting of presaturators and saturating vessel, was completely immersed in a constant temperature bath controlled to ± 0.05°C. Thermometers checked for accuracy against NBS calibrated thermometers were used for measuring the temperature.

3.3.3 Analysis of Dissolved Gas

The experimental method used for the gas solubility measurements has been previously described in detail by Gubbins, Carden and Walker (21). It involved stripping of the dissolved gas from a known volume of the saturated solution with a carrier gas and subsequent chromatographic analysis. This system is shown schematically in Figure 3.3-2. The chromatograph peaks obtained by this procedure were slightly wider and less symmetrical than those obtained by injecting a gas sample directly into the chromatograph sampling post; however, this peak broadening was not sufficient to result in significant loss of accuracy or precision. All analyses were made using a thermal conductivity detector.

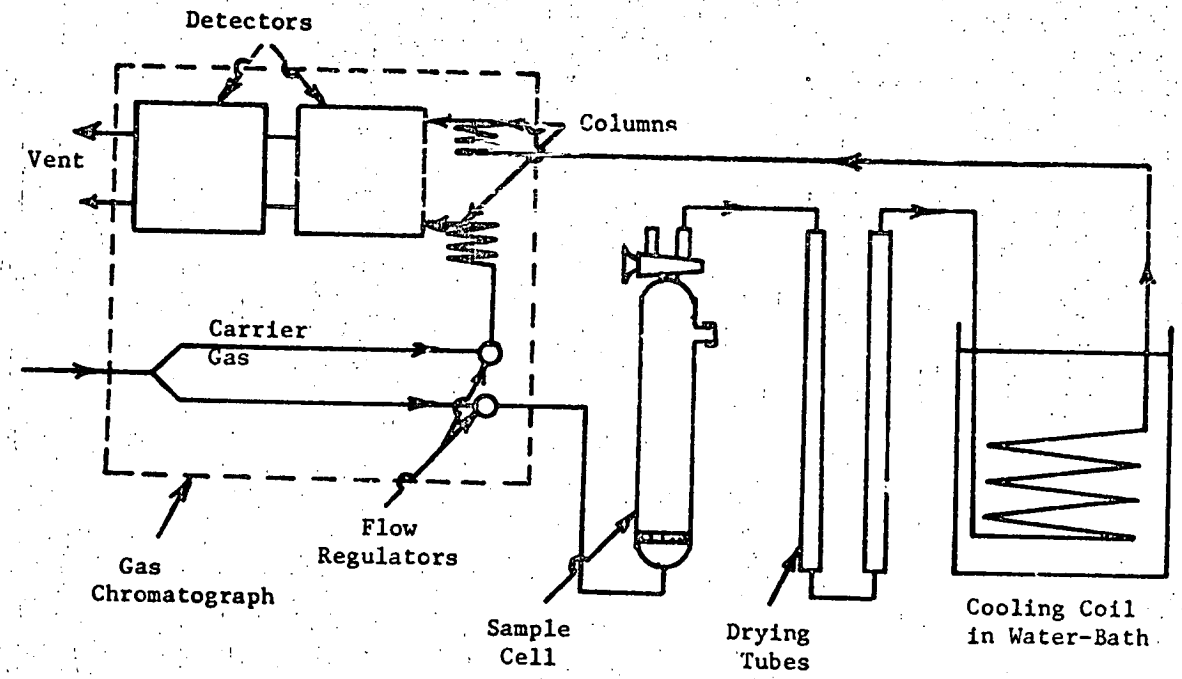

Figure 3.3-2. Apparatus for Gas Solubility Determinations (Method I).

Helium was used as a carrier gas for all solute gases except hydrogen and nelium; for these gases nitrogen or argon was used as the carrier gas.

In determining the solubilities of sulfur nexafluoride and neopentane in 31.6 wt % KOH solution the amount of dissolved gas was found to be too small to obtain accurate results by the above method. For these systems a modified procedure (?) was used in which the gas from a 200 ml sample of solution was concentrated before analysis in a tube immersed in liquid nitrogen. This procedure enabled large samples to be used without loss of accuracy due to broadening of chromatographic peaks. This apparatus is shown in Figure 3.3-3.

The chromatograph was calibrated by injecting an accurately measured volume of pure dry gas and measuring the area of the resulting peak. For those gases where accurate values of the solubility in water at 25°C were available in the literature, the calibration was checked by carrying out the above procedure on a water sample. The relationship of the amount of dissolved gas to the instrument response was checked and was found to be linear within the limits of the experimental error.

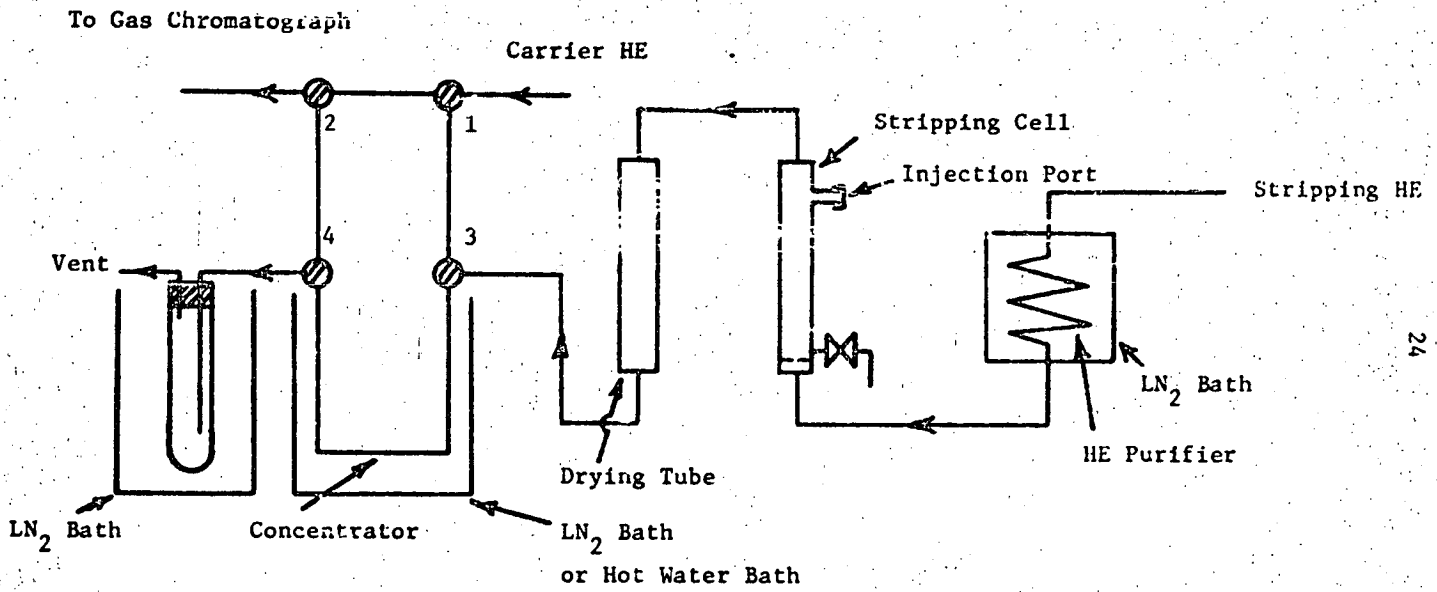

Figure 3.3-3. Schematic Diagram of Method II (Dissolved Gas Stripper and Concentrator).

3.4 Presentation of Experimental Results

The experimental data for the solubility of various gases in KOH and LiOH are presented in Tables 3.4-1 and 3.4-2 as solubility in g.mole/gas/l. solution-atm.; they are plotted in Figures 3.4-1 to 3.4-6.

Activity coefficients of the dissolved gases, calculated from Equation 3.1-10

$$\gamma_1 = \frac{x_1^o(1)}{x_1(1)} \qquad (3.1\text{-}10)$$

are presented in Tables 3.4-3 and 3.4-4, where each value tabulated is the mean of four or more replicate measurements. The precision of the reported data ranged from approximately 1% at the highest solubility (mole fraction in the region of 10^{-5}) to about 5% for the lowest solubilities measured (10^{-7} to 10^{-8} mole fraction). Tables 3.4-5 and 3.4-6 list experimental solubility values from the literature. In most cases agreement is better than 2%. Except for the solubility of hydrogen and oxygen in KOH solutions at the lower temperatures, no other measurements of the solubility in KOH or LiOH solutions seem to have been reported for the other gases studied. Geffcken (15) measured solubilities of oxygen and hydrogen at 15°C and 25°C in solutions 0 to 1.4M in KOH, and Knaster and Apel'baum (16) made similar measurements at 21°, 45° and 75°C for KOH concentrations up to 10M. Ruetschi and Amlie (17) have measured solubilities of hydrogen for KOH concentrations up to 10M at 30°C, while Davis et al. (18) recently reported oxygen solubilities at 0°, 25° and 60°C for KOH concentration to 12M.

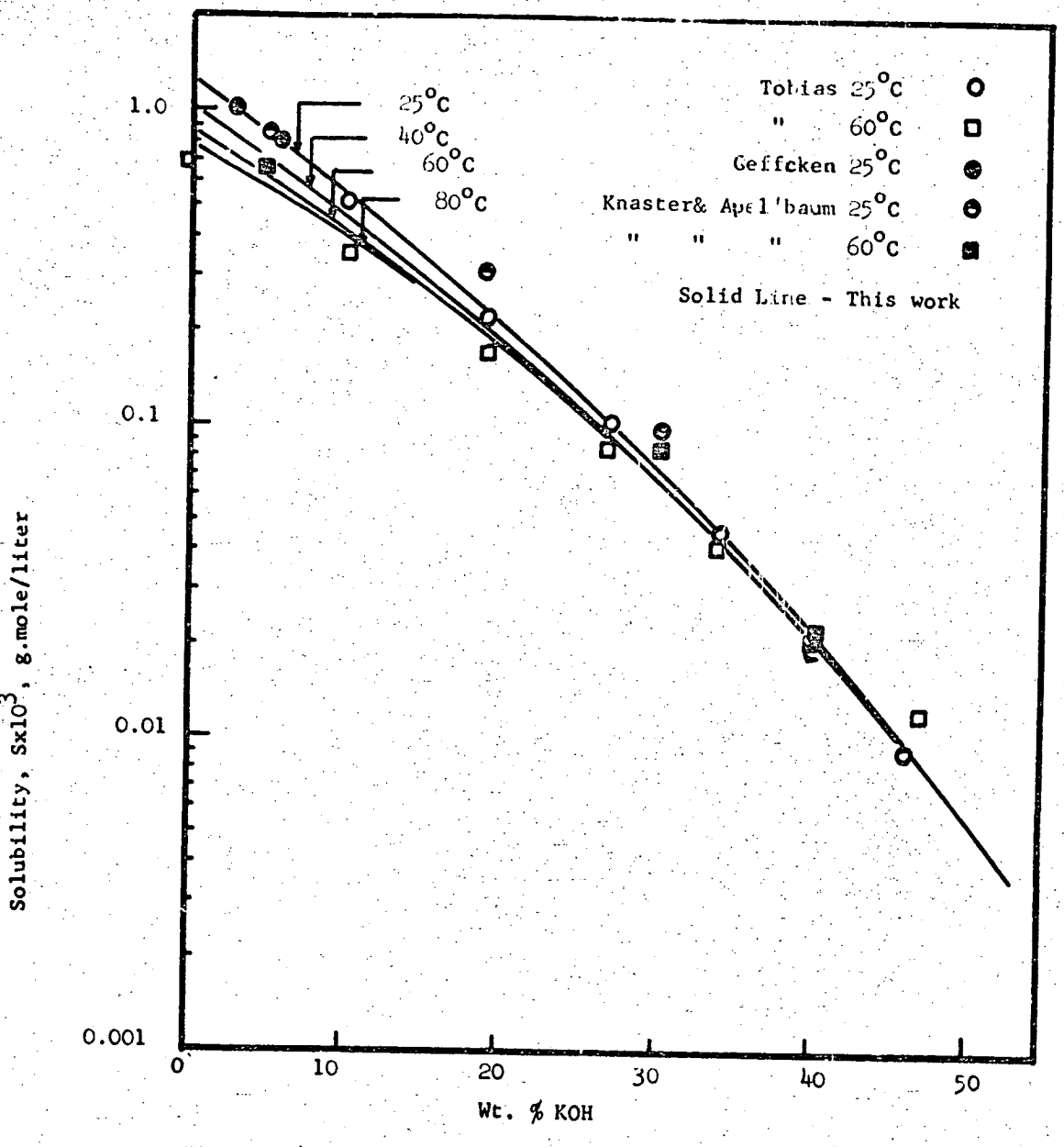

Figure 3.4-1. Solubility of Oxygen in Aqueous Potassium Hydroxide Solutions

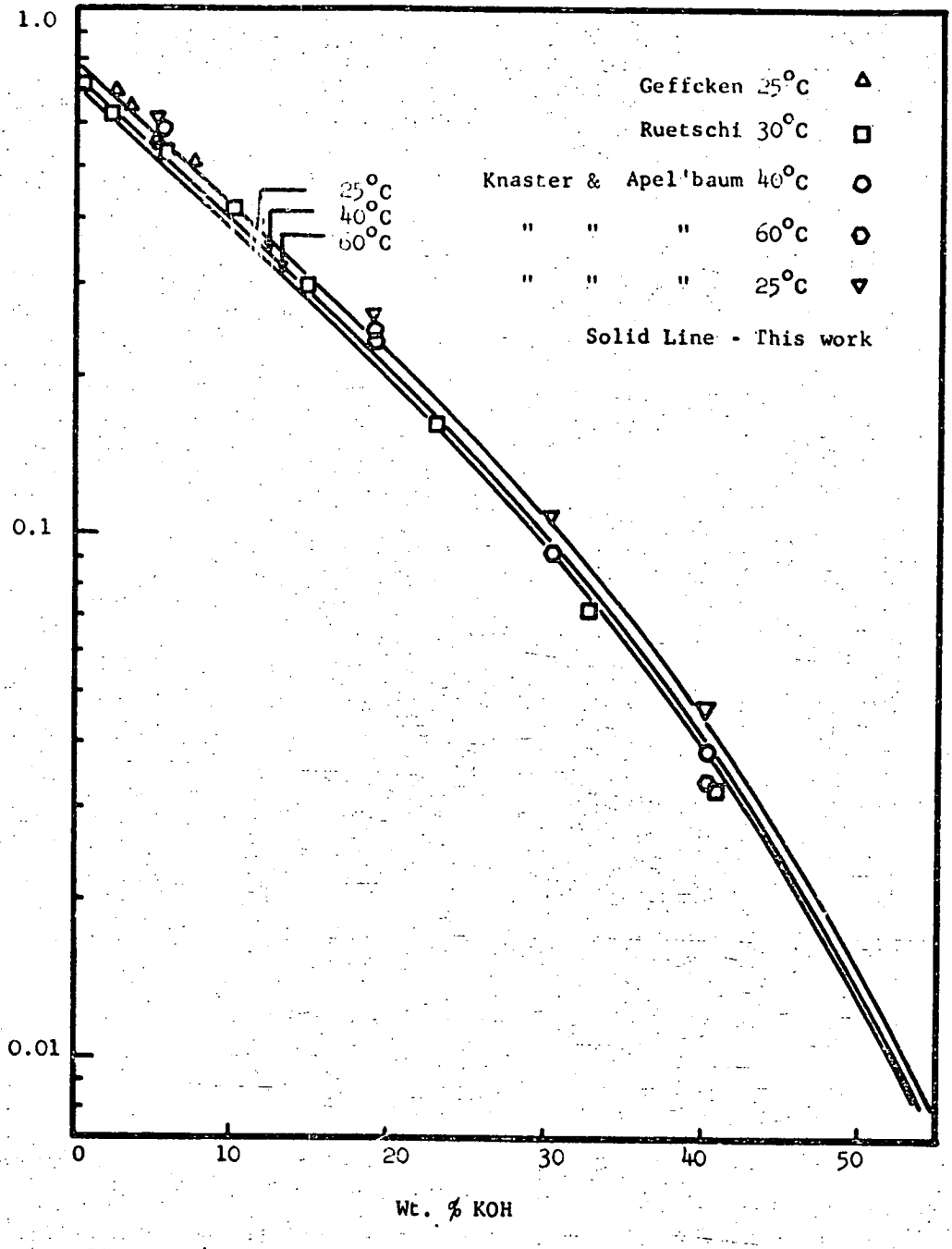

Figure 3.4-2. Solubility of Hydrogen in Aqueous Potassium Hydroxide Solutions

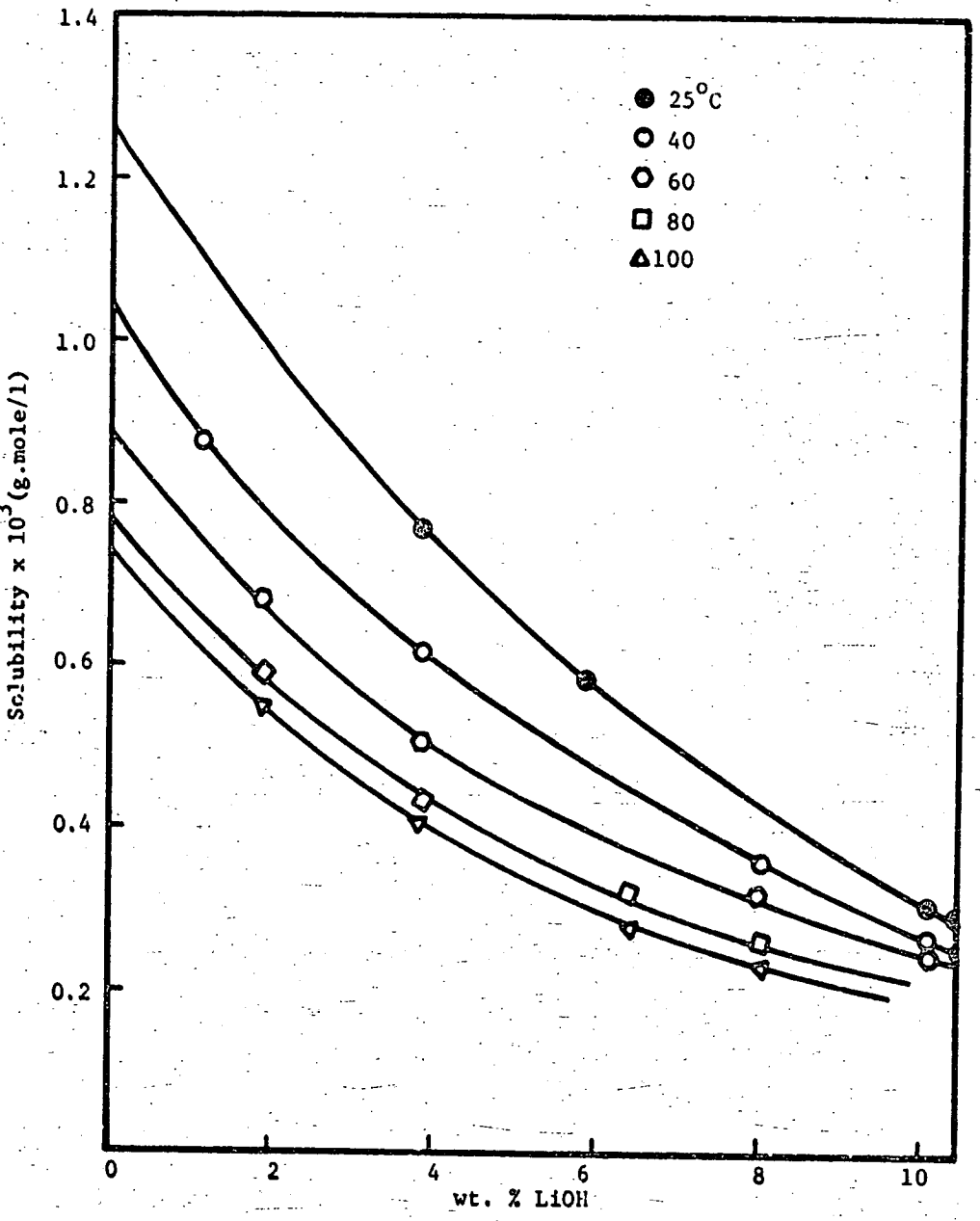

Figure 3.4-3 Solubility of Oxygen in LiOH Solutions

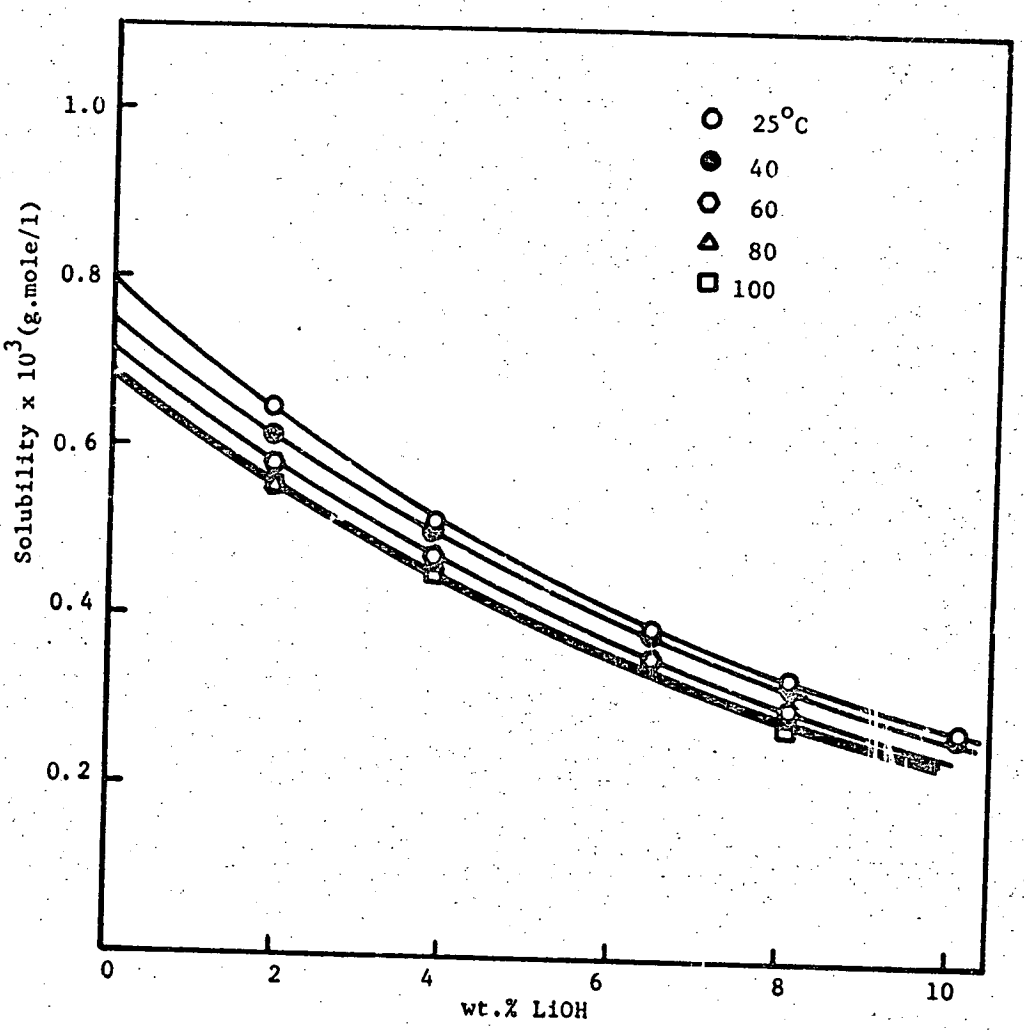

Figure 3.4-4 Solubility of Hydrogen in LiOH Solutions

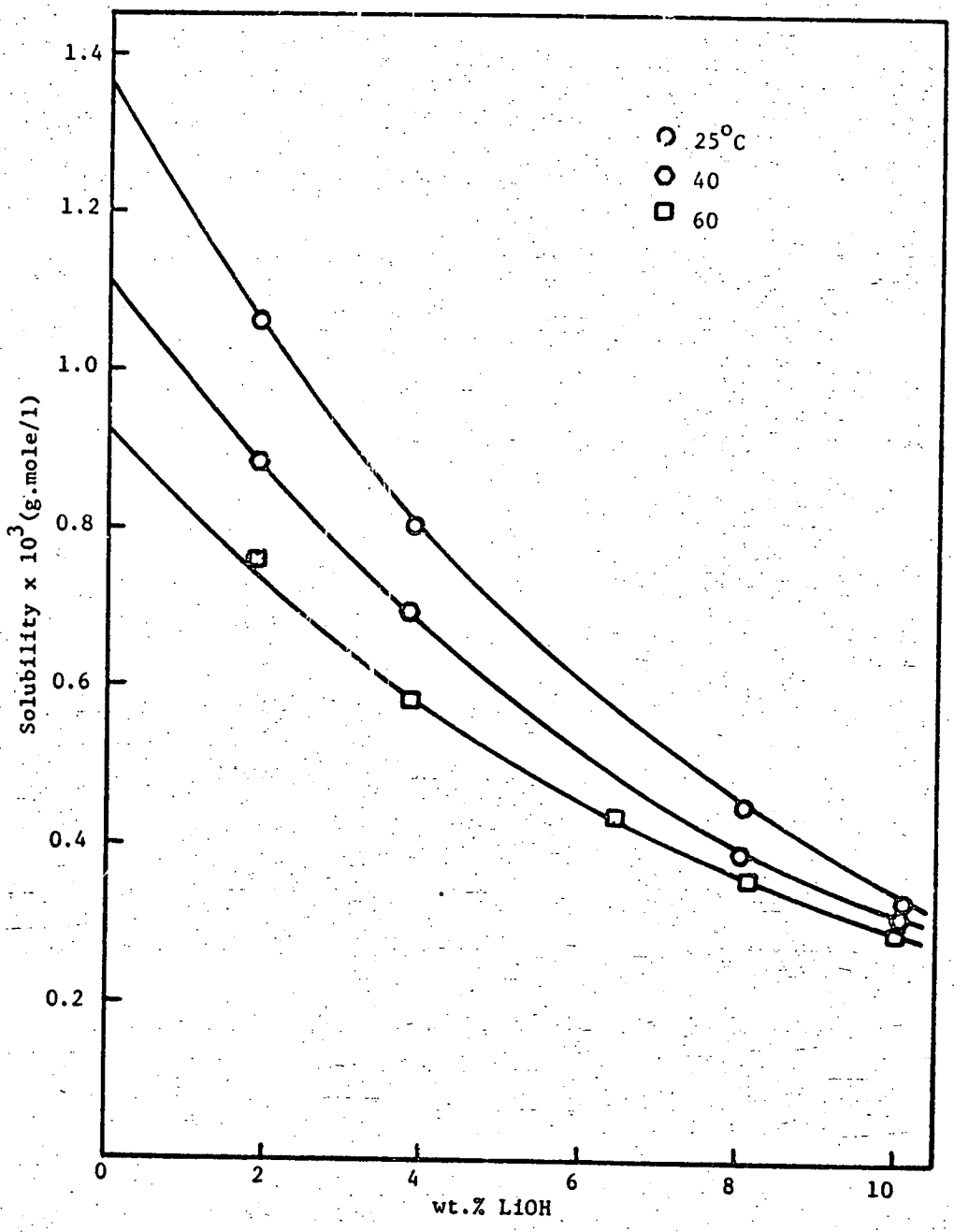

Figure 3.4-5 Solubility of Argon in LiOH Solutions

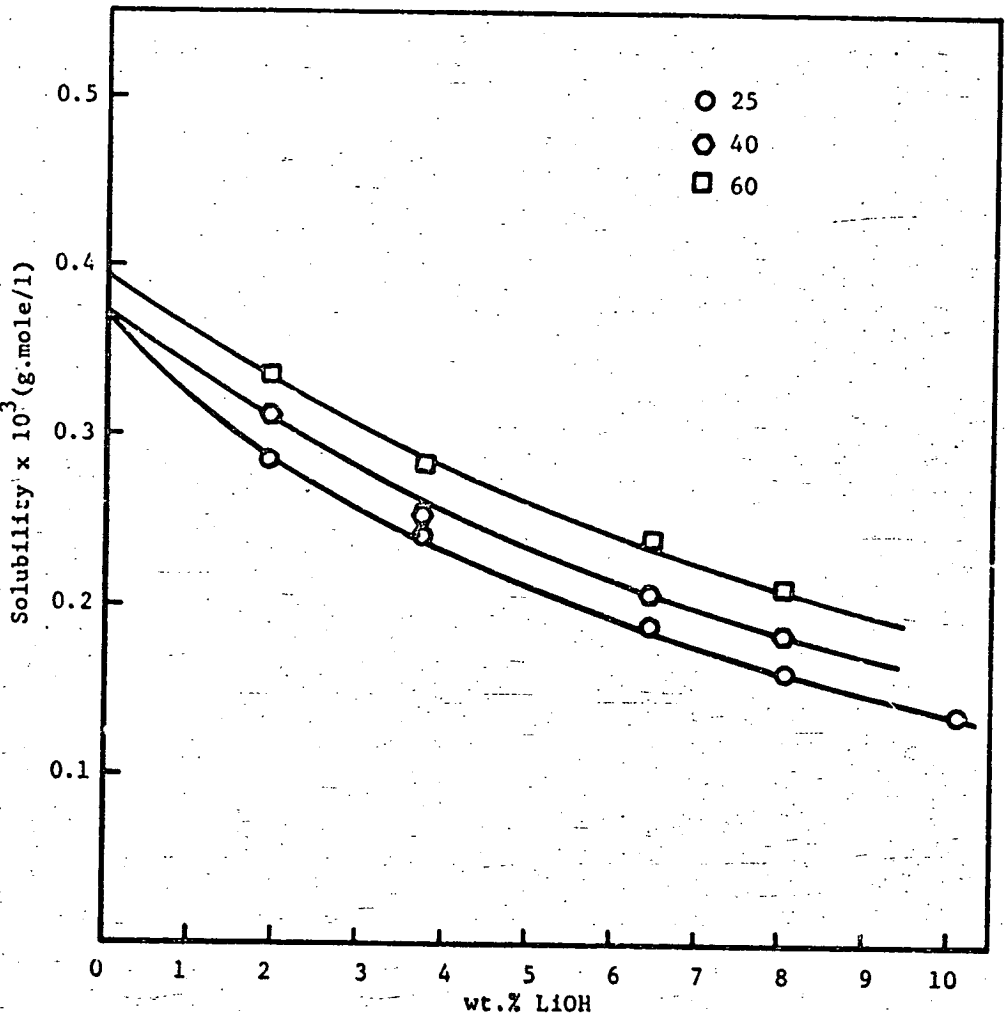

Figure 3.4-6 Solubility of Helium in LiOH Solutions

Table 3.4-1

Solubility of Non-Polar Gases in Aqueous KOH Solutions

Solute Gas	Wt % KOH	Solubility, g.mole/l.-atm., $\times 10^3$				
		25°C	40°C	60°C	80°C	100°C
O_2	0	1.263*	1.049	0.875	0.785*	
	5.00	0.825	0.684	0.605	0.584	
	13.50	0.413	0.365	0.339	0.315	
	23.00	0.155	0.145	0.139	0.137	
	31.60	0.061	0.059	0.056	0.055	
	40.70	0.018	0.020	0.019	0.020	
	50.30	-	0.006	-	-	
	50.65	0.006	-	0.005	0.006	
H_2	0	0.792	0.713	0.742	-	
	5.00	0.583	0.560	0.540	0.539	
	9.00	0.465	0.435	0.410	0.394	
	19.50	0.226	0.217	0.199	0.196	
	32.40	-	0.082	0.078	0.079	
	34.50	0.078	-	-	-	
	38.00	-	-	-	-	0.047
	41.40	0.038	0.035	0.033	0.033	0.034
	52.40	0.011	0.010	0.009	0.010	0.009
	56.40	-	-			0.007
Ar	0	1.407	1.122	0.919	-	
	5.00	0.903	0.758	0.658	0.620	
	13.50	0.442	0.400	0.355	0.334	
	23.00	0.183	0.162	0.157	0.147	
	31.60	-	-	0.064	0.061	
	32.50	0.062	-	-	-	
	36.60	-	0.036	-	-	
	40.70	-	-	-	-	
	41.40	0.002	0.018	0.020	0.020	
He	0	0.378	0.372	0.392	0.43	
	5.00	0.273	0.274	0.286	0.302	
	9.00	0.224	0.225	0.224	0.231	
	19.00	0.109	0.102	0.117	0.117	
	32.4	0.030	0.030	0.031	0.032	

*Literature value (22)

Table 3.4-1 (Continued)

Solute Gas	Wt % KOH	Solubility, g.mole/l.-atm., $x10^3$				
		25°C	40°C	60°C	80°C	100°C
CH_4	0.0	1.341	1.056	0.872	0.789	
	5.61	0.806	0.704	0.594	0.573	
	13.90	0.376	0.343	0.315	0.319	
	23.50	0.135	0.134	0.129	0.129	
	31.61	0.051	0.053	0.054	0.056	
	40.70	0.014	0.017	0.018	0.021	
SF_6	0	0.225	0.151	0.12	0.103	
	5.00	0.1045	0.077	0.065	0.060	
	13.50	0.031	0.024	0.021	0.021	
	23.00	0.005	0.005	0.005	0.005	
	31.60	0.001	0.001	0.001	0.001	
$C(CH_3)_4$	0	0.561	0.378	0.264	0.234	
	5.61	0.257	0.175	0.101	0.122	
	13.90	0.064	0.049	0.040	0.040	
	23.50	0.010	0.009	0.008	0.008	
	31.61	0.003	0.002	0.002	0.002	

* Literature Value (22)

Table 3.4-2

Solubility of Non-Polar Gases in Aqueous LiOH Solutions

Oxygen	Solubility g.mol/l.-atm., $x10^3$				
Wt. % LiOH	25°C	40°C	60°C	80°C	100°C
0.0	1.263	1.045	0.875	0.782	0.75
1.90	0.986	0.814	0.682	0.592	0.548
3.85	0.770	0.617	0.502	0.430	0.405
6.45	0.516	0.426	0.360	0.328	0.275
8.05	0.400	0.363	0.322	0.262	0.230
10.10	0.309	0.265	0.243	-	-

Helium			
Wt. % LiOH	25°C	40°C	60°C
0.0	0.372	0.372	0.392
1.90	0.285	0.314	0.339
3.85	0.264	0.244	0.281
6.45	0.190	0.208	0.245
8.05	0.161	0.181	0.210
10.10	0.135	0.160	0.172

Hydrogen					
Wt. % LiOH	25°C	40°C	60°C	80°C	100°C
0.00	0.792	0.745	0.712	0.692	0.690
1.90	0.650	0.617	0.574	0.550	0.550
3.85	0.517	0.506	0.475	0.462	0.450
6.45	0.390	0.395	0.355	-	-
8.05	0.340	0.335	0.312	0.282	0.275
10.10	0.270	0.264	0.242	-	-

Table 3.4-2 (continued)

Argon	Solubility, g.mole/l.-atm., $\times 10^3$		
Wt. % LiOH	25°C	40°C	60°C
0.00	1.360	1.110	0.918
1.90	1.066	0.896	0.765
3.85	0.809	0.706	0.582
6.45	0.549	0.489	0.437
8.05	0.450	0.388	0.361
10.10	0.329	0.310	0.285

Table 3.4-3

Activity Coefficients of Non-Polar Gases Dissolved in Aqueous KOH Solutions

Oxygen

Wt.% KOH	C_S [a]	Activity Coefficient, γ_1 25°C	40°	60°	80°	100°
0.00	0.00	1.00	1.00	1.00	1.00	1.00
5.00	0.92	1.53	1.54	1.45	1.35	-
13.50	2.67	3.06	2.87	2.58	2.50	-
23.00	5.00	8.15	7.24	6.30	5.73	-
31.61	7.35	20.1	17.8	15.6	14.4	-
40.70	10.12	70.1	53.3	45.3	40.1	38.4
50.65	13.75	230.	-	162.	143.	141.
56.50	16.20	-	-	-	-	338.

Hydrogen

Wt.% KOH	C_S	Activity Coefficient, γ_1 25°	40°	60°	80°	100°
0.00	0.00	1.00	1.00	1.00	1.00	1.00
5.00	0.92	1.36	1.28	1.32	1.33	-
9.00	1.70	1.71	1.64	1.74	1.81	-
19.50	4.12	3.50	3.29	3.58	3.65	-
32.40	7.60	-	8.70	9.16	9.04	-
38.00	9.27	-	-	-	-	15.3
41.40	10.37	20.1	20.4	21.4	21.8	21.9
52.40	14.35	72.0	73.7	76.7	75.4	82.6
56.50	16.20	-	-		-	108.

Helium

Wt.% KOH	C_S	Activity Coefficient, γ_1 25°	40°	60°	80°
0.00	0.00	1.00	1.00	1.00	1.00
5.00	0.92	1.39	1.36	1.39	1.44
9.00	1.70	1.75	1.73	1.96	1.89
19.00	3.99	3.57	3.71	3.59	3.77
32.40	7.60	13.1	12.7	13.0	13.7

Sulfur Hexafluoride

Wt.% KOH	C_S	Activity Coefficient, γ_1 25°	40°	60°	80°
0.00	0.00	1.00	1.00	1.00	1.00
5.00	0.92	2.15	1.97	1.88	1.73
13.50	2.67	7.44	6.53	5.88	4.91
23.00	5.00	43.2	31.9	26.6	22.6
31.6	7.35	234.	146.	112.	84.2

Table 3.4-3
(continued)

Argon

Wt.% KOH	C_S	Activity Coefficient, γ_1 25°	40°	60°	80°
0.00	0.00	1.00	1.00	1.00	1.00
5.00	0.92	1.56	1.48	1.40	1.32
13.50	2.67	3.18	2.81	2.59	2.48
23.0	5.00	7.68	6.93	5.85	5.57
31.61	7.35	-	-	14.5	13.4
32.40	7.60	22.8	-	-	-
40.70	10.15	-	-	-	30.0
41.40	10.37	70.3	58.2	46.1	-

Methane

Wt.% KOH	C_S	Activity Coefficient, γ_1 25°	40°	60°	80°
0.00	0.00	1.00	1.00	1.00	1.00
5.61	1.03	1.66	1.51	1.48	1.39
13.90	2.77	3.64	3.14	2.83	2.50
23.50	5.13	10.2	8.08	6.90	8.22
31.61	7.35	26.7	19.8	16.7	14.4
40.70	10.12	100.	63.4	49.6	38.0

Neopentane

Wt.% KOH	C_S	Activity Coefficient, γ_1 25°	40°	60°	80°
0.00	0.00	1.00	1.00	1.00	1.00
5.61	1.03	2.18	2.17	2.04	1.94
13.90	2.77	8.91	7.87	6.80	5.94
23.50	5.13	56.1	42.0	33.0	28.6
31.61	7.35	288.	220.	158.	138.

[a] Molarity of KOH measured at 25°C

Table 3.4-4

Solubility of Non-Polar Gases in Water at 1 atm Partial Pressure*
(See also Table 3.4-6)

Solute Gas	$x_1^{\circ}(1)\times10^5$							
	25°C		40°C		60°C		80°C	
	This Work	Lit.	This Work	Lit.	This Work	Lit.	This Work	Lit.
O_2 (22)	2.25	2.279	1.99	1.968	1.80	1.791	1.71	1.755
H_2 (22)	1.43	1.415	1.29	1.329	1.19	1.247	-	1.342
He (107,108)	0.671	0.682	0.673	0.674	0.715	0.718	0.796	-
Ar (107,108)	2.53	2.480	2.00	1.948	1.68	1.671	1.52	-
SF_6 (109)	0.402	0.406	2.74	-	2.20	-	1.91	-
CH_4 (22)	2.48	2.421	1.90	1.915	1.62	1.595	1.44	1.461
$C(CH_3)_4$	1.01	1.02	0.685	0.683	0.483	-	0.433	-

* Literature value (Ref. 22) of $x_1^{\circ}(1)$ for O_2 at 100°C = 1.424×10^{-5}

Literature value (Ref. 22) of $x_1^{\circ}(1)$ for H_2 at 100°C = 1.342×10^{-5}

Table 3.4-3

Activity Coefficients of Non-Polar Gases Dissolved in Aqueous LiOH Solutions

LiOH Concentration		Activity Coefficient, γ_1									
		Oxygen					Hydrogen				
Wt. %	g.mole/l.	25°C	40°C	60°C	80°C	100°C	25°C	40°C	60°C	80°C	100°C
0.0	0.00	1.00	1.00	1.00	1.00	1.00	1.00	1.00	1.00	1.00	1.00
1.90	0.78	1.29	1.29	1.28	1.31	1.34	1.24	1.21	1.24	1.25	1.23
3.85	1.69	1.69	1.73	1.77	1.83	1.84	1.58	1.49	1.52	1.51	1.53
6.45	2.87	2.52	2.51	2.51	2.44	2.76	2.12	2.00	2.06	-	-
8.05	3.65	3.28	3.04	2.84	3.10	3.35	2.43	2.33	2.39	2.55	2.58
10.10	4.69	4.51	4.34	4.13	-	-	3.24	3.15	3.19	-	-

LiOH Concentration		Activity Coefficient, γ_1									
		Helium					Argon				
Wt. %	g.mole/l.	25°C	40°C	60°C	80°C	100°C	25°C	40°C	60°C	80°C	100°C
0.0	0.0	1.00	1.00	1.00			1.00	1.00	1.00		
1.90	0.78	1.33	1.20	1.16			1.29	1.25	1.20		
3.85	1.69	1.46	1.56	1.42			1.73	1.61	1.61		
6.45	2.87	2.05	1.86	1.65			2.51	2.36	2.17		
8.05	3.65	2.46	2.17	1.96			3.21	3.03	2.67		
10.10	4.69	3.04	2.57	2.32			4.57	3.94	3.51		

Table 3.4-6

Solubility of Gases in Water at 1 atm Partial Pressure

S, g.mole/l.x10^3

Solute Gas Ref.	25°C This Work	25°C Lit.	40°C This Work	40°C Lit.	60°C This Work	60°C Lit.	80°C This Work	80°C Lit.	100°C This Work	100°C Lit.
Oxygen (22)	1.26	1.263	1.05	1.030	0.875	0.869	0.782	0.786	0.75	0.755
Hydrogen (22)	0.792	0.784	0.745	0.733	0.712	0.714	0.692	0.714	0.69	0.714
Argon (107,108)	1.36	1.374	1.11	1.071	0.918	0.913	-	-	-	-
Helium (107,108)	0.372	0.378	0.372	0.372	0.392	0.392	-	-	-	-

To facilitate the comparison of the results of the present investigation with those of previous workers, the solubility data for oxygen and hydrogen at 25°C have been plotted in Figures 3.4-7 and 3.4-8 in the form of a semilogrithmic plot. This type of plot has been used since most electrostatic theories of salting out predict a linear relationship between the logrithm of the activity coefficient and molar concentration of electrolyte at moderate electrolyte concentrations.

Figure 3.4-1 reveals that the 25°C oxygen solubility values obtained in this work agree within 2% and 5% with those obtained by Geffcken (15) and Davis et al. (16), respectively. The experimental results of these investigators are distributed on both sides of the solid line of Figure 3.4-7. The agreement with the results of Knaster and Apel'baum (16) is good at very low and very high concentrations. However, at intermediate concentration, the disagreement is quite marked, the results of Knaster and Apel'baum falling consistently below the solid line. At 60°C it is possible to compare the present data with that of Davis et al.; the agreement is excellent, being within 2% at low KOH concentrations, and within 10% at the highest concentrations.

Correction: In the Fourth Semi-Annual Report it was stated that the solubility data of Davis et al. (18) for oxygen in KOH solutions at 60°C differed from those obtained in this work by about 15%, and it further suggested that discrepancies might exist at other temperatures. This is incorrect and the authors are happy to correct this error. In fact, the data generated in this work are in excellent agreement with the data of Davis et al. except at the highest KOH concentrations. This unfortunate error arose through our failure to note that Davis et al.

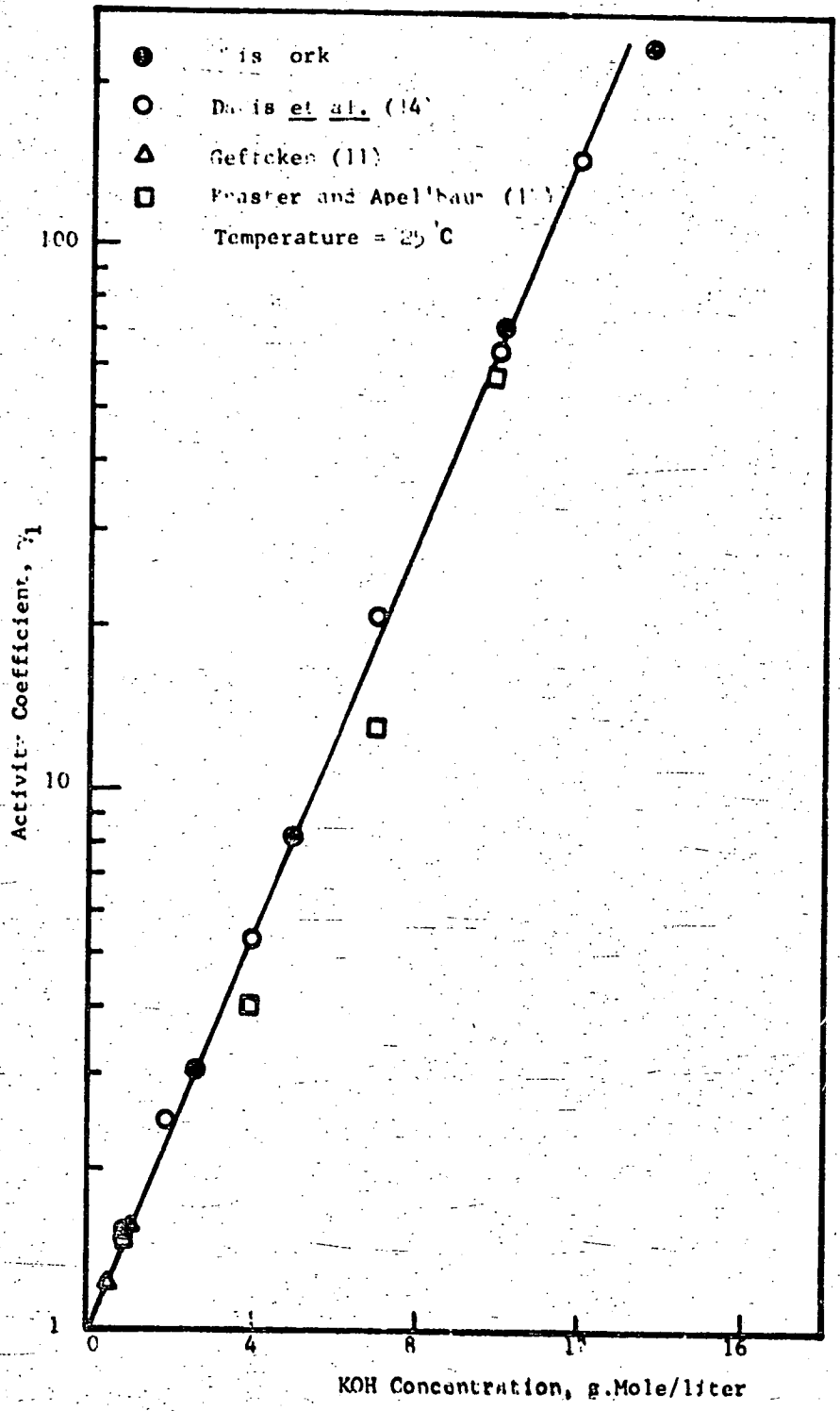

Figure 3.4-7. Activity Coefficients of Oxygen in KOH Solutions

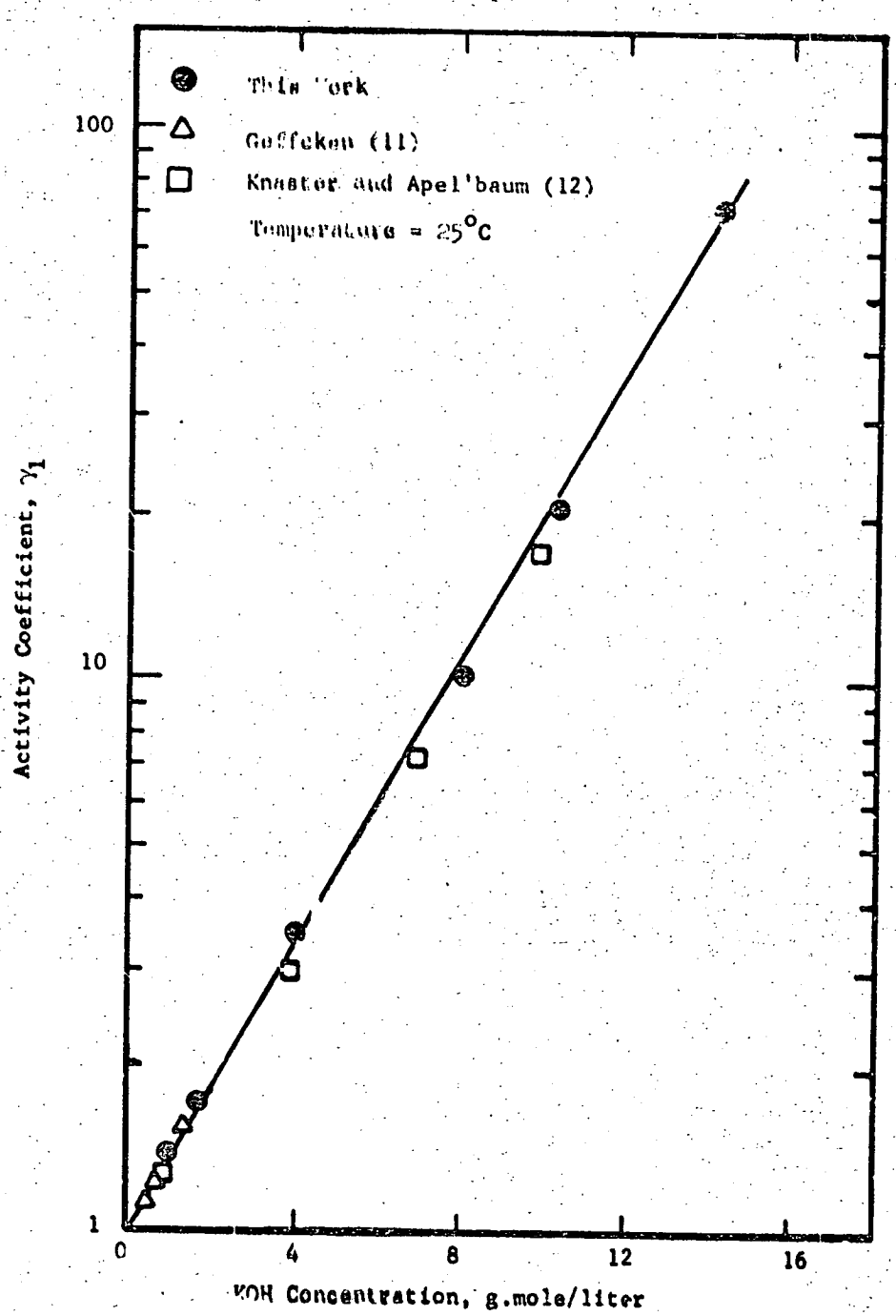

Figure 3.4-8 Activity Coefficients of Hydrogen in KOH Solutions

had reported solubilities at a total pressure of one atmosphere whereas we were reporting data at a partial pressure of one atmosphere. We are grateful that this matter has been called to our attention and that we have this opportunity to clarify the matter.

Figure 3.4-2 shows that hydrogen solubilities in KOH obtained in this work at 25°C are in fairly good agreement with those of other workers. Agreement with the results of Geffcken (15) is within 2%, and with those of Knaster and Apel'baum (16) is within 10%. For dilute KOH solutions, the reported results agree within 3% with those of Ruetschi and Amlie (17). However, the values of activity coefficients obtained by them are consistently lower than those reported here, and these discrepancies are as large as 10% for the higher KOH concentration. At temperatures of 40 and 60°C, the disagreement between the reported results and those of Knaster and Apel'baum (16) is also within 10%.

No literature values are available to compare the experimental solubility of various gases in LiOH solution.

3.5 Discussion of Results

3.5.1 Calculation of Gas Solubilities by Scaled Particle Theory

The scaled particle theory was used to calculate theoretical values for the solubility of various gases in KOH and LiOH solutions. The following equation, developed earlier (3.2-16), was used to make these calculations:

$$\ln(\gamma_1 K_1^o) = \frac{\bar{g}_1^h}{kT} + \frac{\bar{g}_1^s}{kT} + \ln(kT\Sigma\rho_j)$$

The various parameters required for calculation of $\ln(\gamma_1 K_1^o)$ were evaluated in the manner described below.

Values of the Lennard-Jones parameters, σ and ϵ/k, for solute gases were those obtained from second virial coefficient data, and are shown together with polarizabilities in Table 3.5-1. These parameters were taken from Hirchfelder, Curtiss and Bird (23) except where otherwise indicated, and are the same values as used by Pierotti (7), except in the cases of sulfur hexafluoride and neo-pentane. Values of σ, ϵ/k and dipole moment, μ, for water were those used by Pierotti.

Values of σ and ϵ/k do not seem to have been reported for ions. Although crystal radii should provide approximate values for σ, such radii are difficult to determine accurately and considerable disagreement is shown between the values reported by various workers. In view of the sensitivity of the calculated solubilities to the σ values, a procedure similar to that used by Pierotti (7) in determining σ for water was used. Experimental values of $\ln(\gamma_1 K_1^o)$ were plotted against polarizability of the solute molecules at 25°C for 10% and 20% by weight KOH solution. The value of $\ln(\gamma_1 K_1^o)$, extrapolated to zero polarizability,

is the experimental hard sphere value. This may be compared with the theoretical hard sphere value from Equations 3.1-7 and 3.2-15

$$\lim_{\substack{\alpha_1 \to 0 \\ \sigma_1 \to 258\text{A}}} \ln(\gamma_1 K_j^o) = \frac{\bar{g}_1^h}{kT} + \ln(kT\Sigma\rho_j)$$

As the other molecular parameters are known, the resulting equations may be solved for the σ values for the two ions. These values are shown in Table 3.5-2, and are seen to be in good agreement with crystal diameters. The σ value of Li^+ ion was taken as twice the crystallographic radius.

Although experimental values of ϵ/k are not available for ions, several theories afford expressions for the potential interaction due to dispersion forces (24). The Mavroyannis-Stephen theory (25) gives for the dispersion interaction

$$U_{ij}^{(dis)} = -3\frac{a_0^{1/2}e^2\bar{\alpha}_i\bar{\alpha}_j}{2r^6\left[\left(\frac{\bar{\alpha}_i}{Z_i}\right)^{1/2}+\left(\frac{\bar{\alpha}_j}{Z_j}\right)^{1/2}\right]} \qquad (3.5\text{-}1)$$

where $a_o = 0.5292$ Å is the Bohr radius, e is the electronic charge, Z is the total number of electrons in the particle, and $\bar{\alpha}_i$ and $\bar{\alpha}_j$ are polarizabilities for the two species in the mixture. Comparing with the dispersion term of Lennard-Jones (6-12) potential

$$4\epsilon_{ij}\sigma_{ij}^6 = \frac{3a_0^{1/2}e^2\bar{\alpha}_i\bar{\alpha}_j}{2\left[\left(\frac{\bar{\alpha}_i}{Z_i}\right)^{1/2}+\left(\frac{\bar{\alpha}_j}{Z_j}\right)^{1/2}\right]} \qquad (3.5\text{-}2)$$

Table 3.5-1

Molecular Parameters for Solute Gases

Solute Gas	σ_1, Å	ϵ_1/k, °K	$\alpha_1 \times 10^{24}$ cm³/molecule
He	2.63	6.03	0.204
H_2	2.87	29.2	0.802
Ar	3.40	122	1.63
O_2	3.46	118	1.57
CH_4	3.82	137	2.70
SF_6	5.51	200.9	6.21[a]
$C(CH_3)_4$	7.44[b]	232.5[b]	10.36[b]

[a] T. M. Reed, J. Phys. Chem., 59, 428 (1955).

[b] J. H. Bae, Ph.D. Thesis, University of Florida, Gainesville, Florida, 1966.

Table 3.5-2

Molecular Parameters for Solvent Species

Solvent Species	σ, Å	a, Å	a_i, Å	ϵ/k, °K	$\alpha \times 10^{24}$ cm³/molecule	μ Debye
H_2O	2.75[a]	-	-	85.3[a]	-	1.84
K^+	2.60[b]	2.66[c]	2.50[d]	239[b]	0.835[e]	
OH^-	3.30[b]	3.52[c]	0.92[d]	137.2[b]	1.83[b]	
Li^+	1.20[c]	-	-	59.37[b]	0.0313	

a Values from reference (7)

b Calculated in this work

c Diameters from crystal radii, references (28) and (29)

d Diameters from ionic mobility, reference (29)

e Reference (27)

For like pair interactions, after substituting values for a_0 and e, this equation gives

$$\epsilon = 3.146 \times \frac{10^{-24} \alpha^{3/2} Z^{1/2}}{6} \text{ erg} \qquad (3.5\text{-}3)$$

where α and α are in c.g.s. units. The Mavroyannis-Stephen theory gives ϵ values which are in considerably better agreement with values obtained from experimental data than those calculated from most previous theories. Equation 3.5-3 was used to calculate the $\frac{\epsilon}{k}$ value for the K^+ and Li^+ ions shown in Table 3.5-2. For OH^- no polarizability value could be found in the literature, and the value given in Table 3.5-2 was calculated from the relation between polarizability and mole refraction R (26)

$$\alpha = \frac{3}{4\pi} \left(\frac{V}{N} \right) \frac{n^2-1}{n^2+2} = \frac{3R}{4\pi N} \qquad (3.5\text{-}4)$$

where V and N are volume and number of molecules, and n is the index of refraction. Mole refraction data were obtained from the Landolt-Bornstein Tables (27).

A complete sample calculation is given in Appendix 1.

3.5-2 Comparison of Theoretical and Experimental Gas Solubilities

Having evaluated all the molecular parameters we can now predict the solubilities. Predicted and experimental values of $\ln(\gamma_1 K_1^o)$ are compared at two temperatures in Tables 3.5-3 and 3.5-4 for KOH and LiOH solutions, respectively. Hard and soft contributions to the chemical potential in Equation 3.2-15 can now be calculated using the molecular parameters of Tables 3.5-1 and 3.5-2 together with experimental densities from the literature.

Table 3.5-3

Comparison of Predicted and Experimental $\ln(\gamma_1 K_1^{\circ})$ Values for KOH Solutions

	0% KOH[a]		10%		20%		30%		40%		50%	
Solute	Expt.	Theo.	Expt.	Theo.	Expt.	Theo.	Expt.	Theo.	Expt.	Theo.	Expt.	Theo.
						25°						
He	11.86	11.62	12.25	11.98	13.10	12.85	14.05	13.62	-	-	-	-
H_2	11.17	11.10	11.85	11.85	12.41	12.53	13.17	13.42	14.13	14.63	15.2	15.15
Ar	10.62	10.34	11.38	11.03	12.30	11.90	13.36	12.99	14.58	14.16	-	-
O_2	10.66	10.51	11.50	11.33	12.46	12.22	13.54	13.26	14.73	14.57	16.07	16.20
CH_4	10.58	10.58	11.46	11.38	12.49	12.48	13.65	13.66	15.10	15.17	-	-
SF_6	12.38	10.75	13.88	12.38	15.58	14.10	17.52	16.25	-	-	-	-
$C(CH_3)_4$	11.51	11.80	12.99	13.55	14.81	16.43	16.85	19.87	-	-	-	-
						80°						
He	11.74	11.42	12.39	12.11	13.18	12.83	14.10	13.71	-	-	-	-
H_2	11.24	10.67	11.90	11.89	12.55	12.67	13.28	13.62	14.25	14.73	15.29	16.03
Ar	11.10	10.81	11.75	11.56	12.55	12.44	13.50	13.47	14.60	14.72	-	-
O_2	11.13	11.04	11.81	11.72	12.68	12.66	13.63	13.83	14.76	15.13	16.07	16.82
CH_4	11.14	11.18	11.86	12.05	12.70	13.10	13.69	14.35	14.80	15.79	-	-
SF_6	13.17	12.49	14.30	13.99	15.72	15.79	17.36	18.10	-	-	-	-
$C(CH_3)_4$	12.37	14.42	13.61	16.43	15.15	19.40	16.91	23.10	-	-	-	-

[a] Weight percent KOH

Table 3.5-4

Comparison of Predicted and Experimental $\ln(\gamma_1 K_1^\circ)$ Values for LiOH Solutions

	0% LiOH		2% LiOH		4% LiOH		6% LiOH		8% LiOH		10% LiOH	
Solute	Expt.	Theo.	Expt.	Theo.	Expt.	Theo.	Expt.	Theo.	Expt.	Theo.	Expt.	Theo.
						25°C						
He	12.00	11.62	12.21	11.81	12.42	12.18	12.64	12.38	12.82	12.77	12.99	13.04
H_2	11.16	11.10	11.39	11.39	11.63	11.74	11.86	12.07	12.09	12.43	12.28	12.74
Ar	10.61	10.34	10.89	10.60	11.20	10.99	11.50	11.36	11.77	11.77	12.09	12.11
O_2	10.69	10.51	10.86	10.86	11.24	11.22	11.53	11.53	11.83	12.03	12.16	12.37
						60°C						
He	11.84	11.42	12.02	11.80	12.22	12.15	12.38	12.44	12.53	12.76	12.70	13.06
H_2	11.25	10.67	11.47	11.50	11.70	11.88	11.94	12.19	12.18	12.53	12.41	12.84
Ar	10.99	10.81	11.24	10.93	11.51	11.39	11.80	11.75	12.00	12.14	12.22	12.49
O_2	11.04	11.04	11.34	11.14	11.64	11.61	11.90	12.01	12.14	12.40	12.39	12.75

For the dissolution He, H_2, Ar, O_2 or CH_4 at 25°C the agreement between theory and experiment is very good for all KOH concentrations. The same is true for all the gases in LiOH solutions at 25°C. Values of $(\gamma_1 K_1^o)$ agree within a factor of about 2 or better even at the highest alkali concentrations. The agreement for these solutes at 80° for KOH is slightly poorer; however, it should be recalled that σ values for the ions were determined at 25°C. Discrepancies between theory and experiment are larger in the cases of sulfur hexafluoride and neopentane. Because of the large hard core diameter for these molecules, the calculated $(\gamma_1 K_1^o)$ are very sensitive to the value taken for σ of solute gas. Considerable uncertainty is involved in evaluating the Lennard-Jones σ parameter, and it is possible that the values used were in error. Similar considerations apply to the ϵ/k parameter for these molecules, although these have less effect on calculated $(\gamma_1 K_1^o)$ values. Because intermolecular interactions for sulfur hexafluoride and neopentane are both large and acentric, it also seems likely that the assumptions of $S_1^s = 0$ and of uniform molecular distribution around the solute are poor approximations in these cases.

The experimental and predicted temperature dependencies of $\ln(\gamma_1 K_1^o)$ are compared in Figure 3.5-1 for oxygen in 20% KOH solution. The differences seen here appear to arise from the fundamental assumption that a pair potential of the form given by Equation 3.2-6 may be used. In practice it is necessary to choose appropriate constant values for the hard core diameter of each species. However, the real particles do not possess hard cores, and the effective core diameter may be expected

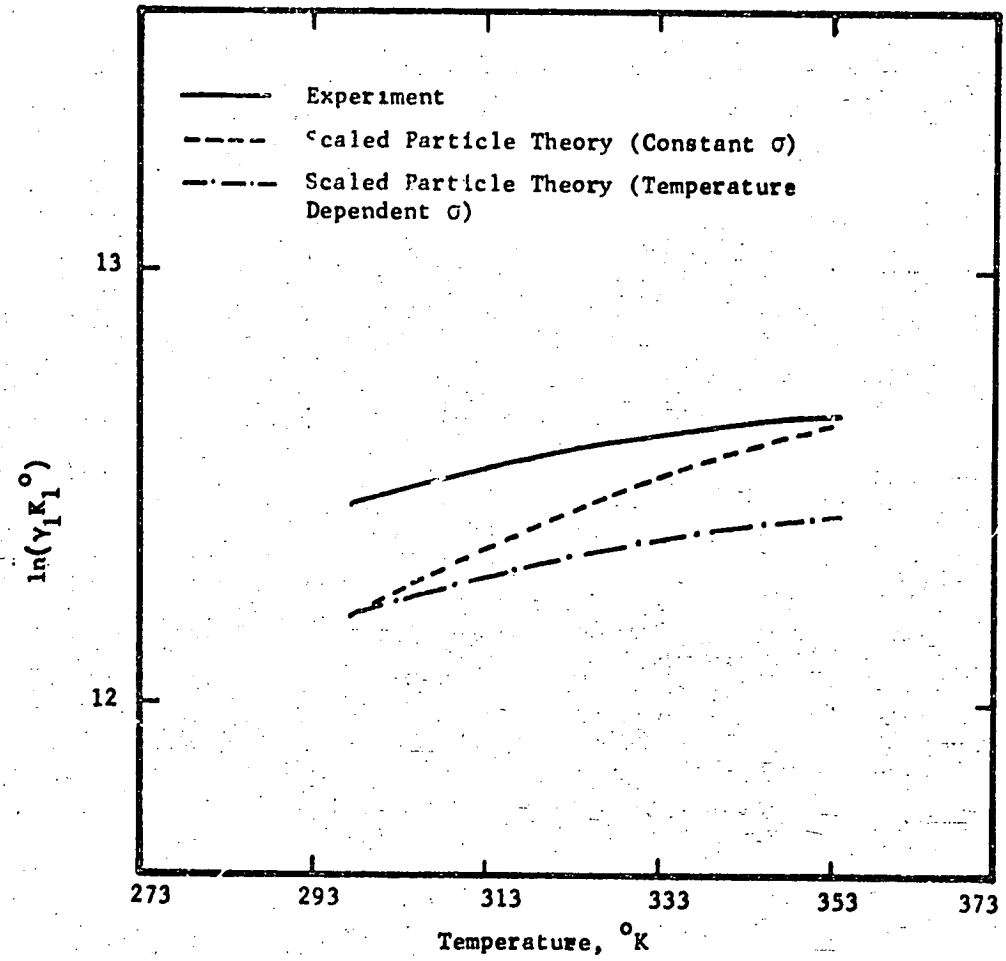

Figure 3.5-1 Effect of Temperature on Activity Coefficient of Oxygen in 20% KOH Solution

to decrease with rising temperature both because of the increase in average particle kinetic energy and averaging over molecular orientation. The temperature dependence of the diameter has been recently discussed in connection with applications of scaled particle theory to gas solubilities (30), and surface tension (9). The predicted temperature dependence for both of these properties is improved if σ is allowed to decrease with rising temperature. In determining σ for water, Pierotti (9) found that the best value was 2.74 Å at 70° as opposed to 2.75 Å at 25°C to illustrate the effect of a small decrease with temperature of the σ values for various species. Calculations were made for oxygen in 20% KOH using the following diameters (Å) at 25 and 80°C

Temperature, °C	σ_{O_2}, Å	σ_{H_2O}, Å	σ_{K^+}, Å	σ_{OH^-}, Å
25	3.46	2.75	2.60	3.30
80	3.45	2.74	2.59	3.28

Diameters at intermediate temperatures were obtained by linear interpolation. The resulting predicted temperature dependence of $\ln(\gamma_1 K_1^o)$ is shown in Figure 3.5-1, and is seen to be much improved.

It is instructive to compare the relative magnitudes of the various terms in Equation 3.2-15; Tables 3.5-5 and 3.5-6 show the contributions for oxygen at 25°C for both KOH and LiOH solutions. The free energy of cavity formation is seen to be the dominant term in Equation 3.2-15; moreover, it is affected by the addition of ions to a much larger extent than is the $\overline{g}_1^s$ term. The success of the scaled particle theory appears to stem in large part from this fact, for the calculation to obtain $\overline{g}_1^h$ may be performed with considerably greater confidence than that needed to obtain $\overline{g}_1^s$. The last term on the right hand

Table 3.5-5

Contributions to $\ln(\gamma_1 K_1^{\circ})$ for Oxygen in KOH Solutions at 25°C

		Nonpolar Interactions			Soft Contributions		
Wt % KOH	$\bar{g}_1^h/kT$	O_2-H_2O	O_2-K^+	O_2-OH^-	Electrostatic Term[a]	$\bar{g}_1^s/kT$	$\ln(kT\Sigma\rho_j)$
0	7.64	-3.73	-	-	-0.60	-4.33	7.20
10	8.79	-3.64	-0.20	-0.23	-0.59	-4.66	7.20
20	9.97	-3.51	-0.43	-0.48	-0.57	-4.99	7.24
30	11.38	-3.36	-0.72	-0.80	-0.54	-5.42	7.24
50	15.31	-2.84	-1.43	-1.57	-0.47	-6.31	7.21

[a] Arising from the water dipole-solute induced dipole interaction term of Equation

Table 3.5-6

Contribution to $\ln(\gamma_1 K_1^o)$ for Oxygen in LiOH Solutions at 25°C

		Soft Contributions					
		Nonpolar Interactions					
Wt % LiOH	$\bar{g}_1^h/kT$	O_2-H_2O	O_2-Li^+	O_2-OH^-	Electrostatic Term	$\bar{g}_1^s/kT$	$\ln(kT\Sigma\rho_j)$ j
0	7.64	-3.76	-	-	-.60	-4.36	7.20
2	8.04	-3.76	-0.02	-0.10	-.60	-4.48	7.23
4	8.56	-3.76	-0.04	-0.19	-.60	-4.59	7.25
6	9.06	-3.76	-0.06	-0.30	-.60	-4.62	7.27
8	9.58	-3.75	-0.09	-0.40	-.60	-4.84	7.29
10	10.04	-3.74	-0.11	-0.51	-.60	-4.96	7.31

side of Equation 3.2-15, which correspond to the free energy for the fixed solute molecules to wander within the solvent, is seen to be almost independent of electrolyte concentration. Of the various contribution to $\bar{g}_1^s$ the electrostatic interaction between solute and water molecules is a relatively small contribution, whereas that of the nonpolar interaction is large. Nonpolar interactions between solute and ions become appreciable at high alkali concentrations. Similar trends are observed for the other solutes and temperatures.

3.5.3 Comparison with Electrostatic Theories

Salting out coefficients can be predicted by the methods of Debye and McAulay, and of Conway with the help of Equations 3.2-2 and 3 2-4. To calculate β in order to use Debye and McAulay theory, the following equation is used

$$\bar{\beta} = \frac{\bar{V}_1}{No} - \frac{6\pi\alpha_1}{Do} \qquad (3.5\text{-}5)$$

where $\bar{V}_1$ is the partial molal value of solute. Equation 3.2-4 was used to calculate salting out coefficient for the system using the following values for the ionic parameters n and r_n

Ion	r_n $\mathring{A}$	n
K^+	2.72	4.1
Li^+	3.28	7.1
OH^-	3.00	5.3

The hydration number for the OH^- ion was not available, and was calculated from the experimental partial molal entropy of hydration using the method proposed by Ulich(31). Predicted values together with experimental values have been plotted in Figures 3.5-2 through 3.5-6.

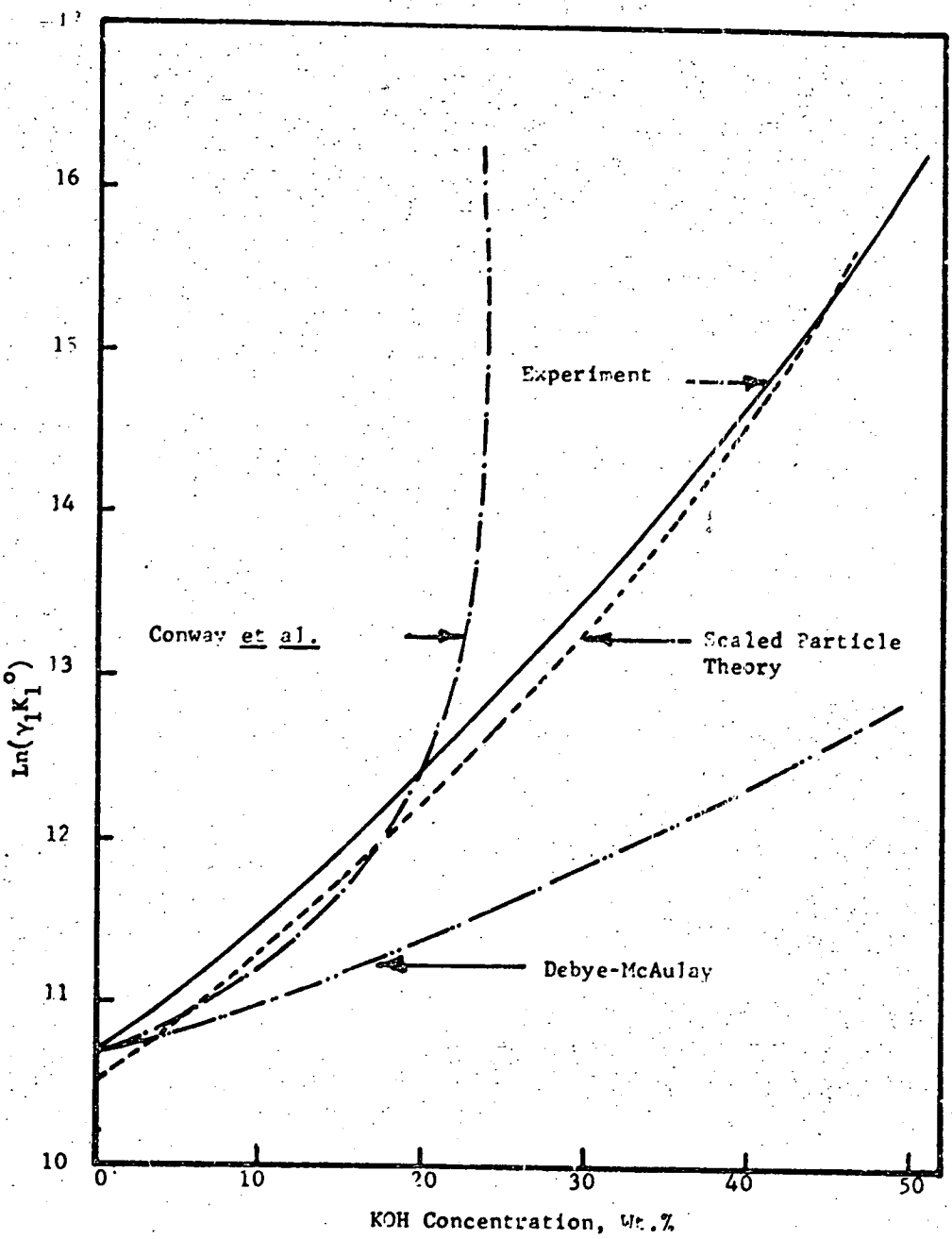

Figure 3.5-2. Theoretical and Experimental Activity Coefficients of Oxygen at 25°C.

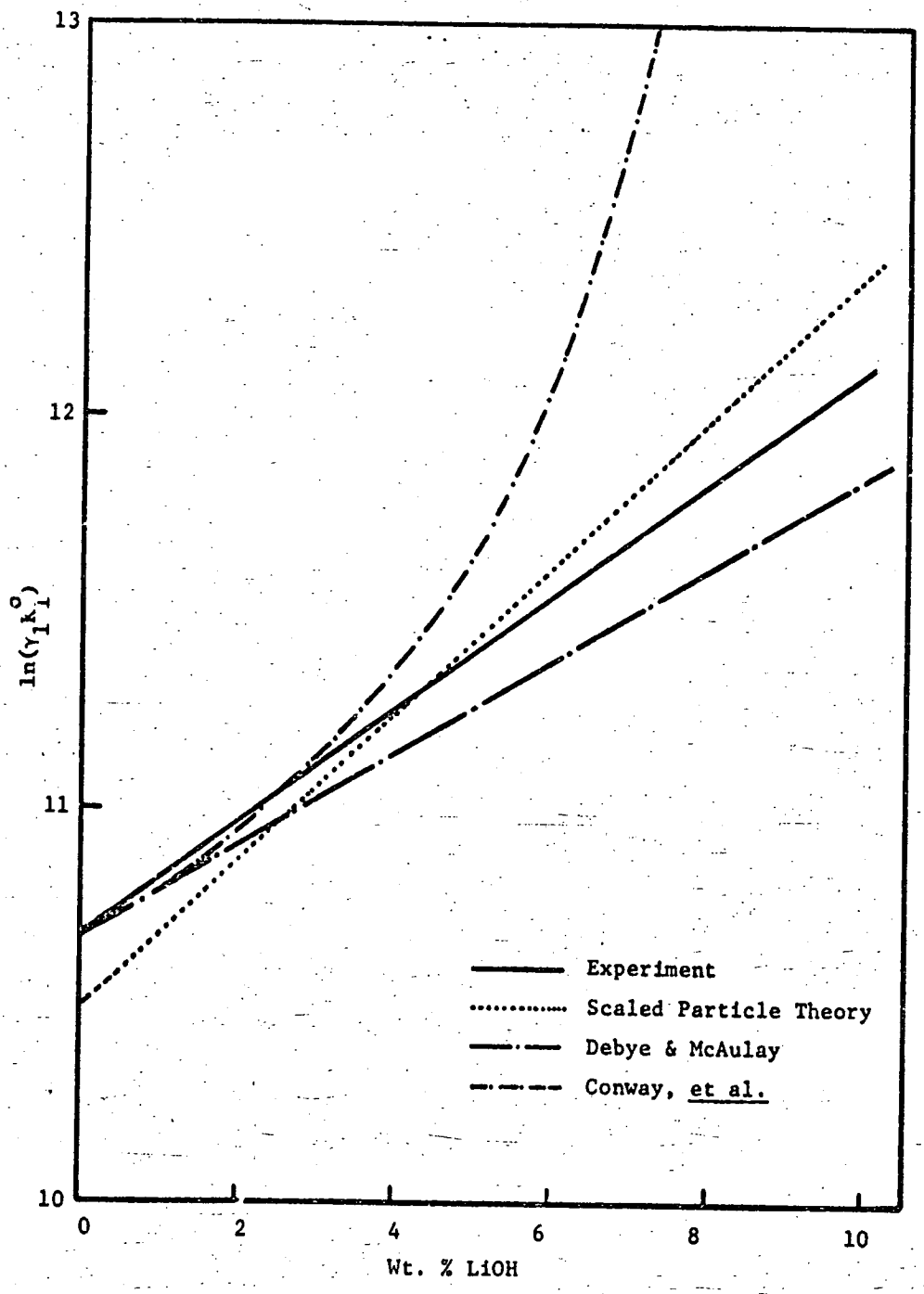

Figure 3.5-3Theoretical and Experimental Activity Coefficients of Oxygen at 25°C.

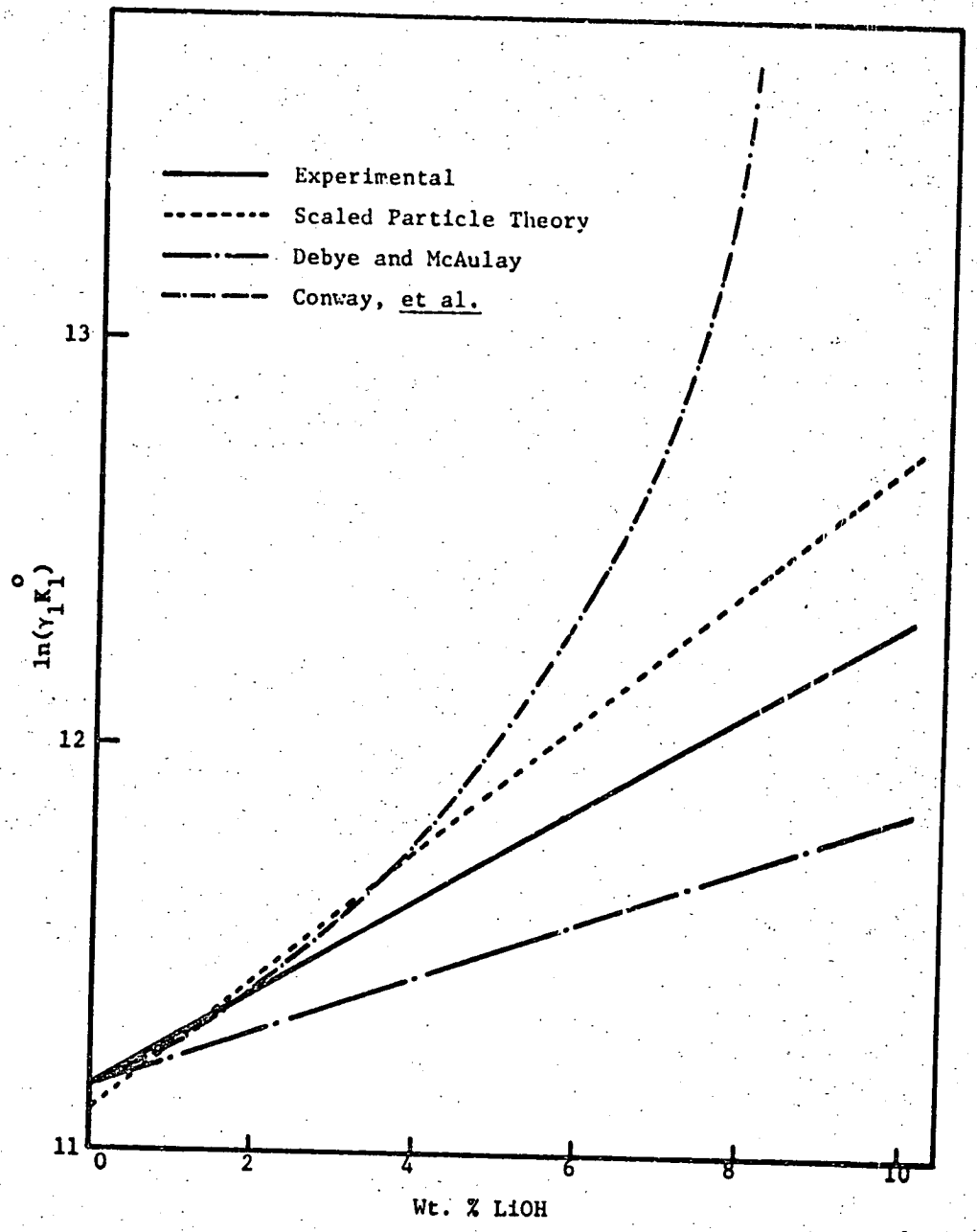

Figure 3.5-4Theoretical and Experimental Activity Coefficients of Hydrogen at 25°C.

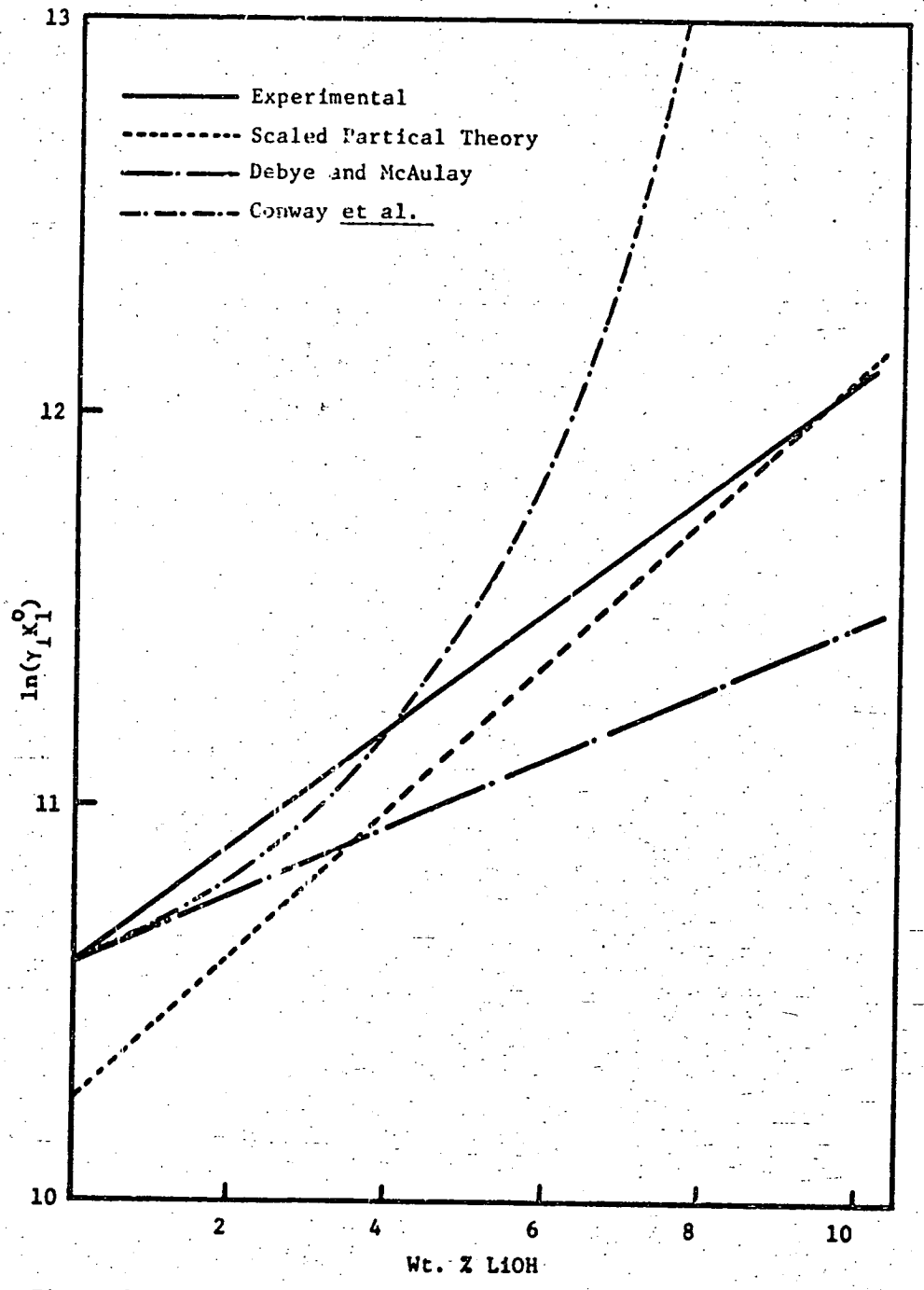

Figure 3.5-5. Theoretical and Experimental Activity Coefficients of Argon at 25°C.

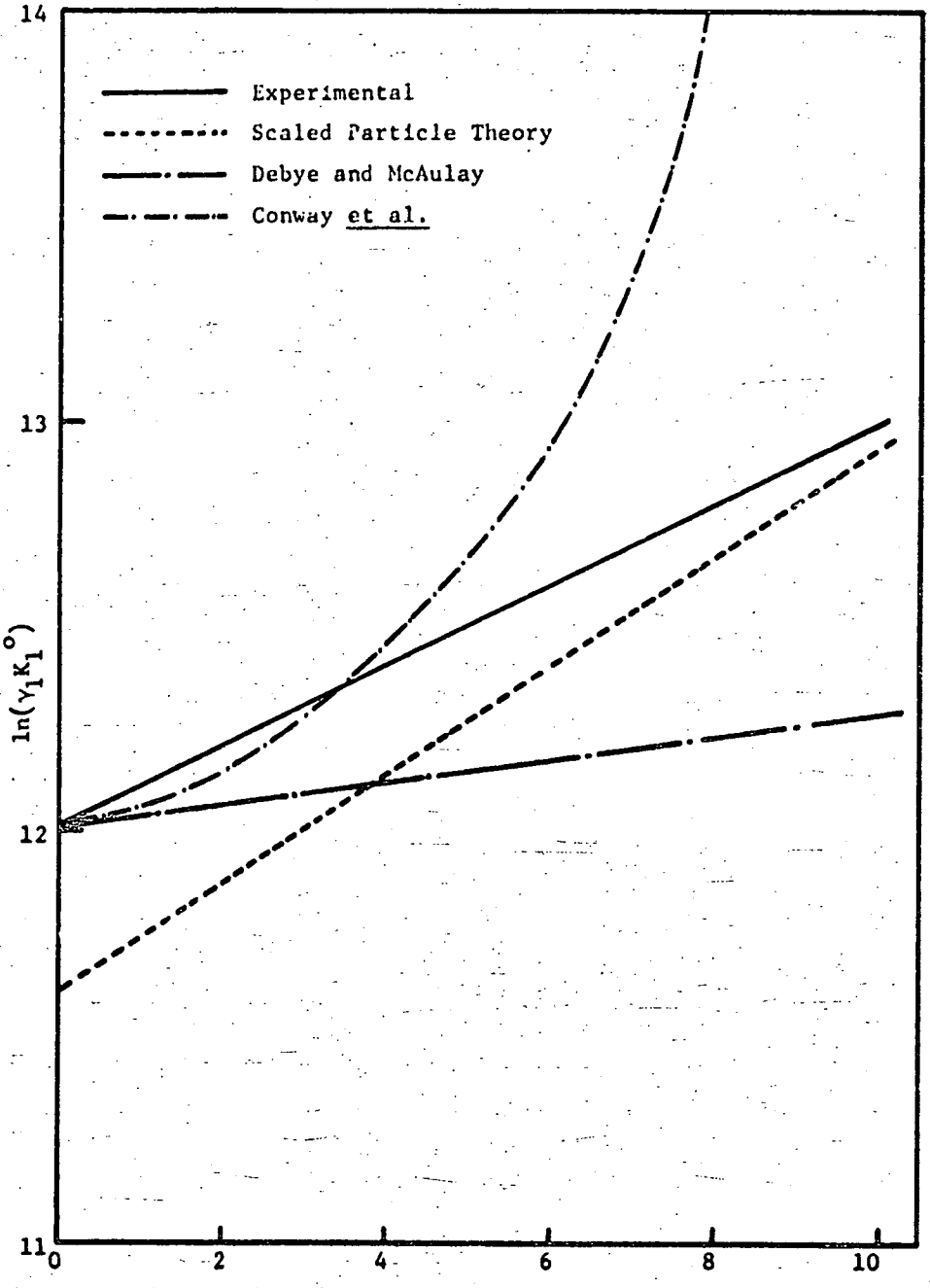

Figure 3.5-6. Theoretical and Experimental Activity Coefficients of Helium at 25°C.

It is apparent that neither of the electrostatic theories predict the observed salting-out coefficient satisfactorily. The Debye-McAulay theory gives results much below experiment for both LiOH as well as KOH solutions. While the theory of Conway et al. gives better results at low electrolyte concentrations, it predicts negative solubilities for higher KOH and LiOH concentrations and is thus invalid in this region. The failure of the electrostatic theories to predict correctly either the effect of solute species or electrolyte concentration on the activity coefficient can be attributed to the assumptions made in these theories. It seems probable that it is oversimplification to treat the solvent as a continuous dielectric medium, and that observed salt effects can be adequately accounted for only if the solute-solvent molecular interactions are explicitly introduced into the theory.

The scaled particle theory has the advantage that the expression for solute chemical potential is derived from the equation of statistical mechanics by a series of well-defined approximation. Salting-out effects are accounted for within the framework of a more general theory that describes the solubility of gases in organic solvents and water (3), and it provides a simple model of the solution process. The theory explains the effect of solute species and electrolyte concentration of salting-out in electrolyte solutions, where salt effects are large. In contrast to the electrostatic theories, it is possible to calculate the solubility of the gas in pure water. Furthermore, the molecular parameters needed are more readily obtained than those involved in electrostatic theories. Unlike many of the electrostatic theories, the scaled particle theory makes no appeal to assumptions

concerning solvent structure, ionic hydration, etc. In addition, the ionic charge has little direct influence on salting-out. The most important effect of such charges appears to be in determining the density of the electrolyte solution.

3.5.4 Calculation of Thermodynamic Properties from Solubilities

The activity coefficients in Table 3.4-3 and 3.4-5 may be used to calculate partial molal enthalpies, entropies and energies of different solution with the help of Equations 3.1-12, 13 and 14. Tables 3.5-7, 8 and 9 show the calculated values of partial molal enthalpies, entropies and energies, respectively, for KOH solutions. Typical plots of heat of solution, entropy of solution, and energy of solution of oxygen in KOH have been shown in Figures 3.5-7, 3.5-8, and 3.5-9, respectively. Similar behavior is observed for other gases. It is seen that the heat of solution is negative at low KOH concentrations and that it becomes less negative as the KOH concentration increases. Also, at lower temperatures the heat of solution is more negative. The same trend is followed by entropies and energies of solutions, too. As seen from Tables 3.5-7, 8 and 9, for a given temperature on KOH concentration, $\Delta\bar{H}_1$, $\Delta\bar{S}_1$ and $\Delta\bar{E}_1$ varies with the solute gas. It is reasonable to expect that this variation of partial molal heats is due to physical characteristics of the solute gas, or at least to its effect on the properties of the solvent. To this end $\Delta\bar{H}_1$, $\Delta\bar{S}_1$ and $\Delta\bar{E}_1$ were plotted against ϵ/k in Figures 5.3-7, 8 and 9. All the partial quantities seem to correlate well with this parameter. It is seen that all these quantities decrease as ϵ/k increases for lower concentrations of KOH but that each exhibits a minimum at higher concentration.

Table 3.5-7

Partial Molal Heats of Solution, $\overline{\Delta H}_1$, cal(g.mole)$^{-1}$

Solute Gas	25°C					40°C				
	0%KOH	20%KOH	30%KOH	40%KOH	50%KOH	0%KOH	20%KOH	30%KOH	40%KOH	50%KOH
O_2	-2820	-1100	-	-	-160	-2080	- 812	-	-	-160
H_2	- 910	- 830	-	-	-700	- 355	- 409	-	-	-490
He	- 720	- 640	- 500	-	-	+ 280	+ 194	+150	-	-
Ar	-2870	-1390	-	- 796	-	-2200	- 992	-	- 440	-
SF_6	-5160	- 540	+ 976	-	-	-3500	- 560	+976	-	-
CH_4	-3630	-1100	-	+1170	-	-2460	- 440	-	+1170	-
neo-C_5H_{12}	-5780	-3110	-1140	-	-	-4430	-2110	-405	-	-
	60°C					80°C				
O_2	-1680	- 635	-	-	-160	- 544	- 446	-	-	-160
H_2	0	- 100	-	-	-250	+ 90	+ 28	-	-	- 80
He	+ 800	+ 693	+ 640	-	-	+1000	+ 934	+ 910	-	-
	-1465	- 465	-	- 130	-	- 760	- 204	-	- 20	-
SF_6	-2100	- 120	+ 976	-	-	- 945	+ 226	+ 976	-	-
CH_4	-1518	+ 100	-	+1170	-	- 860	+ 380	-	+1170	-
neo-C_5H_{12}	-2380	- 739	+ 354	-	-	-1054	+ 4	+1255	-	-

Table 3.5-8

Partial Molal Energies of Solution, $\overline{\Delta E}_1$, cal(g.mole)$^{-1}$

Solute Gas	25°C					40°C				
	0%KOH	20%KOH	30%KOH	40%KOH	50%KOH	0%KOH	20%KOH	30%KOH	40%KOH	50%KOH
O_2	-2229	- 509	-	-	+751	-1458	- 190	-	-	+782
H_2	- 319	- 239	-	-	-109	+ 267	+ 213	-	-	+132
He	- 129	+ 17	+ 91	-	-	+ 902	815	+ 772	-	-
Ar	-2279	- 799	-	- 205	-	-1639	- 378	-	+ 302	-
SF_6	-4569	- 349	+1567	-	-	-2878	+ 62	+1598	-	-
CH_4	-3039	- 509	-	+1761	-	-1838	+ 182	-	+1792	-
neo-C_5H_{12}	-5189	-2519	- 551	-	-	-3808	-1488	+ 216	-	-

	60°C					80°C				
O_2	- 579	+ 26	-	-	+821	- 188	+ 256	-	-	+920
H_2	+ 661	+ 561	-	-	+411	+ 792	+ 724	-	-	+622
He	+1461	+1354	1301	-	-	+1702	+1642	1612	-	-
Ar	- 804	+ 111	-	+ 621	-	+ 40	+ 520	-	+ 662	-
SF_6	-1449	+ 441	+1637	-	-	- 243	+ 922	+1678	-	-
CH_4	- 857	+ 771	-	+1831	-	- 158	+1082	-	+1872	-
neo-C_5H_{12}	-1719	- 78	+1015	-	-	- 352	+ 706	+1957	-	-

Table 3.5-9

Partial Molal Entropies of Solution, $\overline{\Delta S}_1$, cal(g.mole°K)$^{-1}$

Solute Gas	25°C					40°C				
	0%KOH	20%KOH	30%KOH	40%KOH	50%KOH	0%KOH	20%KOH	30%KOH	40%KOH	50%KOH
O_2	- 9.45	- 3.69	-	-	+ 0.54	- 6.65	- 2.59	-	-	+ 0.51
H_2	- 3.05	- 2.77	-	-	- 2.35	- 1.13	- 1.22	-	-	- 1.56
He	- 2.42	- 1.93	- 168	-	-	+ 0.89	+ 0.61	+ 0.48	-	-
Ar	- 9.64	- 4.67	-	- 2.67	-	- 7.22	- 3.19	-	- 0.76	-
SF_6	-17.31	- 3.15	+ 3.28	-	-	-11.18	- 1.79	3.12	-	-
CH_4	-12.21	- 3.69	-	+ 3.92	-	- 7.85	- 1.40	-	+ 3.74	-
neo-C_5H_{12}	-19.4	-10.42	- 3.84	-	-	-14.15	- 6.74	- 1.29	-	-

	60°C					80°C				
O_2	- 3.73	- 1.90	-	-	+ 0.49	- 1.45	- 1.26	-	-	+ 0.46
H_2	0	+ 0.30	-	-	- 0.75	+ 0.25	-	+ 1.02	-	0
He	+ 2.4	+ 2.08	+ 1.92	-	-	+ 2.84	+ 2.67	+ 2.58	-	-
Ar	- 4.40	- 1.50	-	- 0.12	-	- 2.05	- 0.45	-	0	-
SF_6	- 6.33	- 0.36	+ 2.93	-	-	- 2.68	+ 0.64	+ 2.77	-	-
CH_4	- 4.56	+ 0.30	-	+ 3.51	-	- 2.44	+ 1.08	-	+ 3.32	-
neo-C_5H_{12}	- 7.15	- 2.22	+ 1.05	-	-	- 2.99	+ 0.01	+ 3.56	-	-

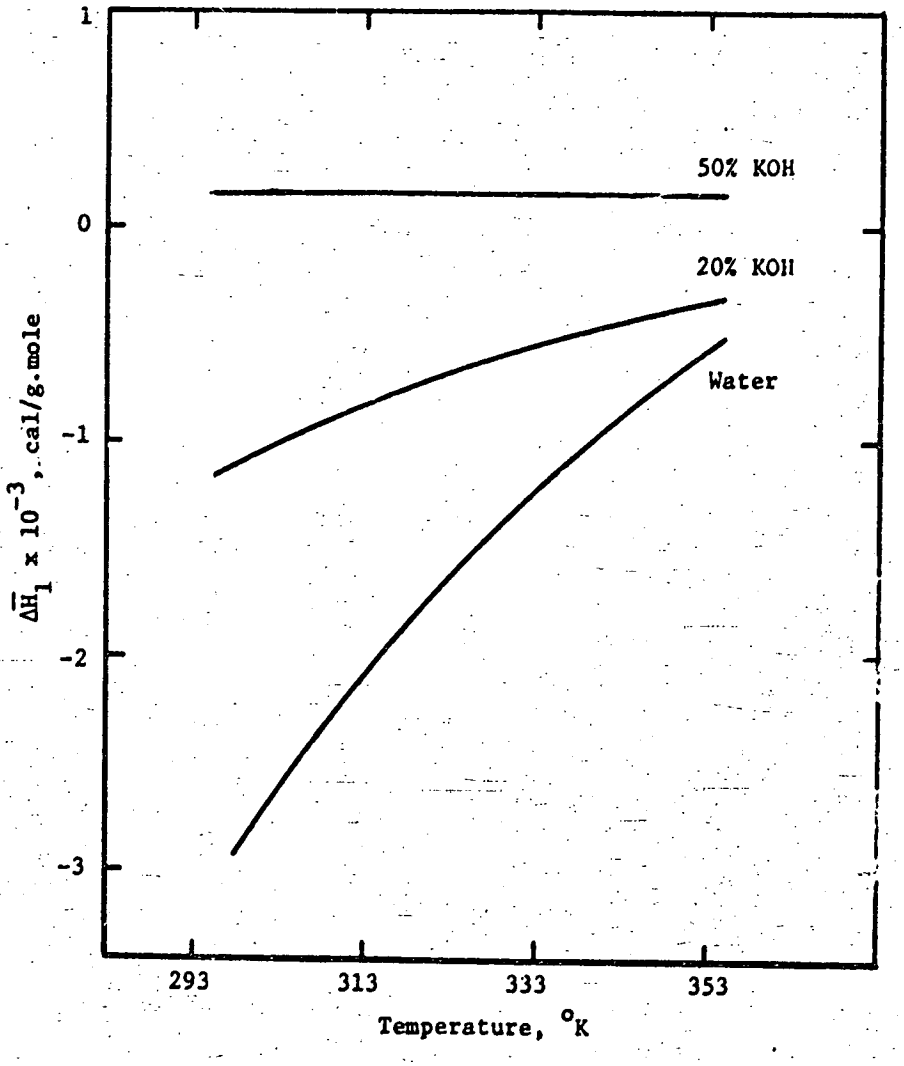

Figure 3.5-7. Partial Molal Heats of Solution for Oxygen.

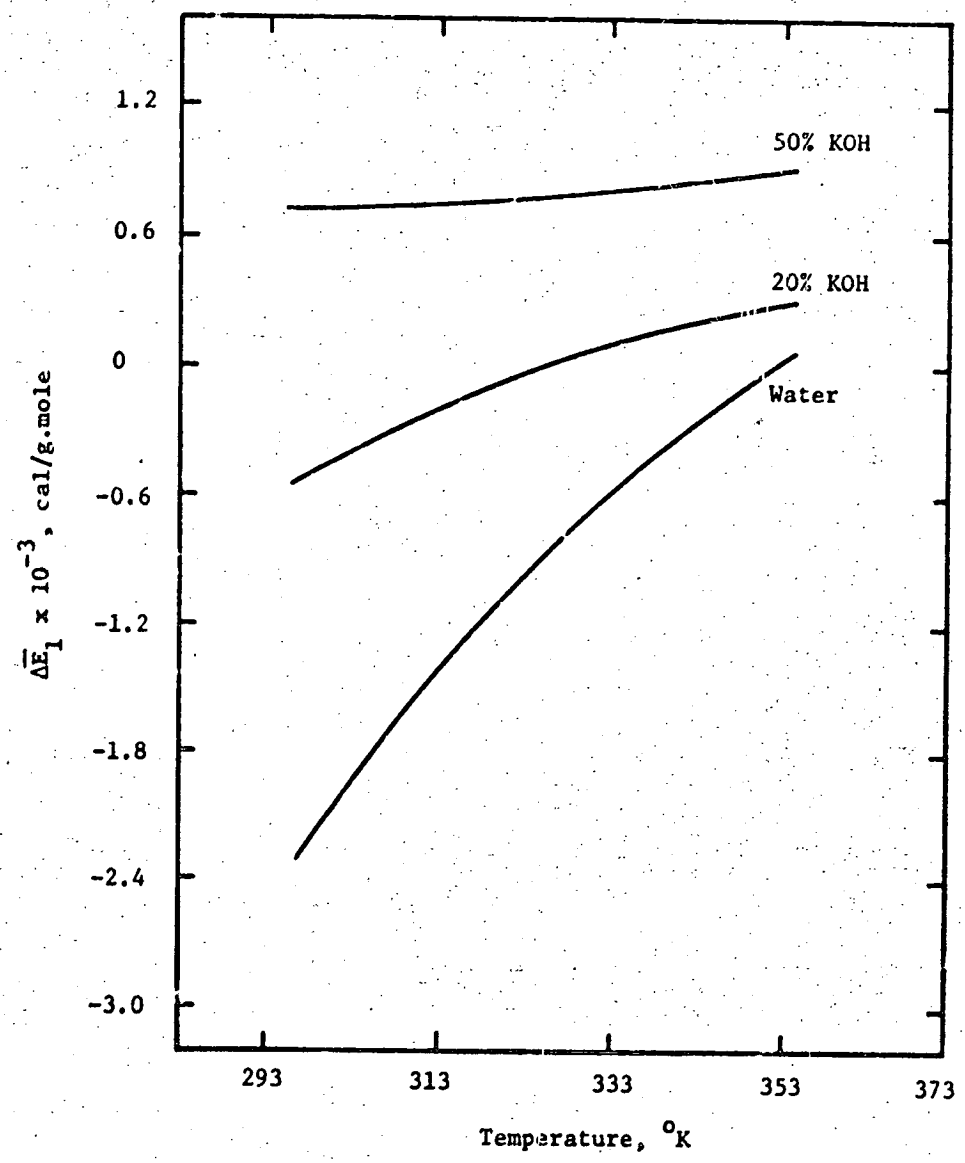

Figure 3.5-8. Partial Molal Energies of Solution for Oxygen.

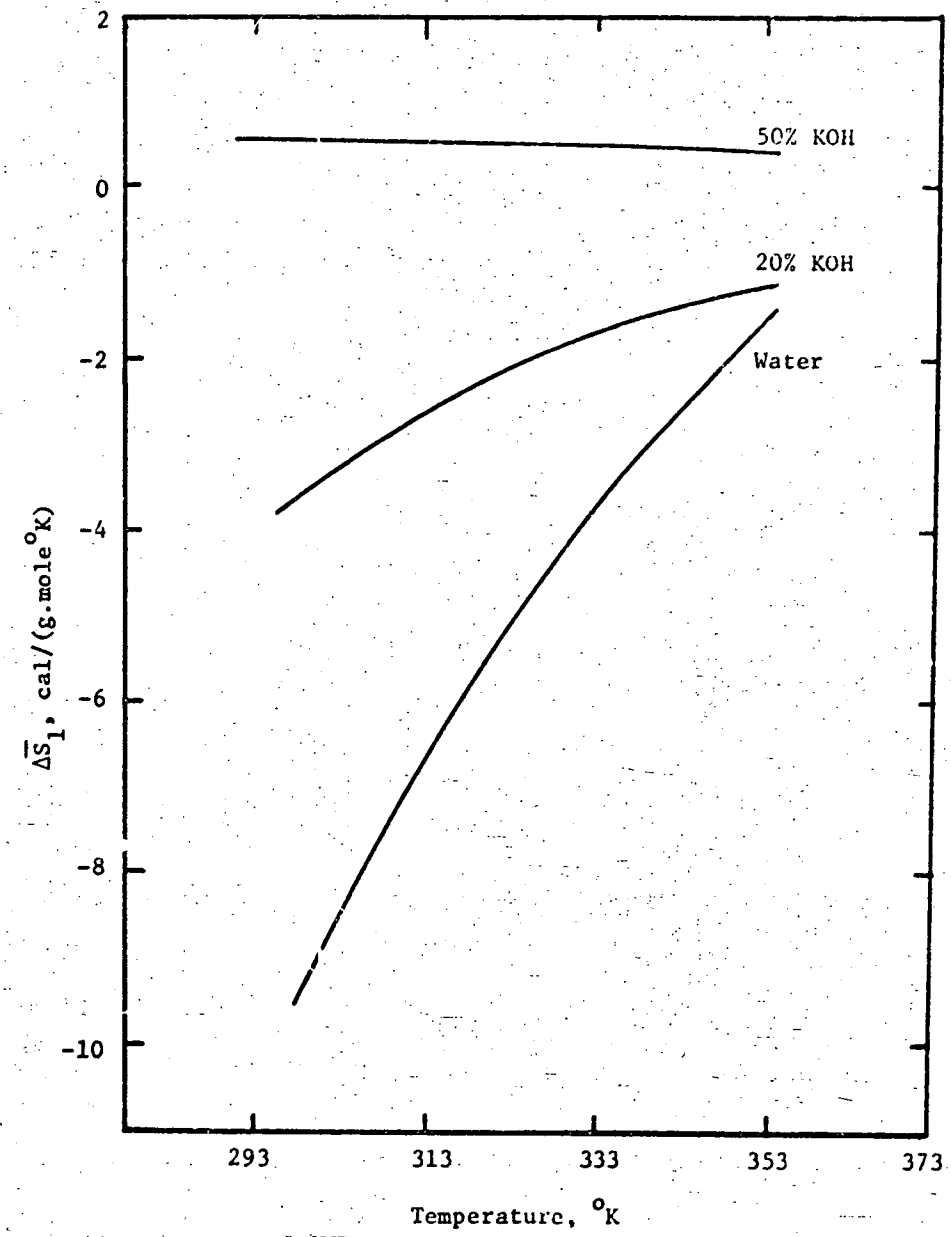

Figure 3.5-9. Partial Molal Entropies of Solution for Oxygen.

ΔH_1, ΔS_1 and ΔE_1 can be calculated for LiOH also and they are believed to behave the same way.

4. Diffusivities of Oxygen and Hydrogen in KOH and LiOH Solutions

A knowledge of diffusion coefficients is very important in many mass transfer processes; unfortunately the existing data on the diffusion coefficients of gases in electrolytic solutions are very scarce. In this work, diffusion coefficients of oxygen and hydrogen in potassium hydroxide, and of oxygen in lithium hydroxide at 25°C, were measured.

Owing to the inadequacy of the theories of liquids the theory of diffusion coefficients of gases in liquids is not well developed. A comparison of the data obtained from this work and the existing theories was made in order to test their validity and to evaluate their usefulness for correlation of experimental data.

4.1 Theories of Diffusion in Liquids

Many theories and empirical correlations have been proposed for diffusion coefficients in liquid systems. Himmelblau (32), and Kamal (33) have given very complete reviews of the existing theories. In the following paragraphs a discussion of irreversible thermodynamics and of the theories of possible relevance to the present work is given.

In the case of diffusion of these gases in electrolytes the solute gas is present in essentially infinite dilution, and the diffusion process is effectively a binary one; attention is therefore given to two component systems.

4.1.1 Classical Irreversible Thermodynamics

Irreversible thermodynamics is useful in identifying the forces and the fluxes in non-equilibrium processes, although it does not allow us to predict these fluxes and the related coefficients. The development is based upon the assumption of local equilibrium, i.e., it is

assumed that equilibrium thermodynamics may be applied to macroscopically small elements of the system which are very close to equilibrium.

Thus, in an open system, an entropy balance gives

$$\frac{ds}{dt} = \frac{(ds)_{ext}}{dt} + \frac{(ds)_{int}}{dt} \qquad (4.1\text{-}1)$$

where $(ds)_{int}$ is the generation of entropy due to the non-equilibrium process. If we let

$$\frac{(ds)_{int}}{dt} = \sigma \qquad (4.1\text{-}2)$$

then it can be shown (106) that the rate of entropy production, σ, is related to the forces producing a flux by an equation of the form

$$T\sigma = \sum_{\alpha} J_{\alpha} Y_{\alpha} \qquad (4.1\text{-}3)$$

where J_{α} = isothermal fluxes

Y_{α} = isothermal forces conjugate to J_{α}.

thus, for an isothermal, isoberic system

$$T\sigma = 1 \sum_{i} \underline{J}_i \cdot \nabla\mu_i \qquad (4.1\text{-}4)$$

where μ_i is the partial molar free energy of component i

J_i is the molar flux with referent to the mass average velocity.

Assuming that J_{α} is a function of the force $\nabla\mu_{\beta}$, where β represents all components, and expanding about the equilibrium condition, which for the case when chemical potential is the only form, gives

$$\underline{J}_{\alpha} = \underline{J}_{\alpha}(0) - \sum_{\beta} L_{\alpha\beta} \nabla\mu_{\beta} + \cdots\cdots$$

The first term is obviously zero, and taking the linear approximation, we have

$$\underline{J}_\alpha = \sum_\beta L_{\alpha\beta} \nabla\mu_\beta \qquad (4.1\text{-}5)$$

$L_{\alpha\beta}$ are called the Onsager coefficients, and according to the Onsager Reciprocal Relation

$$L_{\alpha\beta} = L_{\beta\alpha} \qquad (4.1\text{-}6)$$

The mass-average velocity of the fluid, $\underline{v}$, is defined as

$$\underline{v} = \frac{\sum_i \rho_i \underline{v}_i}{\sum_i \rho_i} \qquad (4.1\text{-}7)$$

where ρ_i = density of species i

$\underline{v}_i$ = velocity of species i

While the molar flux with reference to this mass-average velocity is

$$J_i = C_i(\underline{v}_i - v)$$

C_i = concentration in mole/volume.

The chemical potential gradient in a system at constant temperature and pressure can be written

$$\nabla\mu_j = \sum_{k=1}^{r-1} \frac{\partial\mu_j}{\partial C_j} \nabla C_k \qquad (4.1\text{-}9)$$

so that for a binary system Equations 4.1-5 and 4.1-9 give for the flux of component 1

$$\underline{J}_1 = - \left[L_{11} \frac{\partial\mu_1}{\partial C_1} + L_{12} \frac{\partial\mu_2}{\partial C_1} \right] \nabla C_1 \qquad (4.1\text{-}10)$$

Comparing with Fick's first law

$$\underline{J}_1 = - D_1 \nabla C_1 \qquad (4.1\text{-}11)$$

gives the diffusion coefficient of 1 with reference to the mass-average velocity.

$$D_1 = L_{11} \frac{\partial \mu_1}{\partial c_1} + L_{12} \frac{\partial \mu_2}{\partial c_1} \qquad (4.1\text{-}12)$$

A similar expression is obtained for D_2. It may be shown that $L_{11} = - L_{12}$, and the two diffusion coefficients are related by

$$D_1 \bar{V}_2 = D_2 \bar{V}_1 \qquad (4.1\text{-}13)$$

where $\bar{V}_1$ and $\bar{V}_2$ are partial molar volume.

A similar development can be made for the flux referred to the volume-average velocity.

The volume-average velocity is defined as

$$\underline{v}^* = \sum_j C_j \underline{v}_j \bar{V}_j \qquad (4.1\text{-}14)$$

while the center of volume flux is

$$\underline{J}_i = C_i (\underline{v}_i - \underline{v}^*) = \underline{J}_i - C_i \sum_j \bar{V}_j J_j \qquad (4.1\text{-}15)$$

For a binary system Fick's law is

$$\underline{J}_1 = - D_1^{\circ} \nabla C_1$$
$$\underline{J}_2 = - D_2^{\circ} \nabla C_2 \qquad (4.1\text{-}16)$$

where D_1° is the diffusion coefficient of component 1 with reference to the volume-average velocity. Using Equation 4.1-15 it can be shown that these two diffusion coefficients are related by

$$D_1^{\circ} = C \bar{V}_2 D_1 \qquad (4.1\text{-}17)$$

$$D_2^{\circ} = C \bar{V}_1 D_2 \qquad (4.1\text{-}18)$$

Thus $D_1^{\circ} = D_2^{\circ}$ can be inferred from the above equations.

Experimental diffusion coefficients are usually reported for the volume frame of reference.

4.1.2 Statistical Mechanical Theories

Statistical mechanics provides the most fundamental approach to the formulation of transport properties, and thus to the diffusion coefficients of gases in liquids. Such treatments describe all transport processes, and do not introduce parameters which have no clear meaning. At the present stage, wide application of these theories to predicting diffusion coefficients cannot be made owing to the complexity of the theory and to mathematical difficulties in obtaining solutions. Although these theories represent the most rigorous approaches that have been proposed, there are still some parameters which must be obtained experimentally.

Several theories based on statistical mechanical approaches are discussed briefly in the following paragraphs with a view to assessing their advantages and limitations for predicting the diffusivity of non-polar gases in strong alkali solutions.

The Time Correlation Theory. This theory is derived from a consideration of the time correlation between the movement of different species, and gives for the Onsager coefficient L_{12} of Equation 4.1-12

$$L_{12} = - L_{11} = \frac{1}{3kTV} \int_0^\infty [J_1(0)J_2(t)]\, dt \qquad (4.1\text{-}19)$$

where $J_i = \sum_{k=1}^{N_i} m_i \underline{v}_{ik}$

$\underline{v}_{ik}$ = velocity of molecule of species i.

An expression for the binary diffusion coefficient can be obtained from Equations 4.1-14 and 4.2-1.

This expression requires the time correlation function $[J_1(0)J_2(t)]$ and at present the theory is unable to evaluate this.

The time correlation function may be estimated for a finite number of particles by the method of molecular dynamics using a digital computer. Thus, at the present time, this theory provides final equations, but cannot be used to predict diffusion coefficients

Space distribution function theory. Bearman (3-) developed a statistical mechanical theory of transport processes in solutions based on the work of Kirkwood (35). His work made use of the space distribution function of the molecules. In his development, he defined a frictional force $\bar{F}_1^{(1,1)^*}$ for a ν-component, isothermal and isobaric system as

$$\bar{F}_1^{(1,1)^*} = \bar{F}_1^{(1)^*} - \bar{F}_1^{(1,0)^*} \qquad (4.1\text{-}20)$$

where $\bar{F}^{(1,0)^*}$ is a force which exists even at equilibrium.

$F_1^{(1,1)^*}$ can be defined in terms of distribution function as

$$F_1^{(1,1)^*} = \frac{1}{2} \sum_{\beta=1}^{\nu} NC_\beta(\underline{r}/r) \frac{dV_{1\beta}}{dr} \left(g_{1\beta}^{(2,1)} - g_{\beta 1}^{(2,1)} \right) d^3r \qquad (4.1\text{-}21)$$

where $\hat{V}_1$ = smoothed potential of intermolecular forces between molecules 1 and β

$g_{1\beta}$ = non-equilibrium perturbation

$= g_{1\beta}^{(2)} - g_{1\beta}^{(2,0)}$

$g_{1\beta}^{(2)}$ = pair correlation function (which does not have spherical symmetry)

$g_{1\beta}^{(2,0)}$ = radial distribution function and is related to equilibrium thermodynamic properties.

If we expand $g_{1\beta}^{(2)}$ in a series of spherical harmonics, only the first harmonic will contribute to the integral, and the resultant

expression is

$$\bar{F}_1^{(1,1)^*} = -\sum_{\beta=1}^{\beta} \hat{N} C_\beta \zeta_{1\beta}(u_1 - u_\beta) = \hat{N} \frac{d\mu_1}{dx} \qquad (4.1\text{-}22)$$

where the friction coefficient $\zeta_{1\beta}$ is defined as

$$\zeta_{1\beta} = \frac{1}{6} \int g_{1\beta}^{(2,0)} \frac{\partial V_{1\beta}}{dr} \left\{ \psi_{1\beta}^1 + \psi_{\beta 1}^1 \right\} d^3r \qquad (4.1\text{-}23)$$

The reciprocal relationship $\zeta_{1\beta} = \zeta_{\beta 1}$ is a consequence of the definition of the smoothed potential and the symmetry of the radial distribution function.

For the special case of a binary system with the volume average velocity as reference, Equation 4.2-5 can be expressed as

$$D^\circ = \frac{\bar{V}_2 kT}{\hat{N}\zeta_{12}} \left[1 + \left(\frac{\partial \ln f_1}{\partial \ln C_1} \right)_{T,p} \right] \qquad (4.1\text{-}24)$$

after Equations 4.1-9 and 4.1-14 have been introduced.

Since D° is a function of ζ_{12}, it is also dependent on $g_{12}^{(2,1)}$ by Equation 4.2-5.

If in Equation 4.1-24, component 1 is present in infinite dilution, V_2 becomes the molar volume of pure solvent, and ζ_{12} is represented by ζ_{12}^∞.

Also $\left(\frac{\partial \ln a_1}{\partial \ln C_1} \right)_{T,p} = 1$ [from Henry's Law]

and Equation 4.2-5 will become

$$D_1^{\infty\text{dilution}} = \frac{\bar{V}_2 kT}{\hat{N}\zeta_{12}} \qquad (4.1\text{-}25)$$

4.1.3 Modified Activation Theories of Diffusion

The Eyring theory (36,37) of absolute reaction rates has been applied to the prediction of diffusivities and viscosities with some success. According to this theory, the fluidity of a liquid and the binary diffusion coefficient at infinite dilution may be expressed by

$$\phi = \frac{1}{\mu} = k_\phi \lambda^2 \exp\left(-\frac{\Delta G^*_\phi}{RT}\right) = \frac{k_\phi \lambda^2 h}{(2\pi mkT)^{1/2} V_f^{1/3}} \exp(-\epsilon_\phi/kT) \qquad (4.1\text{-}26)$$

$$D^o = k_d \lambda^2 \exp(-\Delta G^*_d/RT) = \frac{k_d \lambda^2 h}{(2\pi mkT)^{1/2} V_f^{1/3}} \exp(-\epsilon_d/kT) \qquad (4.1\text{-}27)$$

Since strong electrolyte solutions are highly structured (38), the model on which this theory is based is very suitable. Thus, Podolsky (39) has modified Equation 4.1-26 to predict the fluidity of an electrolyte solution, and Ratcliff (40) derived a corresponding equation for the diffusion coefficients of gases in electrolytes. In all these treatments, the presence of ions is assumed to perturb the free energy of activation for diffusion, but its effect on the lattice spacing λ is assumed to be negligible. If δ_1 is the free energy perturbation due to the presence of an ion i, the perturbed free energy of activation will be $(\Delta G^*_o + \delta_i)$. If the distribution of ions in the neighborhood of the solute molecule is assumed to be the same as in the bulk solution, the average free energy of activation for the diffusion of a sparingly soluble gas is

$$\langle G^*_d \rangle = G^*_o + \frac{nx(\nu_1\delta_1 + \nu_2\delta_2)}{(1-x) + (\nu_1+\nu_2)x} \qquad (4.1\text{-}28)$$

where n = number of solvent molecules surrounding an ion

$$\nu_i = \frac{\text{number of g-ions of species i}}{\text{g-mole of electrolyte}}$$

x = mole fraction of electrolyte

Substituting Equation 4.1-28 into Equation 4.1-27, we have

$$\frac{D^o}{D_o} = \exp \frac{-nx(\nu_1\delta_1 + \nu_2\delta_2)}{RT[(1-x) + (\nu_1+\nu_2)x]} \qquad (4.1\text{-}29)$$

This equation predicts a linear relation between $\ln D^o/D_o$ and the quantity $\frac{nx}{(1-x) + (\nu_1+\nu_2)x}$ which is called the species fraction.

This linear relationship was shown to hold for a wide variety of gases in electrolytes by Ratcliff (40). Gubbins and Bhatia (41), using a similar development, arrived at and proved the validity of Equation 4.1-29 for mutual diffusion of potassium hydroxide solution.

4.1.4 Semiempirical and Empirical Correlations

The theories proposed for the prediction of diffusion coefficients are either inadequate or too involved mathematically for engineering calculations. Thus, for the prediction of diffusion coefficients for engineering use, a large number of empirical or semiempirical correlation have been proposed and are widely used in engineering design. A few of them will be discussed in brief here.

Applying the kinetic theory of gases to liquids, Arnold (42) developed an equation for liquid diffusion as

$$D^o = \frac{0.01 \left(\frac{1}{M_1} + \frac{1}{M_2}\right)^{1/2}}{\left(V_1^{1/3}+V_2^{1/3}\right)\left(A_1A_2V_2\mu_2^{1/2}\right)} [1 + b(T-273)] \qquad (4.1\text{-}30)$$

In Equation 4.1-30 subscript 1 refers to the solute and subscript 2 to the solvent. A_1 and A_2 are abnormality factors to account for the molecular association. T is the temperature of the system in degrees Kelvin.

This equation indicates that the diffusion coefficient is proportional to the temperature which is contrary to the usual view that the relation should be exponential. Applying this equation to the diffusion of carbon dioxide in a number of organic liquids, Davies (43) showed that of all the empirical equations tested, his data fitted Equation 4.1-30 best. In contrast to all the predictions that $D^{\circ}\mu_2$ should be a constant at constant temperature, Equation 4.1-30 predicts a constancy of $D^{\circ}\mu^{1/2}$, and this was verified by Davis in his work.

The first correlation based on the hydrodynamic theory was proposed simultaneously by Einstein (44) and Sutherland (45). Their correlation is

$$\frac{D^{\circ}\mu_2}{kT} = \frac{1}{6\pi r_1}\left(\frac{1+3\mu_2/\beta\gamma_1}{1+2\mu_2/\beta\gamma_1}\right) \qquad (4.1\text{-}31)$$

where γ_1 = radius of diffusion particles

β = coefficient of sliding friction

In the extreme case, when,

$$\beta = 0 \qquad \frac{D^{\circ}\mu_2}{kT} = \frac{1}{4\pi r_1}$$

$$\beta = \infty \qquad \frac{D^{\circ}\mu_2}{kT} = \frac{1}{6\pi r_1}$$

For large molecules of solute such as colloidal particles or large polymers, Equation 4.1-31 is found to reproduce experimental data fairly well.

In an attempt to modify this correlation Li and Chang (46) proposed

$$\frac{D^{\circ}\mu_2}{RT}\left(\frac{V_1}{V_1}\right)^{1/3} = \frac{1}{2}\left(1 - \frac{\hat{\sigma}}{\hat{\sigma}}\right) \qquad (4.1\text{-}32)$$

where $\hat{\sigma}$ is the number of closest neighbours in the molecular structure and $\hat{\sigma}$ is the number of closest neighbours in one layer.

Wilke (47), and Wilke and Chang (48) have presented the most widely used correlation; it is based on the Eyring's absolute rate theory and the Stoker-Einstein equations, and it is of the following form

$$D^{\circ} = \frac{7.4\times10^{-8}(XM_2)^{1/2}T}{\mu_2 V_1^{0.6}} \qquad (4.1\text{-}33)$$

where X is an association factor. This correlation requires a knowledge of the association factor, and that is one of its defects. To overcome this, Scheibel (49) modifed Equation 4.1-33 to give

$$D^{\circ} = 8.2\times10^{-8}\left(\frac{1+(3V_1/V_2)^{2/3}}{\mu V_1^{1/3}}\right)T \qquad (4.1\text{-}34)$$

In a recent paper Wise (50) tested six of the empirical correlations on the diffusion coefficients of the slightly soluble gases in water at 10-60°C. He found that none of these correlation fitted the data over the entire range of temperature and molecular size.

4.2 Experimental Methods Considered for the Determination of Diffusion Coefficients

Many methods have been proposed for the measurement of diffusion coefficients of gases in liquids (both mixture and pure compounds). The most widely used techniques differ from each other only

in the method of maintaining linear diffusion and in the quantity measured. Excellent reviews of experimental methods of measuring diffusion coefficients in liquids are given by Himmelblau (32), and Johnson and Babb (51). A brief discussion of the methods considered, as well as their merits and demerits with reference to the present system, is undertaken in the following sections.

4.2.1 Diaphragm Cell Methods

The unsteady state diaphragm cell method depends on measuring the concentration of solute in the compartments on both sides of a diaphragm before and after diffusion has taken place. The diffusion process is confined to the capillary pores of a sintered glass or metal diaphragm and thus avoids the errors due to thermal and mechanical convection. This method of determining diffusion coefficients is a relative one, since it requires the calibration of the cell with a substance of known diffusion coefficients. This method has been applied in numerous cases and it has been developed into a standard method for measuring self and mutual diffusivities of liquids. An excellent review on the experimental procedure for measuring diffusion coefficients in binary liquid mixtures was made by Gubbins and Bhatia (52). A steady state diaphragm cell has also been proposed by Walker (53), and was found to be very reliable for measuring the diffusivities of certain gases in liquids. The problem inherent with sparingly soluble gases is the difficulty of measuring small concentration and the danger of loss of gas on sampling the solution (54). These methods are not particularly suitable for the present system because the solubilities of the gases studied are only of the order of 10^{-5} to 10^{-8} mole fraction

owing to the salting out effect of the potassium hydroxide (3). The corrosive properties of potassium hydroxide also present problems. Thus, prolonging the experiment to obtain a larger concentration change is undesirable, for during the long period to arrive at a measurable change in concentration, the cell constant may change.

4.2.2 Steady State Absorption Method

Steady state absorption methods are based on the assumption that interfacial resistance to mass transfer is negligible and the fact that no resistance exists in the gas phase when pure gas is used. Many types of steady-state flow apparatus of known geometry have been introduced, of which the most widely used are the laminar jet, the wetted sphere, and the wetted wall. Of these, the laminar jet is the most extensively investigated, and it has been shown to give very reliable results in suitable cases (32). This method has the defect that it involves many implied assumptions, both in the model and in the mathematical solution of the differential equations describing the model which have neither been proved nor disproved. In addition, the assumption of no resistance in the gas phase cannot be fulfilled in the present system, for if pure dry gas is used, the concentration and temperature of the solution will be affected due to evaporation. A further limitation of these methods is that it is very difficult to get accurate results when the solubility of the gas is small.

4.2.3 Interferometric Techniques

These techniques represent the type which measures the concentration gradient of the solution as a function of time. Guoy (55)

was the first to use refractive index measurements for diffusion experiments, although it was Wiener (56) who developed the required equation and who first performed experiments using interferometric techniques. This method is a promising and accurate one but has not been widely used for gases dissolved in liquids because of the delicacy of the technique and the cost of the equipment. For very low gas concentrations and concentration differences such as those employed here, it seems doubtful that the interferometer is applicable.

4.2.4 Electrochemical Methods

The oxidizability and/or reducibility of the gases under study make electrochemical methods very attractive. In fact, all the existing data on these systems in the literature were obtained using electrochemical methods. Several such methods are available and are considered below.

Dropping Mercury Electrode

The principle of the dropping mercury electrode depends on measuring the diffusion current at the surface of the dropping mercury. Diffusion at a dropping mercury electrode is spherically symmetrical, but owing to the periodic growth and fall of the mercury drops the area of the diffusion field changes continuously during the life of a drop. Hence the problem is much more complicated than for the case of a stationary electrode.

The diffusion coefficient can be calculated from the experimental results by the modified Ilkovic equation

$$i_d = 607\, n(D)^{1/2} C m^{2/3} t^{1/6} \left(1 + \frac{A D^{1/2} t^{1/6}}{m^{1/2}} \right) \quad (4.2\text{-}1)$$

where n = number of electrons involved in reaction

D = diffusivity, $cm^2/sec.$

i_d = limiting current in μ ampere

C = concentration in millimoles/liter

m = mass flow rate of mercury electrode mg/sec

t = drop time of mercury electrode, sec.

A = constant

There have been some differences of opinion as to the value of A, but experimental data tend to support a value of about 31.5.

Gubbins and Walker (34) used the dropping mercury electrode to measure the diffusion coefficients of oxygen in potassium hydroxide solutions at 25°C. The concentration studied was 0% KOH to 35 wt.%. The estimated error is about ±6%, which is fairly precise for diffusion coefficient measurements. A shortcoming of the method is that it can not be used for measuring the diffusivity of hydrogen in potassium hydroxide solutions (owing to the high hydrogen over potential on the mercury electrode). Also, it is questionable whether this method can be used for high temperature measurements, when one considers that the high thermal capacity of mercury may result in the drop not reaching the solution temperature during its flow through the capillary and this may introduce errors in the diffusion coefficients so determined. Moreover, at high potassium hydroxide concentration the reaction may not be mass transfer limited. Thus, the dropping mercury electrode was not used in the present measurements.

Rotating Disk Electrode

The diffusion coefficient may be obtained from limiting diffusion current to a rotating platinum disk electrode if the solubility is known.

According to the equation of Levich

$$i_d = 0.62nFAc\nu^{-1/6}D^{2/3}\omega^{1/2} \qquad (4.2\text{-}2)$$

where n = number of electrons involved in reaction

F = faraday

A = electrode area

c = concentration of solute

ν = kinematic viscosity

D = diffusivity

ω = rotational speed

This method has the merit over the dropping mercury electrode in that it can be applied to both oxygen and hydrogen diffusion measurements. However, as pointed out by Davis et al. (18), when the rotating disk electrode is used in concentrated potassium hydroxide solutions, activation polarization becomes rate-controlling instead of concentration polarization. This method is therefore ill-suited to the present investigation where diffusion coefficients at high potassium hydroxide concentrations are of interest.

Stagnant Microelectrode

A final method, and the one adopted in this work, is the stagnant microelectrode method developed by Kolthoff and Lingane (57). Modification of this technique was made by Davis, Horvarth and Tobias (18), and it was used by them for the measurement of diffusion coefficients of oxygen in potassium hydroxide solutions with great success. This method combines simplicity with accuracy, and the time involved for each experiment is much shorter than that of diaphragm cell method.

4.3 Measurement of Diffusion Coefficients in LiOH and KOH Solutions

Measurements of diffusion coefficients depend largely on ingenuity in eliminating convection and the method of measuring the diffusion flux or the concentration gradient. The different methods so far proposed differ from each other principally in the ways in which these can be achieved. In the case of the stagnant micro electrode, Laitinen and Kolthoff (58) made use of a capillary to ensure linear diffusion, and they measured the flux of the diffusing species by the electrical current flowing. To eliminate the effect of ionic migration of the diffusing species a large excess of indifferent electrolyte was used. Among others von Stackelberg (59), Lingane (60), and Davis (18) used this method for diffusion coefficient measurements.

4.3.1 Theory of the Stagnant Microelectrode

The mathematical model of this system depends on the assumption of linear diffusion of the reactant in a direction parallel to the axis of a capillary. Consider a capillary with a large length to diameter ratio as shown in Figure 4.3-1. Assume that the capillary is filled with solution of uniform concentration of the diffusing species. When a step change in concentration is made at one end of the capillary, the diffusion process will start instantaneously owing to the concentration gradient. At any point in the capillary, the concentration will be changing with time. The concentration of the solution for that point at any instant in time can be found by solving the appropriate partial differential equation with the appropriate initial and boundary conditions. A brief discussion of the derivation will be made here; for further details the reader is referred to Kolthoff and Lingane (57).

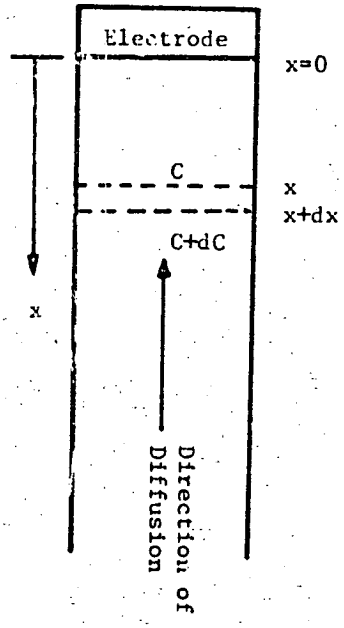

Figure 4.3-1. Schematic Diagram of a Capillary.

According to Fick's second law, for linear diffusion

$$\frac{\partial C}{\partial t} = D \frac{\partial^2 C}{\partial t^2} \qquad (4.3\text{-}1)$$

where C = concentration of the diffusing species

t = time

x = axial distance

D = diffusion coefficient of the diffusing species

with the initial condition for all x $C = C_o$ $t = 0$ (I.C.)

and boundary conditions $x = 0$ $C = 0$ $t > 0$ (B.C.1)

$x = \infty$ $C = C_o$ $t > 0$ (B.C.2)

These boundary conditions imply that the step change imposed is of magnitude C_o, and the electrode will never "see" the bulk of the solution.

The concentration profile at any time t results from solving Equation 4.3-1 with the above initial and boundary conditions, and is given by

$$C(x,t) = \frac{\partial C_o}{\sqrt{\pi}} \int_o^{x/2\sqrt{Dt}} e^{-y^2} dy \qquad (4.3\text{-}2)$$

where y is an integration variable.

In electrolytic solutions, Equation 4.3-1, which assumes a purely diffusion process, is applicable only when the limiting current is equivalent to the diffusion current, that is to say, the migration current is zero. This can be fulfulled when an excess of indifferent electrolyte is present and the current through the solution is carried entirely by the large excess of indifferent ions.

In practice, boundary condition I is achieved by causing the diffusing species to react as soon as it reaches the platinum electrode (x=0). Assuming no activation polarization by applying high enough voltage condition I is satisfied. Davis (18) has shown that Equation 4.3-2 is valid even though condition I is not satisfied provided one allows enough time for the actual concentration profile to coincide with that required by Equation 4.3-2. The reaction at the electrode gives rise to an electrical current which is directly proportional to the diffusive flux.

The current flowing is given by

$$i_t = nFAD \left(\frac{\partial C}{\partial x} \right)_{x=0}$$

$$= nFAC_o \sqrt{\frac{D}{\pi t}} \qquad (4.3\text{-}3)$$

By rearranging Equation 4.1-3, we obtain

$$D = \left(\frac{i_t}{nFAC_o} \right) \pi t \qquad (4.3\text{-}4)$$

Equation 4.3-4 predicts a linear relationship between i_t and $t^{-1/2}$; this was confirmed by Kolthoff and Lingane (57), and by Davis *et al.* (18). Thus, the linearity can be used as a criterion to test the reliability of an experimental run.

The boundary conditions introduced are less stringent than they appear. Condition I can be easily fulfilled if the voltage applied is such that it corresponds to a diffusion limiting condition. Under this condition, any reactant diffusing to the surface of the electrode will react as soon as it reaches the surface, and the concentration will be practically zero at the electrode surface.

The second boundary condition can be insured by having a long capillary, the length of which is much greater than the diameter of the capillary. Using a 0.15 cm. diameter and 2.5 cm long capillary, Davis, Horvarth and Tobias (18) have shown that "the correction for the finite length of the bore is found to be negligible for time periods of several hours".

4.3.2 Apparatus

Diffusion vessel I

This vessel was used for studying diffusion of gases in solutions, and is shown in Figure 4.3-2. It was so designed that diffusion will take place in the downward direction. Microelectrode A was a pyrex capillary of uniform bore closed by a disk of platinum foil. A platinum wire spot-welded to the platinum disk in the microelectrode was immersed in a column of mercury in tube B. The lead from the polarograph (the voltage source) was then immersed in the mercury through the other arm of B. Fritted disk C was used to dispense the gas under study during the saturation process. Counter electrode D was made of pure silver and of dimension 5.25 x 4.5 cm. The large area of the counter electrode was required to insure that concentration polarization took place at the microelectrode above. The silver counter electrode was connected to the lead of the polarograph by means of a silver wire welded to it. E was a vent for the gases and F an opening for inserting the hypodermic syringe into the cell; the latter was closed with a tapered plug (not shown) during any saturation or diffusion process. G was a cylindrical vessel with a male tapered joint at the top which fitted

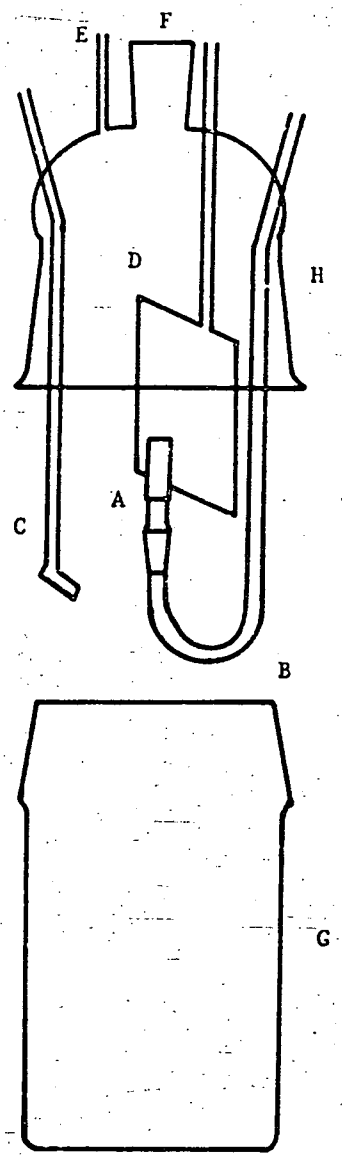

Figure 4.3-2. Diffusion Vessel I.

snugly into the female joint H with all the above accessories attached to it. The two parts were held together tightly by means of springs (not shown).

Diffusion Vessel II

This vessel, shown in Figure 4.3-3, was designed for measuring the diffusion current when diffusion was taking place in the upward direction. The vessel consisted of a cylindrical container A fitted with a rubber stopper through which was inserted a fritted gas bubbling disk C, a microelectrode B, a silver counter electrode D and a small tube used as a vent. The parts of the diffusion cell were similar to that of diffusion vessel I except that the reacting surface of the platinum surface was facing the bottom of the vessel, so that diffusion has to take place in the upward direction. This vessel was used for calibrating the microelectrode, and for determining the diffusion limiting potentials.

The Microelectrode

An enlarged view of the microelectrode was shown in Figure 4.3-4. The pyrex capillary x was of uniform diameter. The diameters of the capillaries used were from 1.75 ± 0.02 to 2.75 ± 0.035 mm depending on the viscosity of the solutions and the flux of current expected. β was a bright platinum disk with a platinum wire attached. The platinum disk was pretreated as described below and was cemented between the two sections of tubing with a fluoro-carbon epoxy cement. The assembly was cured for three hours at $400^{\circ}F$ and one hour at $450^{\circ}F$. γ was a capillary with a 10 mm. tapered joint attached to it, the latter was fitted into the female counter part at the end of part B of the diffusion vessel.

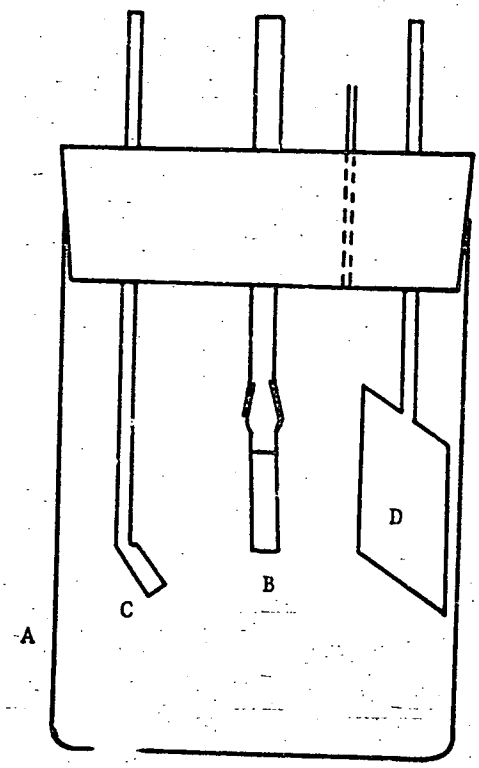

Figure 4.3-3. Diffusion Vessel II.

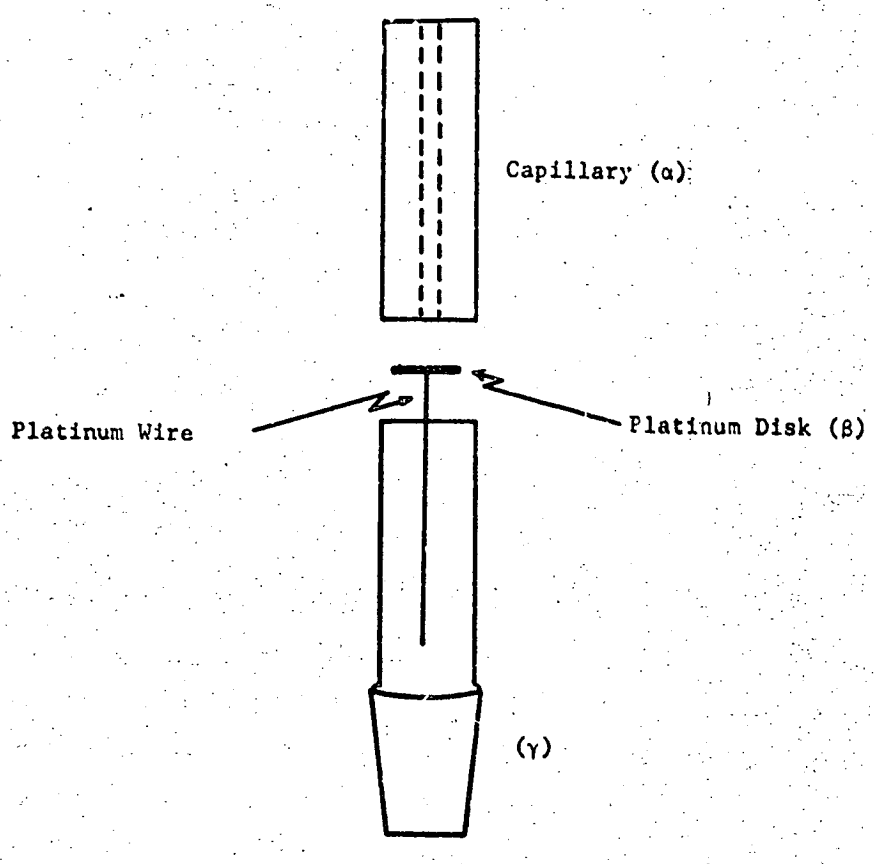

Figure 4.3-4. Enlarged View of Microelectrode.

Voltage Supply

Voltage supply and current measurement were by a Sargent Model XV Polarograph complete with a microrange extender. The polarograph can run on the current-time or current-voltage basis. The leads from the polarograph were connected with the microelectrode and the silver counter electrode for electrical contact.

4.3.3 Reagents and Solutions

Potassium Hydroxide Solutions

A.C.S. Reagent grade potassium hydroxide pellets with about 1% potassium carbonate were used. The solution was prepared by dissolving the potassium hydroxide pellets in doubly distilled water to the desired strength. It was then standardized with standard HCL solution using methyl orange as indicator. The carbonate content was checked by titration using phenolphthalein as indicator; it was found to be less than 1% and the increase in its concentration during storage was negligible. The potassium hydroxide solutions were stored in polyethylene bottles to prevent contamination.

Standard HCL Solutions

Standard 1 N HCL solutions were prepared with capsules of "Acculute" standard volumetric solutions. These capsules were diluted with doubly distilled water to one normal solution in a one liter volumetric flask.

Standard Potassium Ferrocyanide Solutions

The standard potassium ferrocyanide solution in 0.1 N KCL solution was prepared by diluting a capsule of "Acculute" standard volumetric solution of potassium ferrocyamide with 0.1 N KCL solution to the

required concentration (0.0004M in this case). The concentration was checked by titrating the solution with a standard zinc solution acidified with 4N sulfuric acid and with addition of $(NH_4)_2 SO_4$ using 3-3' dimethyl napthidine as indicator

Zinc Solution

The standard zinc solution was prepared by dissolving a weighed amount of analytical grade grannular zinc metal in dilute sulphuric acid in a volumetric flask and making up to the desired volume with doubly distilled water.

4.3.4 Procedure for Measuring the Limiting Current

This experiment depends on the measurement of diffusion current at a given controlled temperature and concentration of potassium hydroxide solutions. The measured diffusion current was used, together with solubility data and calibrated area (Section 4.3.7) of the capillary, to calculate the diffusion coefficient using Equation 4.3-4. As can be seen from Equation 4.3-4, the diffusion coefficient D is proportional to the square of the diffusion current, i_t, and inversely proportional to the square of the solute concentration. A small error in the measurement of the diffusion current or failure to fully saturate the solution can produce a large error in the value of the diffusion coefficient. The importance of thorough saturation of the solution and attainment of thermal equilibrium with the bath cannot be overemphasized.

The apparatus was set up as shown in Figure 4.3-5. The diffusion vessel was filled with potassium hydroxide solution and immersed in the bath. Diffusion vessel I was used to produce downward diffusion of the reactant. Gas, saturated with water vapor (Section 4.3.5), was allowed

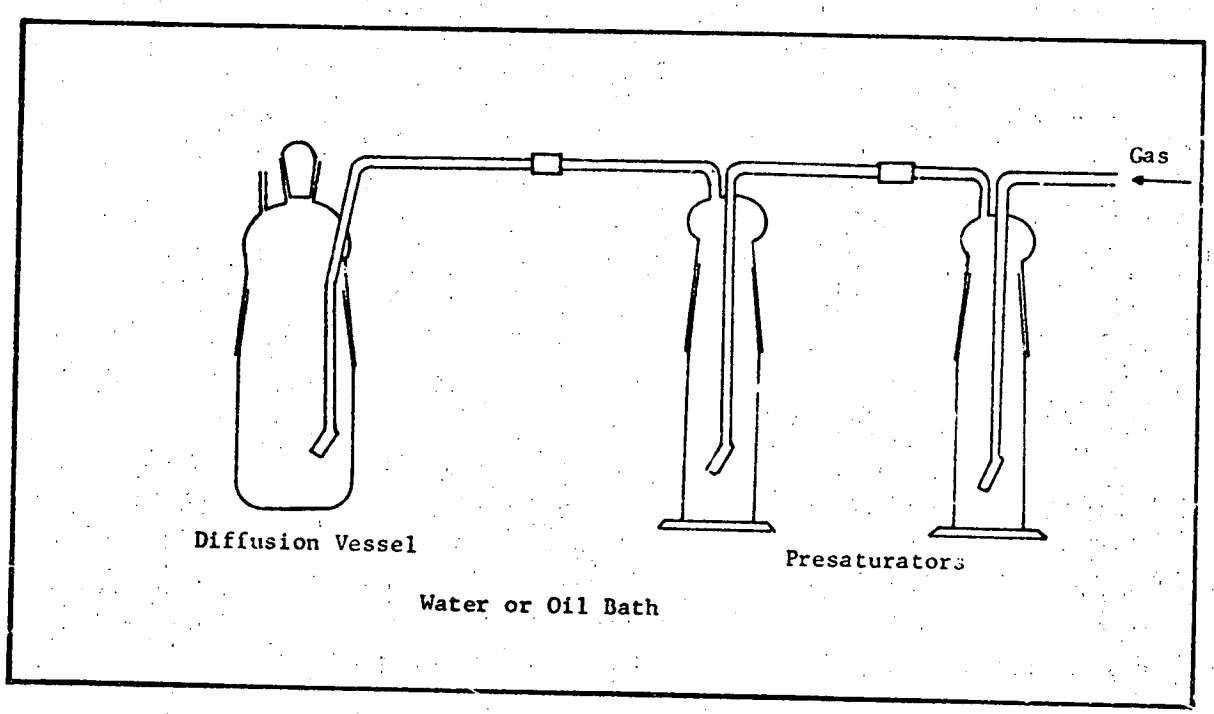

Figure 4.3-5. Apparatus Arrangement

to bubble through the solution for thirty minutes to make sure that both thermal equilibrium and saturation of the solution with gas was attained. Owing to the turbulence introduced by the gas bubbles thermal equilibrium is achieved rapidly.

While the gas was still bubbling through the solution, the gas-saturated solution was drawn into the microelectrode with a hypodermic syringe. The solution in the syringe was then flushed into the bulk of the solution. This drawing and flushing was repeated four times, after which the gas flow was stopped. In the filling process care should be taken to withdraw the plunger very slowly, otherwise degassing will take place. The turbulence in the solution was allowed to die down and the solution allowed to equilibrate with the surroundings for ten minutes. Then, the desired fixed voltage was applied across the electrode (-0.4 to -0.65 volt for O_2 measurements, +0.1 to + 0.25 volt for H_2 measurements all referred to the saturated calomel electrode), and the resulting current was recorded as a function of time. The measurement was carried on for twenty minutes, then the applied voltage was removed. After the current-time curve was obtained, the constancy of $i_t\sqrt{t}$ was tested. If the function was constant throughout the 20 minute period (the measurement for the first four minutes being discarded), the experiment was repeated. During the repetition, the gas saturation process was allowed to take place for ten minutes only. Five to six repetitions were made for each measurement. After this the residual current was measured (Section 4.4-5) and was deducted from the arithmetic mean of the above measurements to obtain i_t. Diffusion coefficients were calculated from these values of i_t, solubility data, and by effective area of the electrode by means of Equation 4.3-4.

If the quantity $i_t\sqrt{t}$ was not constant, the electrode was cleaned by either cathodic evolution of hydrogen or anodic evolution of oxygen, and then activated at -0.2 volt for one minute. If the data did not show any improvement after several repetitions of this pretreatment (especially if irregular disturbances of the curve were observed), the microelectrode was assumed to be poisoned. The microelectrode was then changed, and the experiment repeated.

4.3.5 Saturation Procedure

Care was necessary to insure the presaturation of the gas, as well as the saturation of the potassium hydroxide solution with the gas under study. The arrangement of the apparatus was as shown in Figure 4.3-6. Dry gas from the gas cylinder was presaturated with water by bubbling it through two gas washing bottles (presaturators) filled with potassium hydroxide solution of the same concentration as that under study. The whole apparatus (including the connections between vessels) was immersed in an oil bath controlled with a Fisher proportional controller to within $\pm 0.05^{\circ}C$ of the desired temperature. No condensation of water vapor in the connecting lines was allowed. This insured that the vapor phase in the diffusion vessel was saturated with water vapor. Thus, no change in concentration of the potassium hydroxide solution should take place, and the solubility of the gas was that corresponding to the barometric pressure less the vapor pressure of the potassium hydroxide solution at the bath temperature. An oil bath was used to insulate the diffusion vessel from electrical disturbances from the heaters and stirrers.

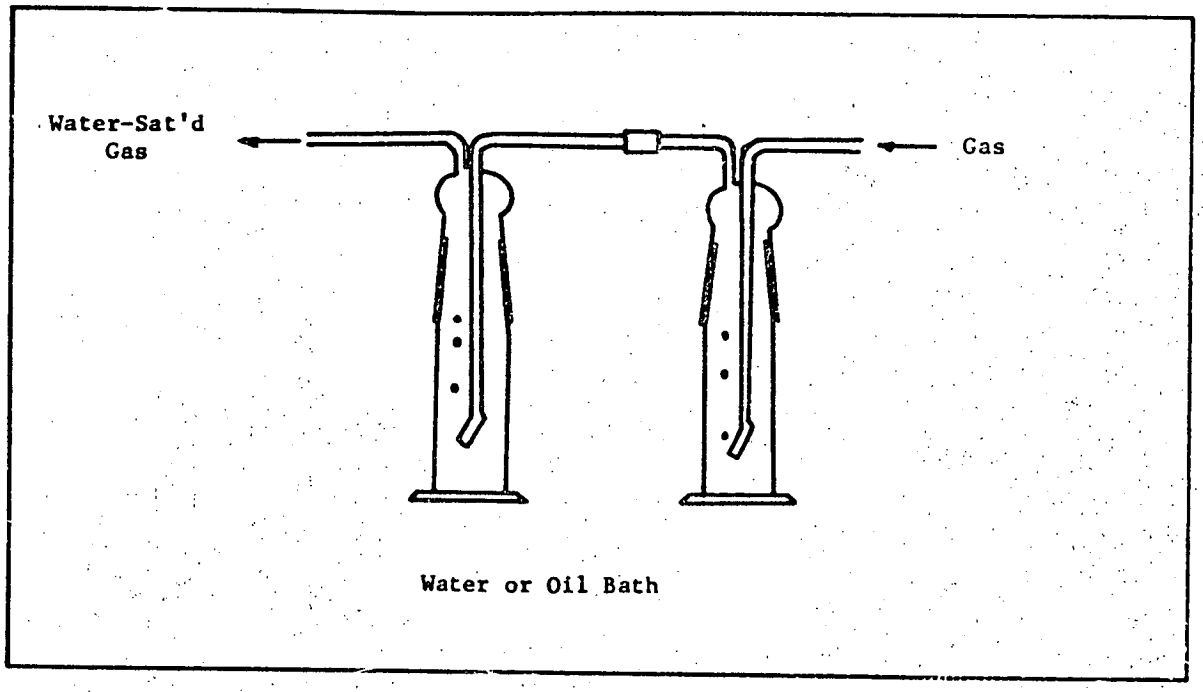

Figure 4.3-5. Gas Presaturation Arrangement.

4.3.6 Pretreatment of the Microelectrode

The most critical feature of this method is the emphasis on purity. The platinum microelectrode was very sensitive to impurities, and it was found that a small amount of impurity poisoned the electrode to such an extent that it had to be cleaned with strong acid before it could be used again. Initially, the electrode was cleaned by dipping in fuming nitric acid, and then rinsed with distilled water. If the rinsing process was not thorough enough to remove all the nitric acid, erratic results were obtained. This may be due to the presence of nitrate ions on the electrodes. The procedure proposed by Bockris (61) was subsequently followed in this work and found to give electrodes of much improved performance. In this procedure, the platinum disk was soaked in acetone for about five minutes to remove impurities, and then rinsed with distilled water several times. It was then cleaned with concentrated sulfuric acid and then thoroughly rinsed with distilled water until all the sulfuric acid had been removed. To remove any traces of sulfate ions remaining, the electrode was immersed in potassium hydroxide solutions for fifteen minutes. The electrode was then again thoroughly rinsed with distilled water, dried and sealed into the capillary as described earlier.

4.3.7 Calibration of the Microelectrode

For the calculation of the diffusion coefficient using Equation 4.1-4, the area of the diffusion path is needed. This can be obtained by either measuring the diameter of the bore directly or by calibrating with a substance of known diffusion coefficient. The latter approach was adopted here. Such a procedure gives a much more accurate

result than the mechanical measurement, and by this method any errors in the measurement and calibration should largely cancel. For the calibration of the electrode, measurements were made of the diffusion current in a solution which was 0.0004M in potassium ferrocyamide solution 0.1N in KCL.

The experimental technique was similar to that reported by Kolthoff and Lingane (57), and only a brief description of the method will be given here. The main difference between the present calibration and the oxygen and hydrogen diffusion measurement is that the diffusion should be in the upward direction to prevent bulk flow due to density gradients. Hence, diffusion vessel II must be used.

Diffusion vessel II and presaturators were filled with the potassium ferrocyamide solution and immersed in the bath controlled at 25°C. Nitrogen gas was passed through the apparatus to strip out any oxygen that might be present; after the stripping process, the microelectrode was filled with the oxygen-free solution using a hypodermic syringe. A voltage of +0.7 volts was applied across the electrodes, and the diffusion current was recorded as a function of time. The experiment was allowed to proceed for 20 minutes, then the applied voltage was removed. After this, fresh solution was drawn into the capillary and the experiment repeated; the process was repeated five times.

To measure the residual current, the same experiment was repeated for 0.1N KCL solutions after stripping with nitrogen. This, too, was repeated several times to minimize errors. The difference between the diffusion and residual current gave the corrected diffusion current for the experiment. The area of the capillary can be calculated

from this corrected diffusion current by rearranging Equation 4.3-4 to give

$$A = \frac{i_t}{nFC_o}\sqrt{\frac{\pi t}{D^o}} \qquad (4.3\text{-}5)$$

D^o is the diffusion coefficient of potassium ferrocyamide in 0.1N KCL solution and was measured accurately by von Stackelberg, Pilgrim and Toome (59) to be $0.768 \pm 0.03 \times 10^{-5}$ cm^2/sec.

4.3.8 Determination of the Diffusion Limiting Potential

In order that boundary condition I be satisfied, the voltage applied across the electrodes should be at least that corresponding to the diffusion limiting potential. This was measured as described below.

The apparatus was arranged as shown in Figure 4.3-5, diffusion vessel II being used. The only difference between this measurement and in the calibrating process is that instead of the microelectrode, a stationary wire electrode was used. The stationary platinum wire was pretreated as described above, then the apparatus was immersed in the oil bath and the solution was saturated with the gas under study in the same manner as described in Section 4.3-5. After the solution became quiescent, the measurement was started. In this experiment the polarograph was utilized to measure the change in current density with increase in voltage. Thus, a given range of voltage was selected and the current was recorded as a function of the applied voltage. A voltage corresponding to the middle of the plateau of the current-voltage curve was used on the diffusion limiting potential. In the case of oxygen, the first of the two plateaus, which corresponds to

the reduction of oxygen to hydrogen peroxide, was used. The experiment was repeated several times until well-defined, reproducible current-voltage curves were obtained.

4.3.9 Determination of Residual Current

In this experiment the same apparatus as in the diffusion current measurements was used. Nitrogen gas saturated with water vapor was used to strip out any oxygen and hydrogen dissolved in the solution. The microelectrode was then filled with the nitrogen-saturated solution in the same manner as described in Section 4.3.5. The same voltage as the diffusion current measurement was applied and the current was recorded as a function of time. The process was repeated several times until there was no further decrease in current for two successive measurements.

4.4 Diffusivities of Hydrogen and Oxygen in KOH and LiOH Solutions

4.4.1 Experimental Data

The experimental data for the diffusion coefficients of oxygen and hydrogen in potassium hydroxide solution are tabulated in Tables 4.4-1 and 4.4-2. In Table 4.4-3 are also tabulated a few diffusion coefficients of oxygen in LiOH solutions at 25°C. The deviations shown are the standard deviations from the arithmetic mean for five to six measurements. A sample calculation for a typical experimental run is given in Appendix 2.

The diffusion coefficient measured are integral values. However, since the concentration of dissolved gas was very low, the values obtained are for all practical purposes equivalent to the differential diffusion coefficients.

Table 4.4-1

Diffusion Coefficients of Oxygen in Aqueous Potassium Hydroxide Solutions in $cm^2/sec \times 10^5$

Wt % KOH	$Dx10^5, cm^2/sec.$				
	25°C	40°C	60°C	80°C	100°C
3.5		2.45±0.02			
5.0			3.40±0.012	5.15±0.03	
6.0	1.45±0.018				
10.2	1.18±0.02	1.75±0.01			
13.0			2.45±0.021	3.70±0.035	
19.0	0.85±0.015	125±0.019	1.80±0.016		
24.0				2.22±0.031	3.70±0.045
26.0	0.60±0.018	0.90±0.01			
32.5			1.05±0.02	1.64±0 049	
40.2	0.40±0.01	0.57±0.02			
42.5			0.85±0.01	1.25±0.03	1.71±0.07
51.5	0.30±0.012	0.45±0.015	0.72±0.01	1.04±0.04	1.48±0.06

Table 4.4-2

Diffusion Coefficients of Hydrogen in Aqueous Potassium Hydroxide Solutions

Hydroxide Solutions in $cm^2/sec \times 10^5$

Wt % KOH	$Dx10^5, cm^2/sec.$				
	25°C	40°C	60°C	80°C	100°C
5.0	3.01±0.015	4.60±0.028	7.55±0.043	11.60±0.086	
13.0	2.36±0.02	3.60±0.017	5.82±0.06	8.70±0.054	
24.0	1.85±0.01	2.74±0.01	4.46±0.032	6.70±0.039	9.90±0.2
32.5	1.55±0.023	2.40±0.01	3.46±0.051	5.40±0.066	
42.5	1.25±0.01	1.95±0.02	2.89±0.11	4.40±0.095	
51.5	1.10±0.01	1.80±0.02	2.53±0.04	3.80±0.12	5.59±0.13

4.4.2 Estimation of Accuracy of Measurements

The KOH and LiOH concentrations were determined by titrating with standard HCL solution, and represent the total alkalinity. It is estimated that the analysis accuracy was 0.2% of the concentration value. Numerous earlier analyses had revealed that the carbonate content of the LiOH and KOH was a little less than one percent.

The temperature in the bath was controlled to $\pm 0.05^{\circ}C$; the bath temperature was measured with a precision thermometer calibrated against a National Bureau of Standards certified thermometer.

The overall accuracy of the measured diffusion coefficients is estimated to be $\pm 10\%$. This estimation was made by considering the possible errors that can be introduced from all sources, including the uncertainty in solubility data.

4.4.3 Comparison with Literature Data

The data for oxygen are compared with those of Davis *et al.* (18), and Gubbins and Walker (54) in Figure 4.4-1 and the data for hydrogen are compared with that of Ruetschi (17) at $30^{\circ}C$ in Figure 4.4-2. In general, agreement of the data with those of other investigators is reasonably good; however, the diffusivity of hydrogen in KOH solution measured by Ruetschi showed a much stronger concentration dependence than was found in this work. Figure 4.4-3 shows the diffusion coefficients of O_2 in LiOH. No other data on the diffusion coefficient of oxygen in LiOH appear to be available.

By extrapolation to infinite dilution, values of the diffusion coefficients of oxygen and hydrogen in water at $25^{\circ}C$ were estimated to be 2.0×10^{-5} and 3.7×10^{-5} $cm^2/sec.$, respectively. These figures agree

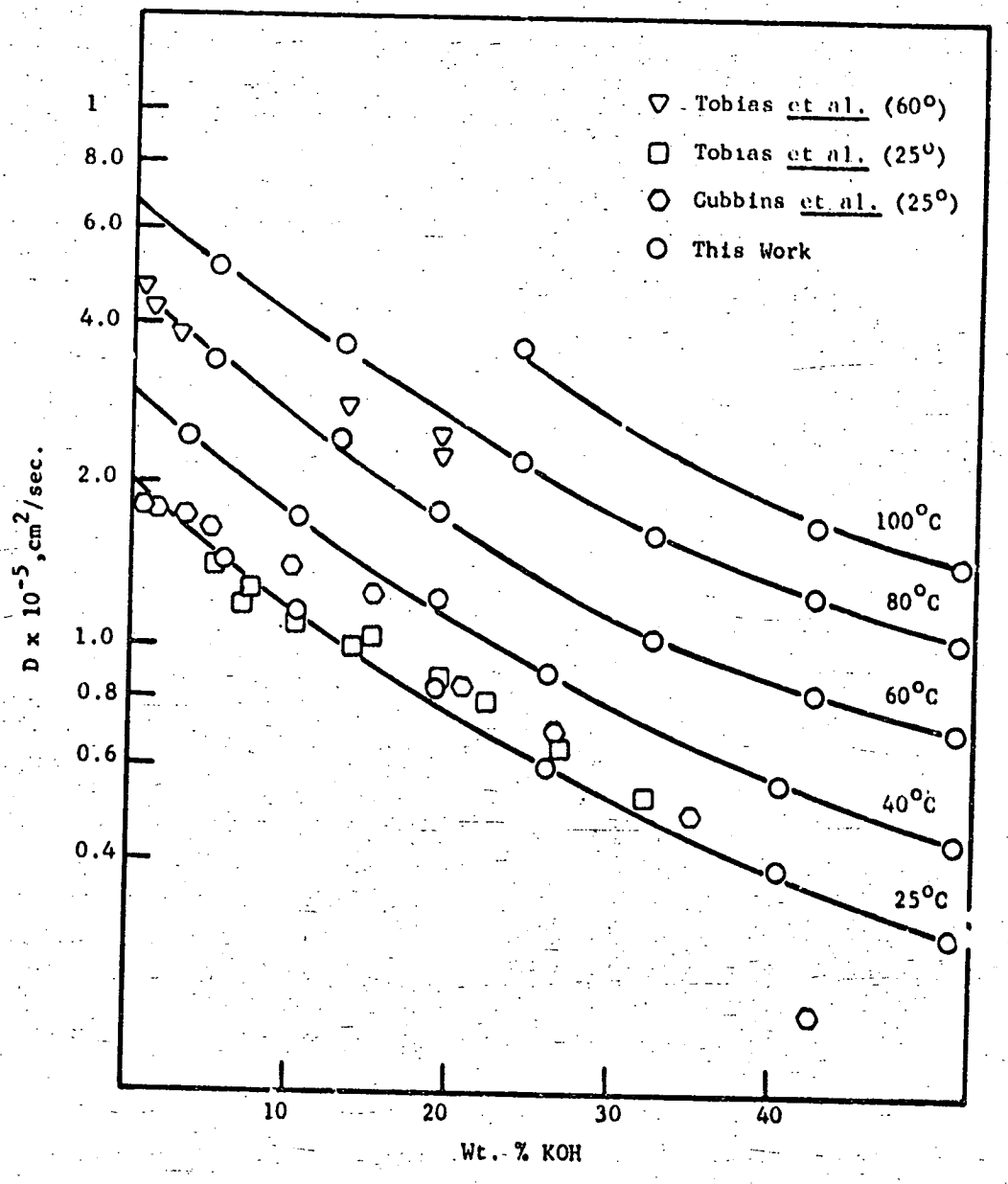

Figure 4.4-1. Diffusion Coefficients of Oxygen in KOH Solutions.

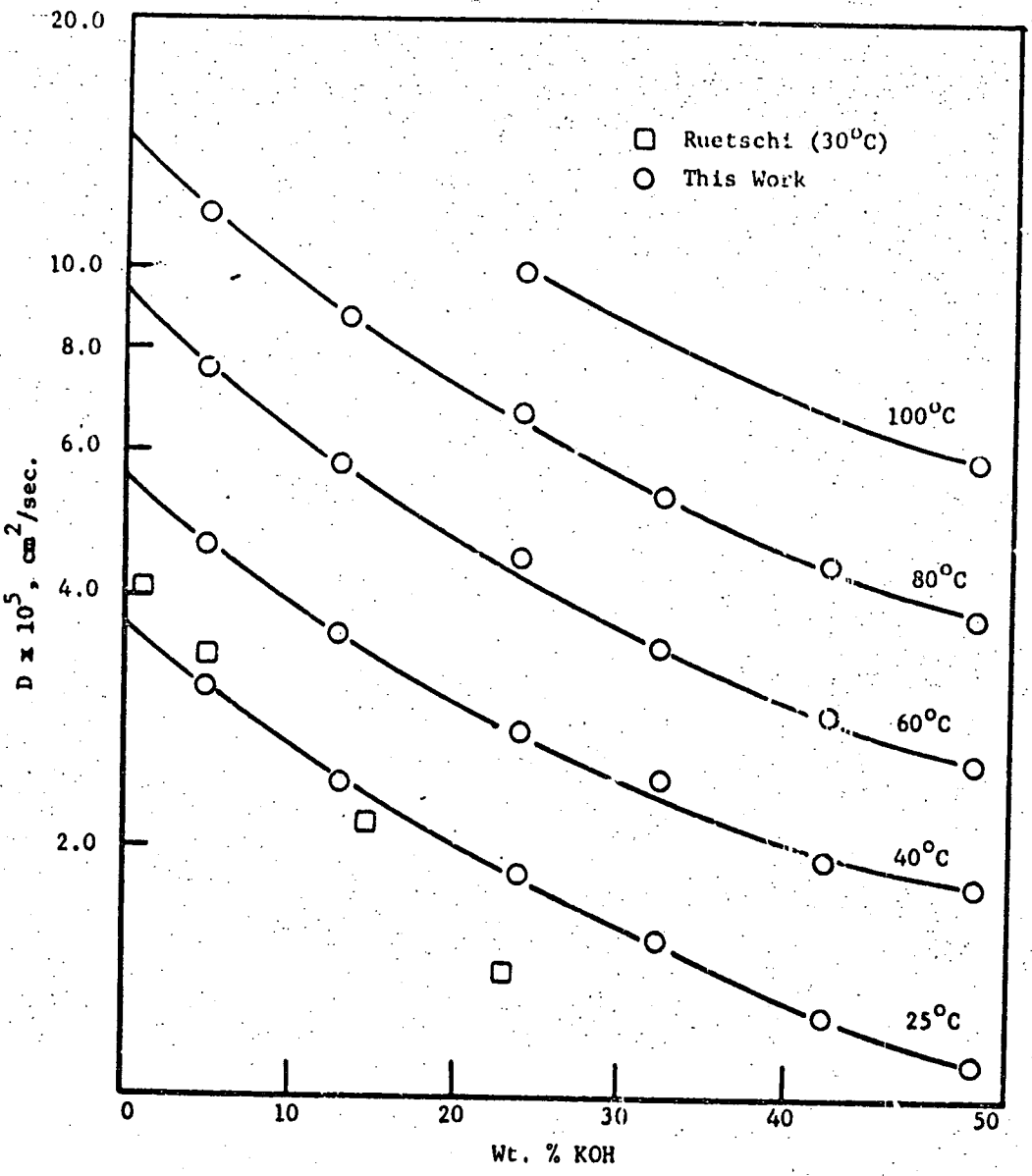

Figure 4.4-2. Diffusion Coefficients of Hydrogen in KOH Solutions.

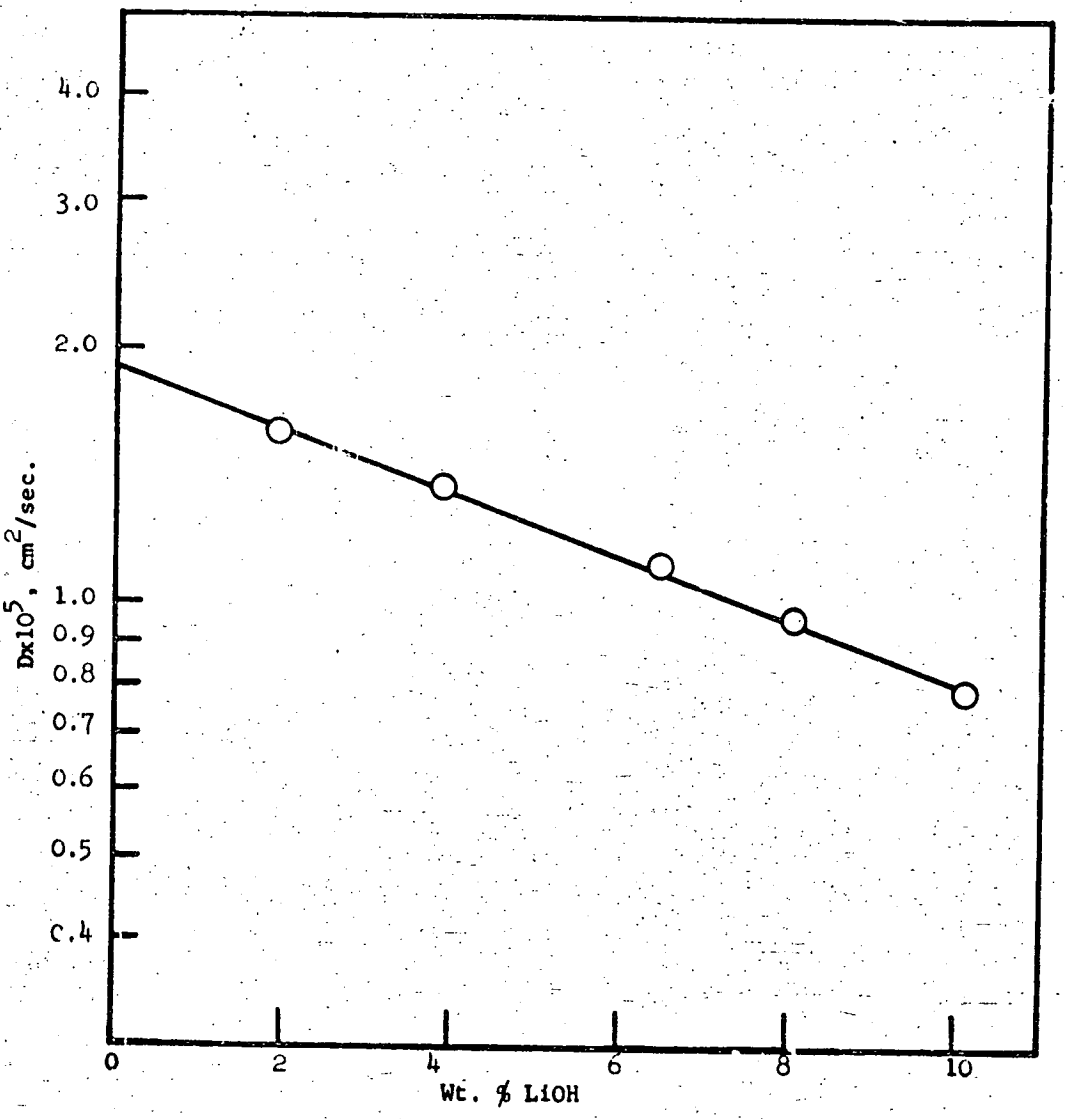

Figure 4.4-3. Diffusion Coefficient of Oxygen in LiOH Solutions

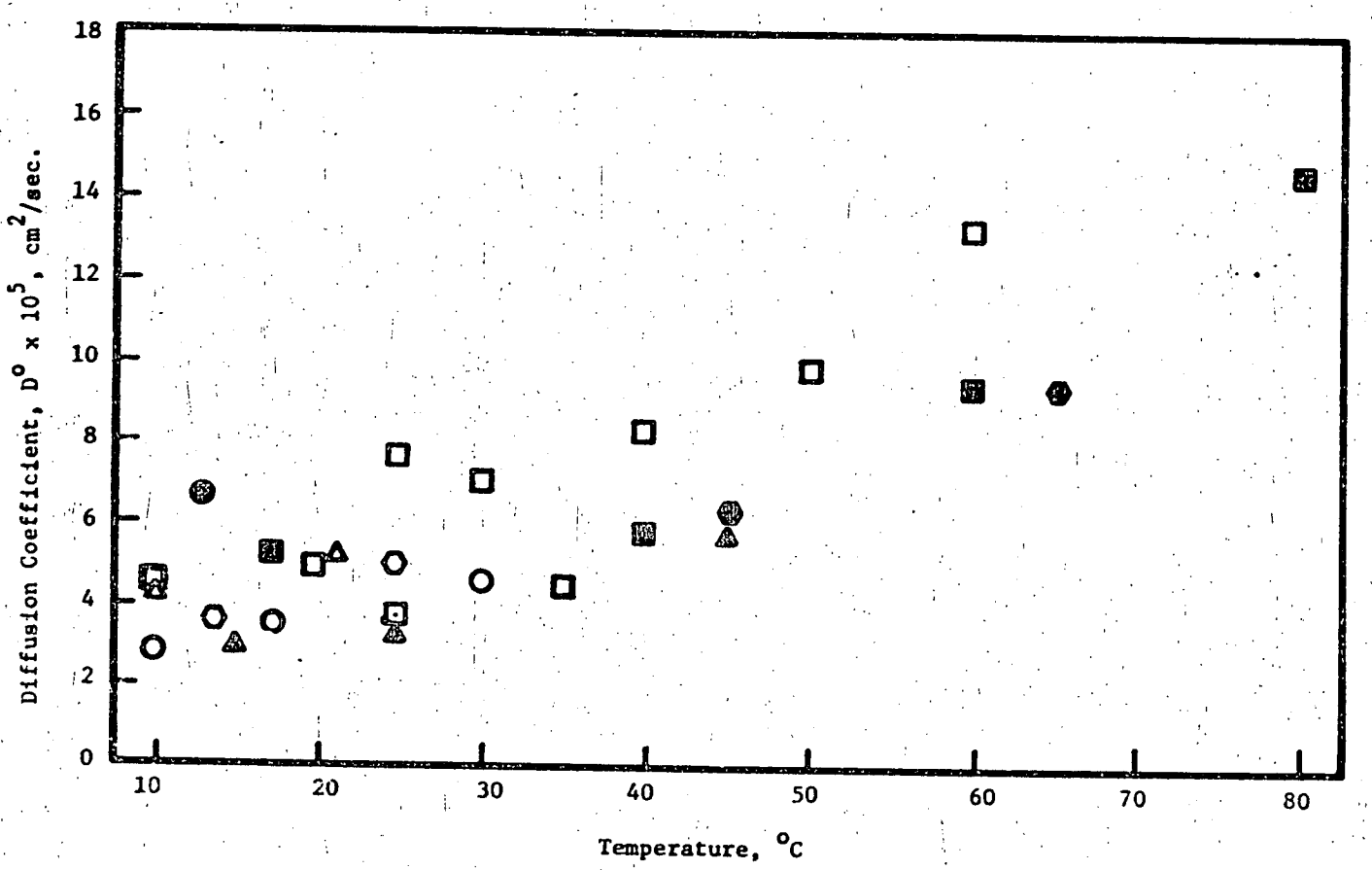

Figure 4.4-4. Temperature Dependence of Diffusion Coefficient of Hydrogen in Water ○, Ref. 62; △, Ref. 64; □, Ref. 50; ◍, Ref. 63; ⬡, Ref. 65; ▲, Ref. 66; ■, Ref. 67; ⬢, Ref. 68.

well with the most generally accepted literature values. The diffusivities of hydrogen and oxygen in water at various temperatures are plotted in Figures 4.4-4 and 4.4-5. The values at 25°C represent the two extremes of the existing data, but most of them are clustered around the values obtained in this work.

Table 4.4-3

Diffusion Coefficients of Oxygen in Lithium Hydroxide Solutions at 25°C

Wt % LiOH	1.9%	3.85%	6.45%	8.05%	10.10%
$D^{o} \times 10^{5}$ cm^{2}/sec	1.60±0.03	1.38±0.01	1.12±0.01	0.96±0.02	0.79±0.01

4.5 Discussion of Results and Conclusions

The results presented in Tables 4.4-1, 4.4-2 and 4.4-3 indicate that the diffusivities decrease rapidly with increase in KOH or LiOH concentration, whereas they increase with increase in temperature. The effect of concentration on diffusivities appears to be more pronounced for oxygen than for hydrogen. It is interesting to examine these effects in the light of the theoretical and empirical correlations that have been proposed.

4.5.1 Temperature Dependence of the Diffusion Coefficients

Most of the theoretical and semitheoretical relationships do not really shed any light on the temperature dependency of the diffusion coefficients, since they contain terms which are also temperature dependent. According to Eyring's theory of absolute reaction rates and its modifications, the diffusivity is related to the absolute temperature by an expression of the form

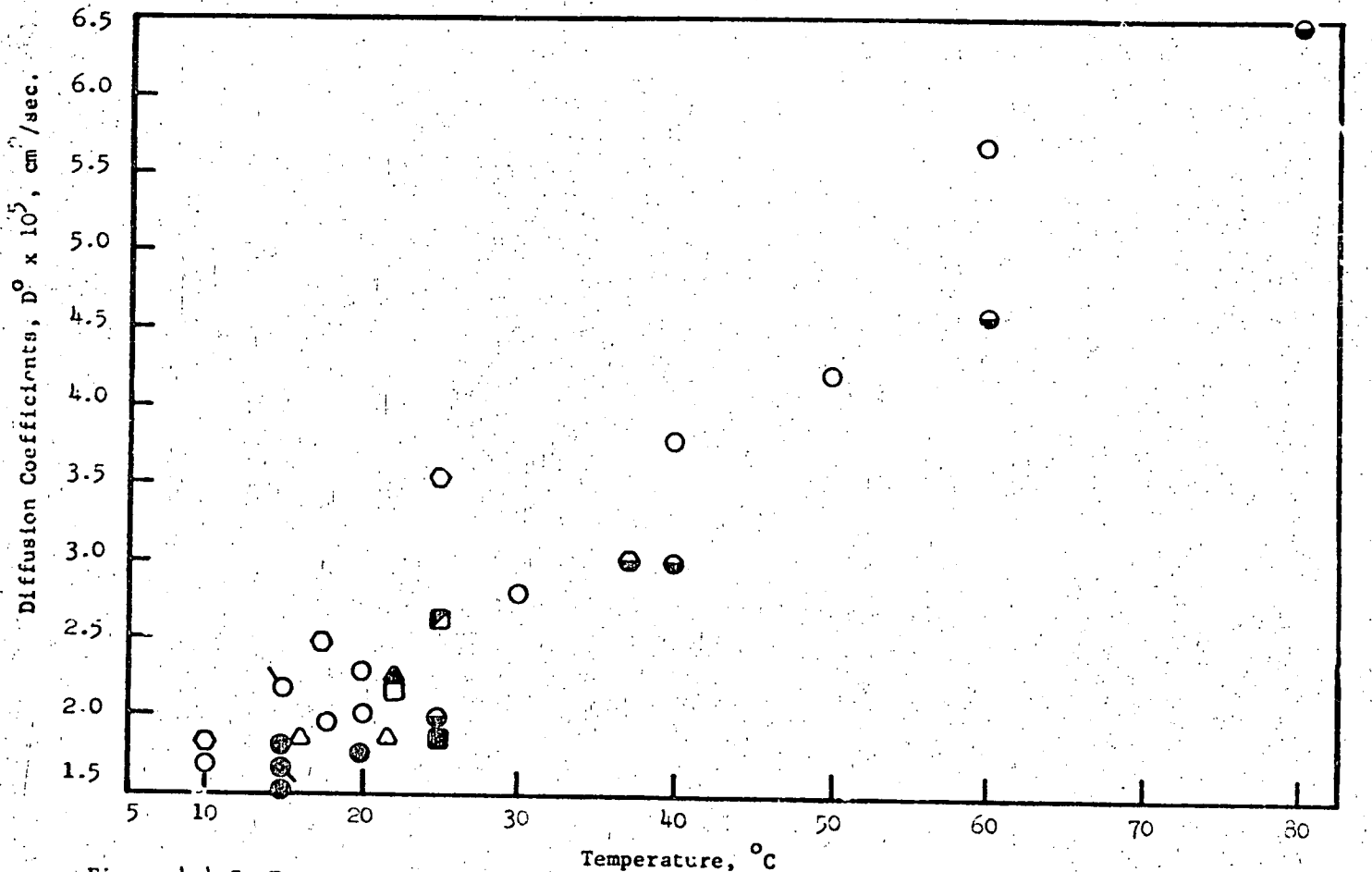

Figure 4.4-5 Temperature Dependence of Diffusion Coefficient of Oxygen in Water
○, Ref. 62; ○, Ref. 50; ○, Ref. 63; ◒, Ref. 69; ●, Ref. 67; △, Ref. 64; ○, Ref. 70; ▲, Ref. 71;
□, Ref. 72; ■, Ref. 73; ▨, Ref. 74; ◒, Ref. 75.

$$\ln D/T = B - A/RT \qquad (4.5\text{-}1)$$

If we assume that within a short range of temperature A and B are constants, Equation 4.5-1 predicts a linear relation between ln(D/T) and 1/T.

In Figures 4.5-1 and 4.5-2, the values of D/T were plotted against 1/T in a semi-logarithmic plot. Within experimental error, such a linearity was observed for both oxygen and hydrogen diffusivities for the temperature range tested.

4.5-2 The Relationship Between Viscosity and Diffusivities

In the study of diffusivities of oxygen in potassium hydroxide solutions, Davis et al. (18) reported that the product of viscosity and diffusivity (and thus $D^{o}\mu/T$) was constant at constant temperature, after an initial decrease in value. The rapid initial falling off in the value of $D^{o}\mu/T$ was also observed in this work (Table 4.5-1), but these values increased after passing through a minimum instead of remaining constant.

Bearman (34) showed that for a "regular" solution, the product of $D^{o}\mu$ should be independent of concentration. The term "regular" implies that the radial distribution function is independent of concentration. This is valid only when all species in a solution are identical, i.e., it holds rigorously only for a pure liquid. The second assumption implied in a regular solution is that the volumes are additive. The present system does not fulfill the requirements stated above for a regular solution, especially for high concentrations. Thus, the product of $D^{o}\mu$ should not be expected to remain constant at constant temperature.

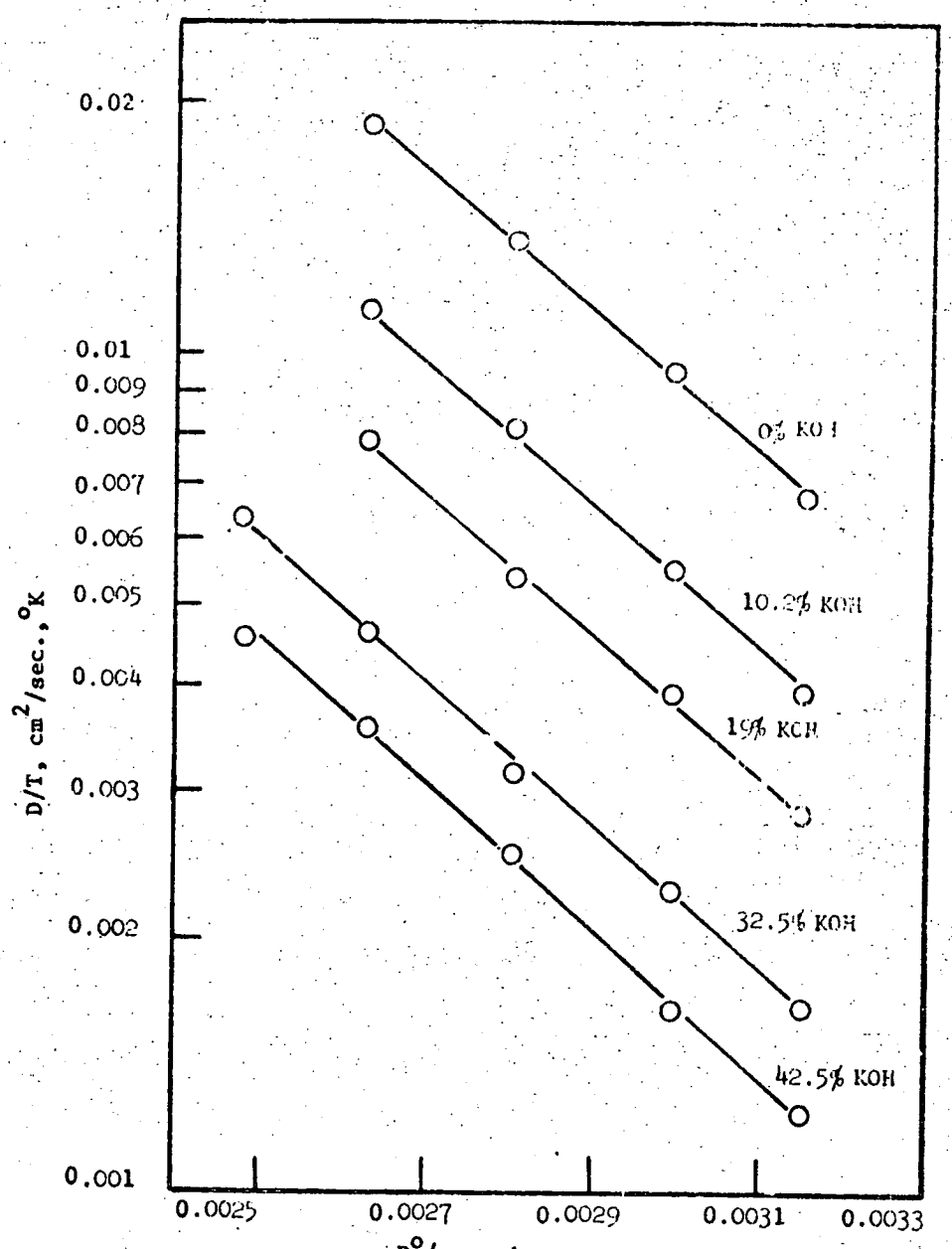

Figure 4.5-1 $\ln D^{o}/T$ vs $\frac{1}{T}$ for O_2 Reciprocal Temperature, $^{o}K^{-1}$

Temperature Dependence of Diffusivity of Oxygen

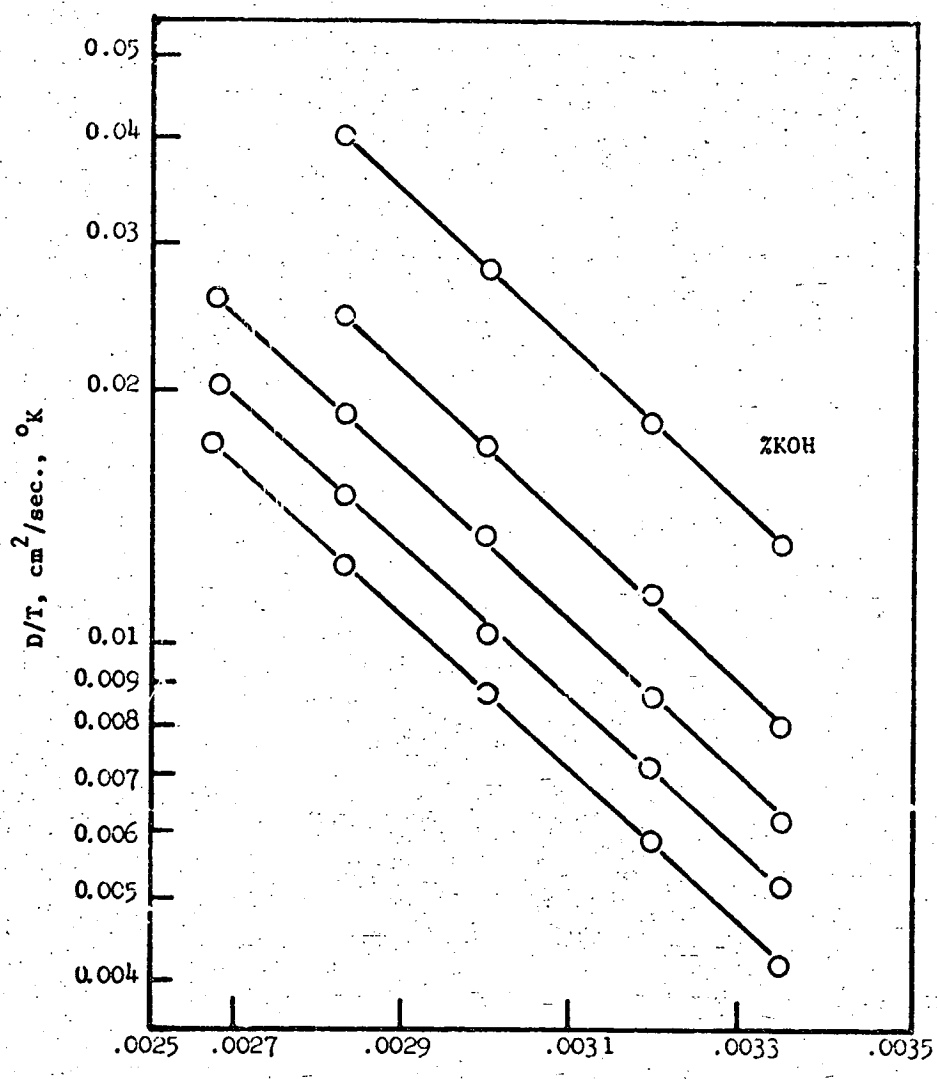

Figure 4.5-2 $\ln D^{o}/T$ vs $\frac{1}{T}$ for H_2 Reciprocal Temperature, $^{o}K^{-1}$

Temperature Dependence of Diffusivity of Hydrogen

Most of the semi-empirical correlations - such as the Wilke-Chang Equation (48) - predict the constancy of $D^{\circ}\mu/T$ for a given solvent or a solution of fixed concentration. In Tables 4.5-1 and 4.5-2 values of $D^{\circ}\mu/T$ for oxygen and hydrogen in potassium hydroxide solutions are given, and within experimental error, such a constancy was observed for each fixed concentration.

4.5-3 Effect of Concentration on Diffusivities

The modified Eyring theory given by Equation 4.1-29, when applied to an electrolyte solution, predicts a linear relation between $\ln(D/D_o)$ and species fraction, where the latter is defined as

$$\text{species fraction} = \frac{x}{1 - xt(\nu_1+\nu_2)x}$$

where ν_1 and ν_2 are the number of ions of species 1 and 2 into which an electrolyte molecule dissociates.

D_o is the diffusivity in pure water.

Typical plots of $\ln D/D_o$ against species fraction for oxygen and hydrogen at 25 and 60° are shown in Figures 4.5-3, 4.5-4, 4.5-5 and 4.5-6. The linear relationship predicted by the theory was found to hold for both systems up to 35% potassium hydroxide concentration, while at higher concentrations distinct deviations from linearity were observed. These deviations appear to be attributable to assumptions that have been made in the modifications of Eyring theory.

Ratcliff and Holdcroft (40) in their modification of the absolute rate theory assumed firstly that the presence of ions would not affect the lattice spacing λ and secondly, that the distribution of ions in the neighbourhood of the solute is the same as in the bulk solution.

Table 4.5-1

$\frac{D^o\mu}{T}$ for Oxygen in KOH Solutions

	25°C			40°C			60°C		
Wt % KOH	$D^o x10^5$ cm^2/sec	$\mu x10^{2(1)}$ g/cm sec	$D^o\mu/Tx10^9$ $gcm/sec^{2o}K$	$D^o x10^5$ cm^2/sec	$\mu x10^5$ g/cm sec	$D^o\mu/Tx10^9$ $gcm/sec^{2o}K$	$D^o x10^5$ cm^2/sec	$\mu x10^5$ g/cm sec	$D^o\mu/Tx10^9$ $gcm/sec^{2o}K$
5	1.52	1	0.510	2.25	0.72	0.517	3.45	0.50	0.518
10	1.18	1.12	0.443	1.75	0.825	0.458	2.70	0.575	0.466
20	0.77	1.46	0.380	1.13	1.09	0.390	1.74	0.78	0.400
30	0.52	2.20	0.383	.79	1.6	0.403	1.15	1.16	0.400
40	0.40	3.68	0.493	.58	2.6	0.481	0.875	1.8	0.472

Table 4.5-2

$\frac{D^o\mu}{T}$ for Hydrogen in KOH Solutions

5	3.10	1	1.040	4.80	0.725	1.110	7.50	0.5	1.12
10	2.60	1.12	0.977	3.60	0.825	0.950	5.80	0.575	1.00
20	2.00	1.46	0.980	3.00	1.090	1.01	4.60	0.78	1.07
30	1.60	2.2	1.18	2.40	1.60	1.22	3.65	1.16	1.27
40	1.305	3.68	1.60	2.02	2.60	1.67	3.00	1.8	1.62

(1) Viscosity data were obtained from "Caustic Potash", Solvay Technical and Engineering Series Bulletin No. 15, Solvay Potash Process Division, Allied Chemical Corp., 1960.

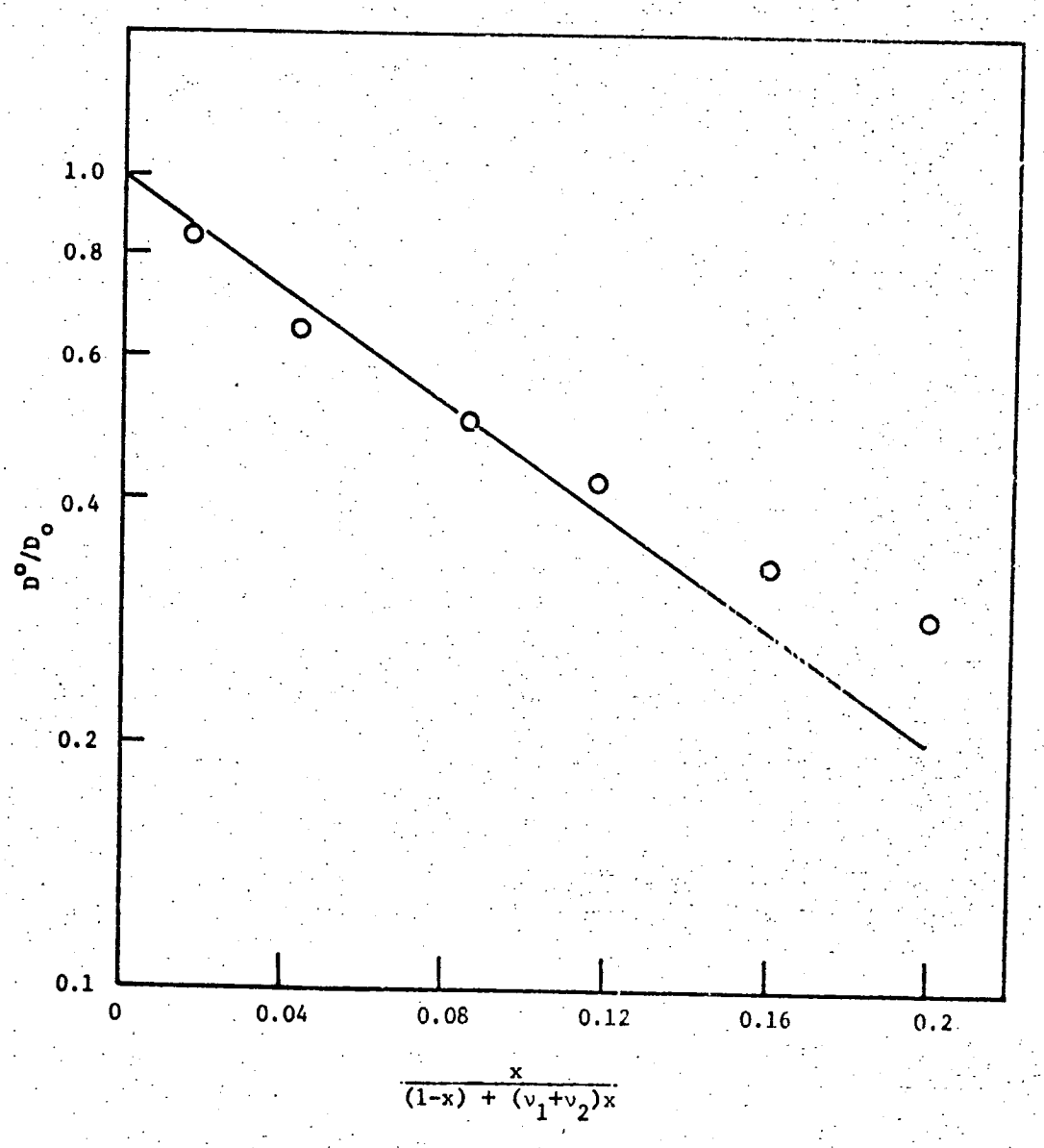

Figure 4.5-3. $\ln D^o/D_o$ vs. Species Fraction for O_2 at 25°C.

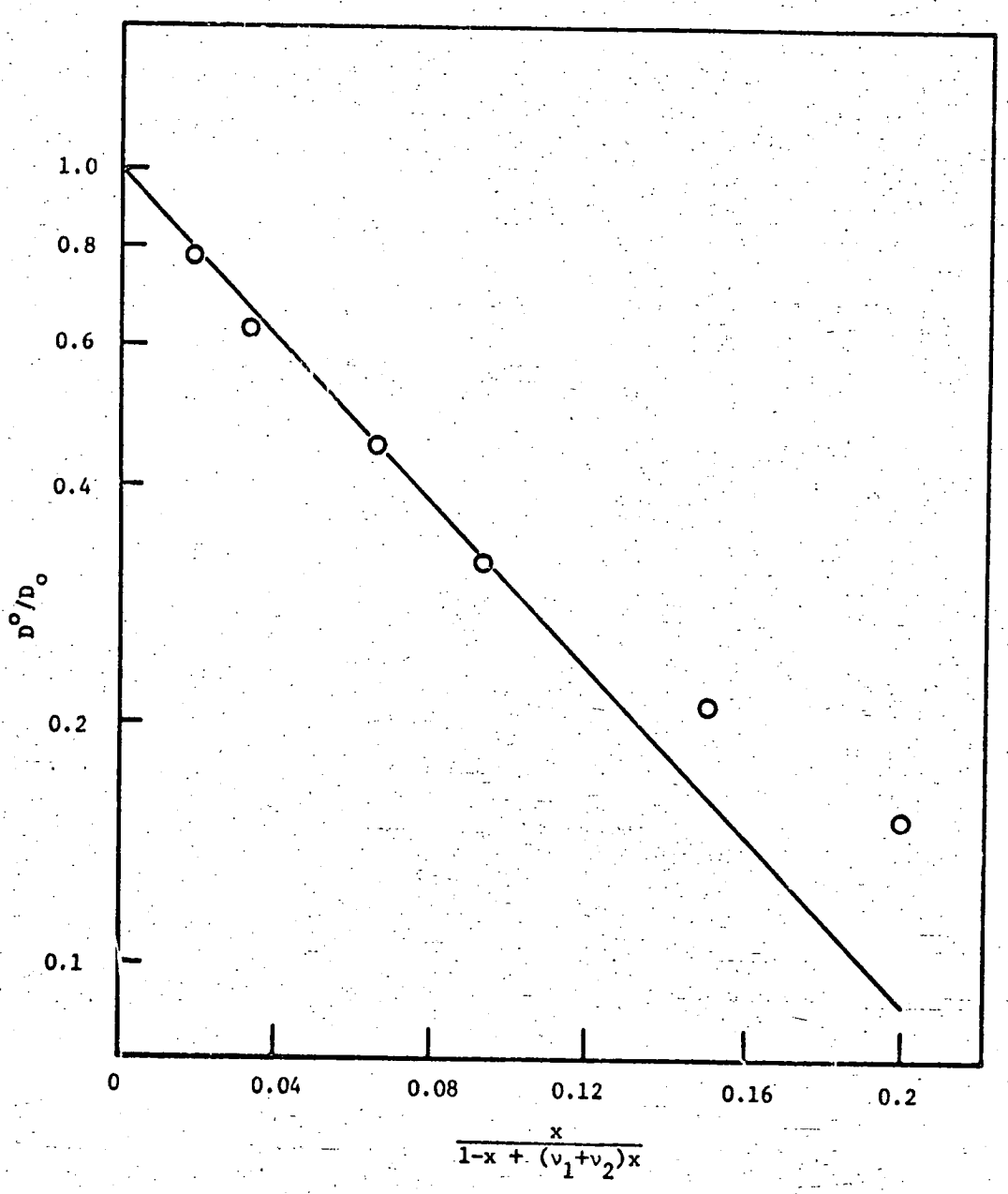

Figure 4.5-4. $\ln D^o/D_o$ vs. Species Fraction for H_2 at 25°C.

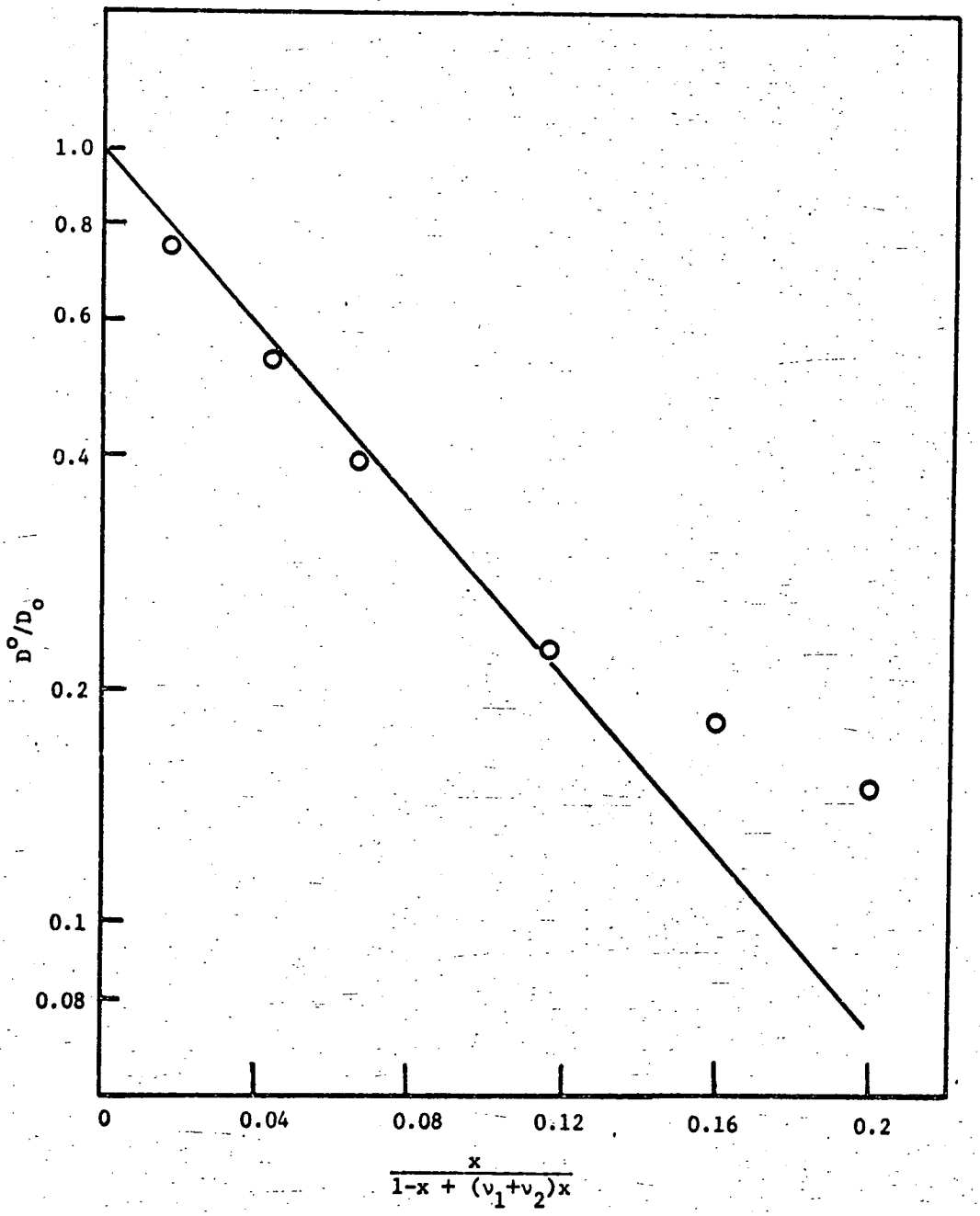

Figure 4.5-5. $\ln(D^o/D_o)$ vs. Species Fraction for O_2 at 60°C.

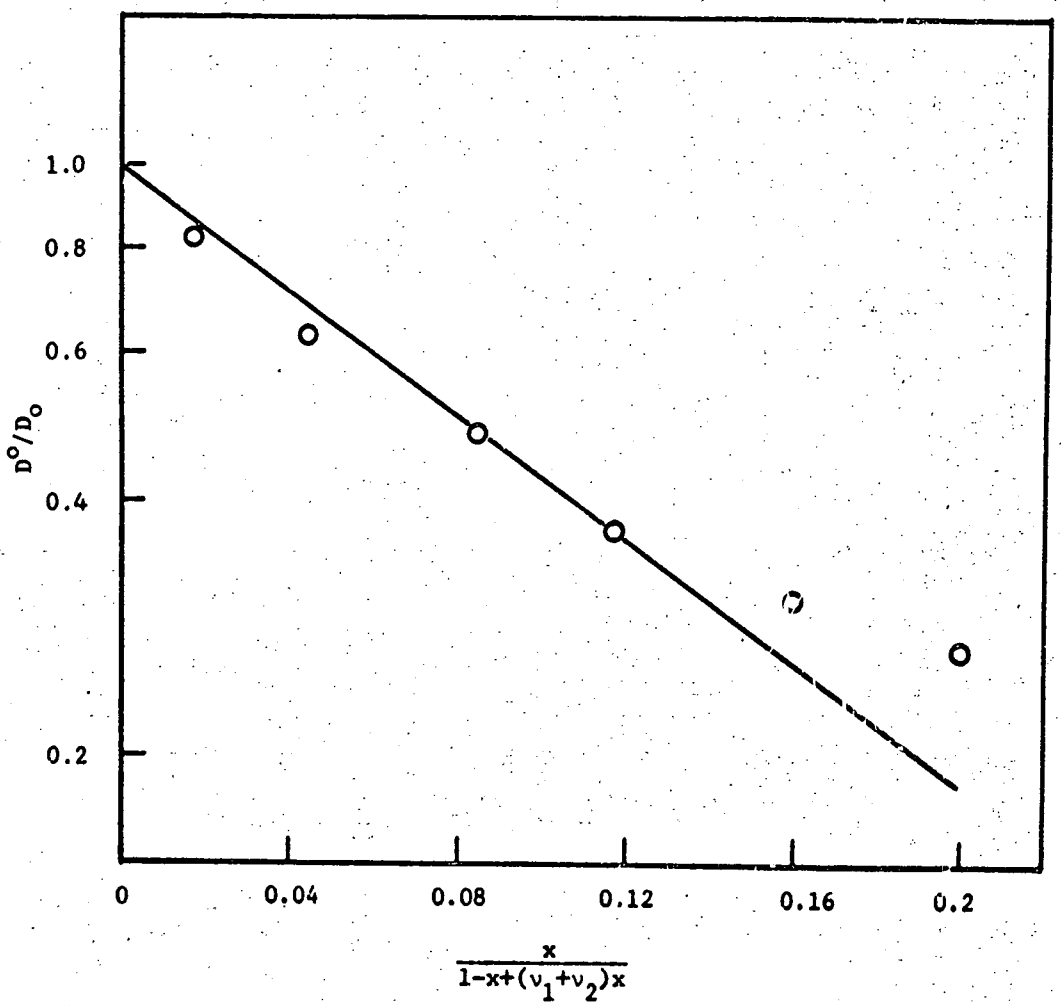

Figure 4.5-6. $\ln D^o/D_o$ vs. Species Fraction for H_2 at 60°C.

These assumptions would not be valid at high concentration because association of the ions will be important. Thus, the definition of species fraction must be modified. Therefore, these assumptions limit the application of the theory to the solutions which contain not more than 35% KOH.

As shown in Figure 4.4-3, the plot of D^o vs. weight percent LiOH for oxygen is linear. This relation was also predicted by Ratcliff and Holdcroft (40) in their modification of absolute reaction rate theory for dilute electrolyte solutions.

Values of the diffusion activation energy for oxygen and hydrogen in potassium hydroxide solutions are presented in Table 4.5-3 and 4.5-4.

4.5.4 Conclusions and Recommendations

The constancy of $D\,\mu/T$ at constant temperature and the linearity of $\ln D/T$ vs. $1/T$ will allow the interpolation of existing data for intermediate temperatures. Extrapolation should be done with care, since the linearity of $\ln D/T$ vs. $1/T$ is valid only when A and B in Equation 4.5-1 are constant. However, these terms are not, in general, constant over wide ranges of temperature.

The modified absolute rate theory predicts moderately well the effect of concentration on diffusion coefficients up to 35% KOH solutions, but it fails at higher concentrations. This shows the inadequacy of the theory, and a more rigorous theory is required for concentrated gas-electrolyte systems. To develop a sound theory for diffusion of gases in electrolytes, it is suggested that a systematic investigation should be made on the effects of electrolyte

concentration, type of electrolyte, molecular size and structure of solute, on the diffusivity of the solute. Such an investigation, taking into account the effects of molecular properties, could be used as a basis for developing a general theory for diffusion in electrolytes.

Table 4.5-3
Activation Energy for Hydrogen Diffusion in KOH Solution

Wt % KOH	Activation Energy cal/g.mole
0	4158
13	4245
24	4301
32.5	4351
42.5	4351

Table 4.5-4
Activation Energy for Oxygen Diffusion in KOH Solution

Wt % KOH	Activation Energy cal/g.mole
0	3896
10.2	3972
19.0	3868
32.5	3992
42.5	3939

5. Mutual Diffusion in Aqueous KOH Solutions

In hydrogen-oxygen fuel cells the reactions at the electrodes may be written as

Anode: $H_2 + 2OH^- = 2H_2O + 2e$ (5.0-1)

Cathode: $O_2 + 2H_2O + 4e = 4OH^-$ (5.0-2)

Thus, the mass transfer processes at each electrode involve diffusional fluxes of both the reactant gas and of water. Although the original proposal did not include work on mutual diffusion of water, it was concluded that a fuller understanding of the role played by diffusion of water in fuel cell electrolytes was of considerable importance and this work was undertaken with the concurrence of the technical representations of NASA.

The present work involved the measurement of mutual diffusion coefficients in aqueous KOH solutions for concentrations up to saturation over the temperature range 25° - 75°C. Similar studies in LiOH could not be included for lack of time, but these are planned for the near future.

5.1 Apparatus and Experimental Procedure

Liquid diffusion coefficient measurements have considerably exercised the ingenuity of experimentalists. This is evidenced from the great variety of experimental methods that have been devised. All of these methods may be divided into steady-state methods based on Fick's first law, $J = - D \frac{\partial C}{\partial z}$, and unsteady-state methods based on Fick's second law, $\frac{\partial C}{\partial t} = \frac{\partial}{\partial z} (D \frac{\partial C}{\partial z})$.

In the statements of Fick's laws, J is the molar flux referred to a molar average velocity, D is the diffusivity, C is the concentration of diffusing substance, and z is the direction in which diffusion occurs. Strictly speaking, Fick's laws are only approximations, and it is necessary to consider diffusion of all components in the system. However, if one defines flows with respect to a plane across which no transfer of volume occurs, then both diffusion coefficients of a binary system are equal and one can write

$$D_1^v = D_2^v = D_{12}^v = D \qquad (5.0.3)$$

where subscripts 1 and 2 refer to components 1 and 2, respectively. This common coefficient is then termed a mutual diffusion coefficient.

Liquid diffusion measurement techniques have been the subject of numerous reviews and books. Johnson and Babb (51) have reveiwed the experimental techniques for measuring liquid diffusion coefficients of non-electrolytes. Harned (76), and Harned and Owen (77) have presented in a systematic form an analysis of the most accurate determinations of diffusion coefficients of electrolytes. More recently Robinson and Stokes (78), and Geddes and Pontius (79) have described methods for the measurements of diffusion coefficients, while Himmelblau (32) has reviewed methods for the measurement of diffusion coefficients of dissolved gases in liquids. The most precise techniques today appear to be those utilizing optical methods, wherein changes of concentration with distance and time are analyzed continuously in a cell.

In the literature on diffusion and its measurement the diaphragm cell method figures prominently as one which best combines accuracy with experimental simplicity, and it was chosen for the present work. By confining

the diffusional process to the pores of a sintered glass, plastic, or metal diaphragm this technique avoids most of the difficulties inherent in the earlier methods, such as errors due to thermal and mechanical convection. Also, the use of large concentration gradients considerably reduces the time for a measurement.

Since this technique has been the subject of exhaustive reviews by Gordon (80), and recently by Gubbins and Bhatia (52), only a brief discussion is presented here. Subsequent sections describe details of the experimental apparatus and procedure used, with emphasis on special precautions needed for the systems studied here.

5.1.1 The Diaphragm Cell Method

A Stokes' type cell consists of a porous diaphragm connecting two compartments in each of which the respective liquid concentrations are maintained uniform. Diffusion is allowed to take place, and from the change in concentrations of the liquid in the two compartments and the time of the run the diffusion coefficient is evaluated. An initial diffusion period is allowed in order to establish a linear concentration gradient through the diaphragm. This is followed by the diffusion run, for which it is assumed that the diaphragm is in a quasi-steady state. Barnes (81) has shown that this assumption introduces negligible errors. Figure 5.1-1 gives the initial and final conditions in a diaphragm cell. If the diaphragm be assumed to offer an effective cross-section A and a path L to the diffusing liquids, then it has been shown (78) that the diaphragm cell integral coefficient $\bar{D}$ is given by

$$\bar{D} = \frac{1}{\beta t} \ln \frac{C_1 - C_2}{C_3 - C_4} \qquad (5.1\text{-}1)$$

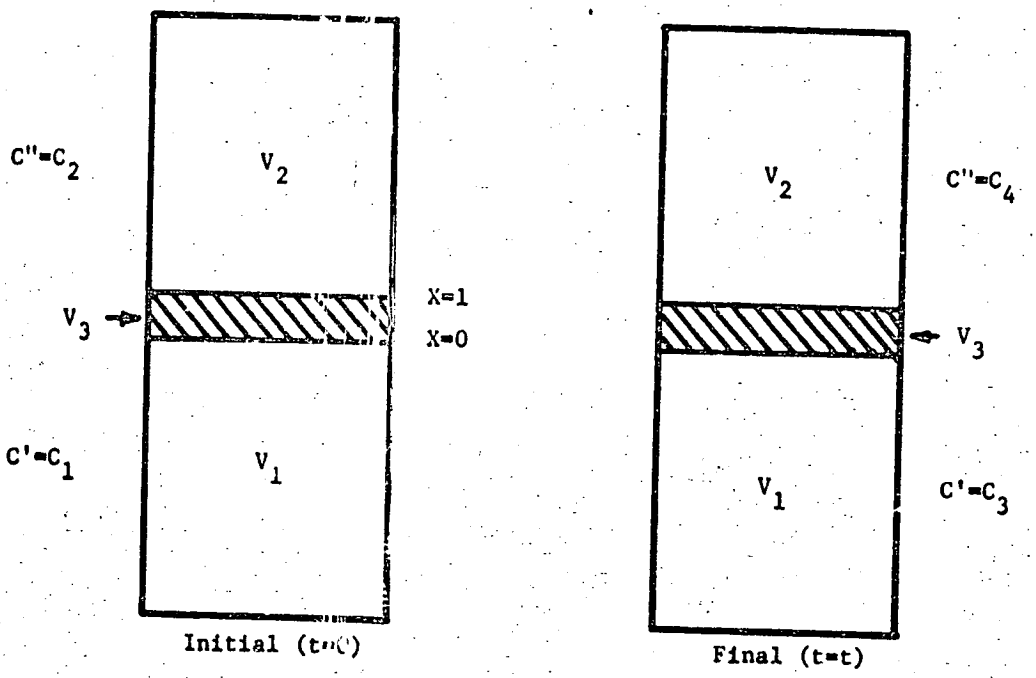

Figure 5.1-1. Initial and Final Conditions in a Diaphragm Cell.

where

β = cell constant

$$= \frac{A}{L} \cdot \left(\frac{1}{V_1} + \frac{1}{V_2} \right) \qquad (5.1\text{-}2)$$

$$\bar{D} = \frac{1}{t} \int_0^t dt \; \frac{1}{C' - C''} \int_{C''}^{C'} D\,dC \qquad (5.1\text{-}3)$$

$$C' = \frac{C_1 + C_3}{2} \quad \text{and} \quad C'' = \frac{C_2 + C_4}{2}$$

The initial concentration C_1 of the lower compartment is obtained by a material balance and is given by

$$C_1 = C_3 + (C_4 - C_2) \left[\frac{V_2 + V_3/2}{V_1 + V_3/2} \right] \qquad (5.1\text{-}4)$$

V_1, V_2, V_3 are the volumes of the lower compartment, upper compartment and the diaphragm, respectively. This diffusion coefficient obtained from the diaphragm cell measurement is a double average over the concentration and time, termed the integral coefficient. From these $\bar{D}$ values, the differential diffusion coefficient D for a given concentration can be determined by procedures discussed in Section 3.5.

5.1.2 Experimental Apparatus

For the present work diaphragm cells of the modified Stokes' type (78) were employed. Figure 5.1-2 and Figure 5.1-3 give details of construction and the mounting arrangement of one such cell. The cells were fabricated from Plexiglass, and diaphragms employed were of Teflon (Grade G, 9μ). Compartment volumes varied from 30 ml. to 45 ml. All glass joints and stopcock bearing surfaces were Teflon-clad. This

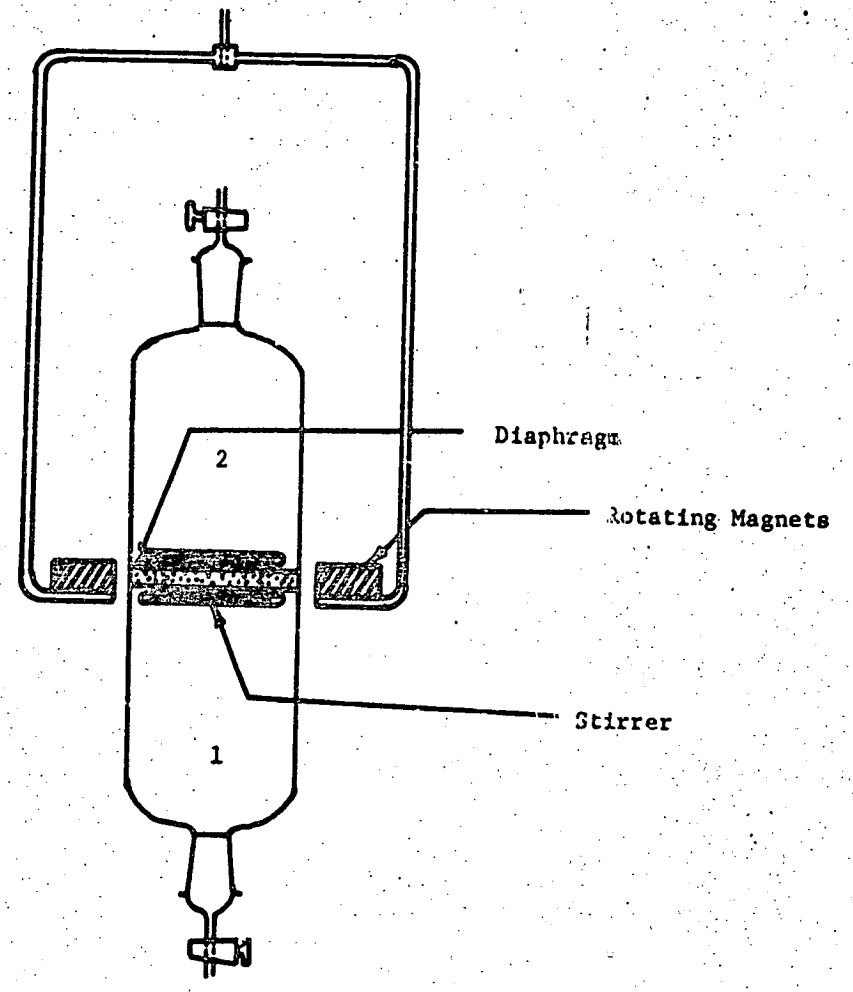

Figure 5.1-2. Diaphragm Cell.

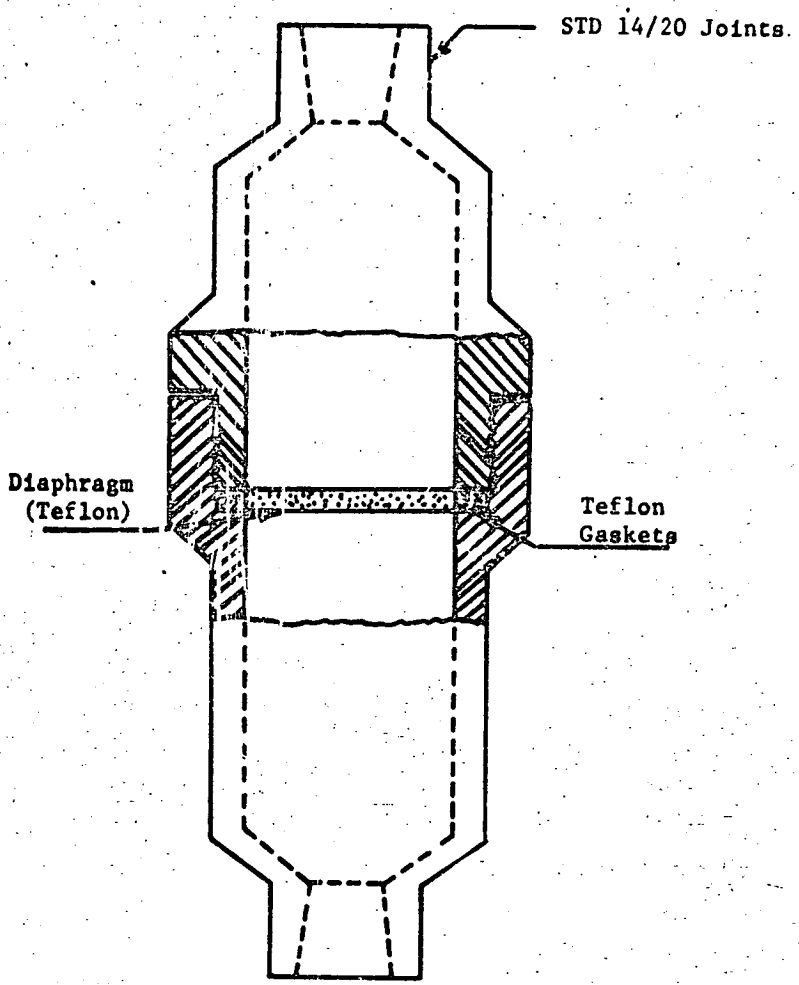

Figure 5.1-3. Diaphragm Cell (Plexiglass).

Scale Full Size

ensured vacuum-tight joints without the use of greases, which might have contaminated the diaphragm. Stirrers consisted of thin iron wires enclosed in glass and were rotated by externally mounted magnets at 48 rpm. A single AC motor (1/70 HP) was used to rotate the magnets through a pulley arrangement. Special silicone rubber 'O' rings were employed as belts. A Fisher proportional temperature controller ($\pm 0.05^{\circ}C$) was used to control the constant temperature stainless steel bath. A laboratory vacuum pump was used for filling the cells and degassing the solutions. Solutions were prepared by diluting a highly pure stock solution having a carbonate content of less than 0.02%. Adequate precautions were taken to prevent CO_2 absorption, and this was checked by periodic titration. Specially distilled (all glass/Teflon still) water was used after degassing to prepare all solutions. Potassium chloride used for calibration purposes was analytical grade and was used as such without further purification. Hydrochloric acid solutions were prepared from reagent grade concentrated acid. Thermometers, checked for accuracy against NBS calibrated thermometers, were used.

5.1.3 Experimental Procedure

The procedure employed was essentially that of Stokes (78). The procedure for filling the cell has been described in detail elsewhere (52). Briefly, it involves evacuation of the cell, followed by introduction of pure degassed water, care being taken to ensure that the diaphragm was completely filled with liquid. The cell was then thermostatted and water was carefully removed from the upper cell compartment, and replaced by the KOH solution, this solution having been previously brought to the desired temperature. The time of the diffusion run varied from

about 2 days at 25°C to 15 hours at 75°C, because of the high value of the diffusion coefficient at the latter temperature. After a run was completed, the cell was removed from the bath and the top compartment carefully emptied. The cell was then quickly inverted (this marked the end of the run) and liquid from the other compartment was decanted. Samples from both compartments (after cooling to room temperature) were then analyzed by titrating with standard hydrochloric acid. Duplicate titrations agreed to within 0.02 ml. Analyses of solutions before and after the experiment showed negligible change in the carbonate content.

For this work the solutions were not replaced by fresh solutions after the preliminary diffusion period. Instead a time correction for the unsteady period was applied as described by Bhatia (68), and Gubbins and Bhatia (52). An effective diffusivity $\bar{D}'$ during the unsteady state period is defined as

$$\bar{D}' = \frac{1}{\beta' t} \ln \frac{C_1 - C_2}{C_3 - C_4} \qquad (5.1\text{-}5)$$

where

$$\beta' = \frac{A'}{L'} \left(\frac{1}{V_1} + \frac{1}{V_2} \right)$$

A', L' are the apparent area and thickness of the diaphragm, respectively. It has been found that if the time for the total diffusional run is corrected by the factor

$$2 \sum_{n=1}^{\infty} (-1)^n \left(\frac{-pL'^2}{\bar{D}' \pi^2 n^2} \right)$$

steady-state conditions may be assumed for the total run. This procedure was employed to calculate the corrected integral diffusion coefficients. A material balance check for the diffusional runs was performed with the help of Equation 5.1-4. The cell compartment and diaphragm volumes were estimated by a series of weighings with water.

After an experiment was completed the cells were carefully cleaned, first with water, and then with dilute hydrochloric acid. This was continued until repeated water washings showed no trace of alkali.

5.1.4 Calibration of Cells

Since the ratio A/L for a diaphragm is not conveniently determinable, most experimenters use the method of Northrop and Anson (82) of characterising the diaphragm by calibration with a solute of known diffusion coefficient. Although there is still disagreement about the best choice of a calibration standard, most workers use KCl since accurate diffusion data of Harned and Nuttall (76) is available. For this work both KCl and HCl were used for calibration since accurate data in a suitable form is also available for the latter (83). Also, since HCl is one of the fastest diffusing electrolyte, diffusional times were short. One of the cells which was calibrated using KCl was used to check the integral coefficient for HCl tabulated by Stokes (83). Table 5.1-1 shows the close agreement obtained.

TABLE 5.1-1

Integral Diffusion Coefficients of HCl at 25°C (C_2=0)

C_1	Stokes Value $\bar{D}$	This Work $\bar{D}$
1.0246	3.220	3.273

The solutions were analyzed by simple titrations using a microburet. KCl solutions were titrated against standard $AgNO_3$ using dichlorofluorescein as indicator, and standard KOH was used to titrate HCl samples with phenolphtalein as indicator. Table 5.1-2 shows the reproducibility of the β values for the cells, and the agreement was within $\pm 0.7\%$. Measurements 1 and 2 represent replicate determinations made at the same time near the start of the measurements. Measurement 3 was made toward the end of the measurements in order to check on possible changes of β with time. Such changes might arise from wear of the diaphragm due to action of the stirrers, in which case β would increase with time. However, the values shown agree within experimental error with those made earlier, so that any such effect is small.

TABLE 5.1-2

Calibration Constants for the Cells

Measurement	Cell I	Cell II	Cell III
1	0.1450	0.2380	0.1814
2	0.1465	0.2384	0.1793
3	0.1474	0.2377	0.1789

There does not seem to be any evidence of the variation of the cell constant with temperature and most experimentalists have assumed it to remain constant. Chang and Wilke (84) have presented experimental measurements of cell constants at various temperature, which indicate the cell constant is essentially invariant with temperature.

5.1.5 Calculation of Differential Diffusion Coefficients

The diaphragm cell integral coefficient $\bar{D}$ is a complicated double average coefficient given by Equation 5.1-3, and is not simply converted to the differential diffusion coefficient D, especially when there is an appreciable volume change on mixing.

For a binary system the flux past a stationary point in terms of the mutual diffusion coefficient is given by

$$\underline{N}_A = - D \nabla C_A + C_A(\underline{N}_A \bar{V}_A + \underline{N}_B \bar{V}_B) \qquad (5.1\text{-}6)$$

where $\underline{N}_i$ = molar flux of i relative to stationary coordinates

The experimentally measured diffusivities will differ according to the geometry and convective flow conditions of the measuring device, unless the last term in the above equation is also accounted for. The quantity in the parenthesis represents the volume-average velocity and in order that the measured diffusion coefficient equal the mutual diffusion coefficient D, this volume-average velocity must be zero at all points of the diffusion path. This condition is exactly fulfilled for diaphragm cells only if the partial molal volumes of each component are constant in the range of concentration over which the experiment is performed. For the system KOH-water, calculations are presented in Section 5.1-6 to show that the volume change effects, though not entirely absent, are insignificant.

In recent years various papers have appeared on the analysis of liquid diffusivity measurements for diaphragm cells which incorporate volume changes on mixing. Dullien and Shemilt (85), and Robinson (86) have presented equations for calculating differential diffusivities

in such systems. However Olander (87) claims that they erred in their derivations, and, himself recognizing the considerable mathematical difficulties which the problem in its completely rigorous form poses, has presented equations which permit the calculation of an approximate correction factor. He also gives a rapid method of checking whether volume change effects are significant for a particular system. Using the latter procedure calculations have been made for the KOH-water system and the results are presented later. The calculations show that the volume change effects on diffusivities are insignificant for this system.

The method adopted in this work for calculating differential diffusivities is that of Stokes (83). He defines $\bar{D}^o$ as the integral diffusion coefficient for a run of vanishingly short duration given by

$$\bar{D}^o = \frac{1}{C} \int_0^C D dC \qquad (5.1\text{-}7)$$

Gordon (80) has shown that $\bar{D}$ is related to the differential diffusion coefficient D by the equation

$$\bar{D} = \frac{1}{(C'_m - C''_m)} \int_{C''_m}^{C'_m} D dC \qquad (5.1\text{-}8)$$

where $C'_m = (C_1 + C_3)/2$ and $C''_m = (C_2 + C_4)/2$. Denoting $\bar{D}^o(C'_m)$ and $\bar{D}^o(C''_m)$ as the values of $\bar{D}^o$ with initial concentrations C'_m and C''_m respectively, it is easily shown that

$$\bar{D}^o(C'_m) = \bar{D} - (C''_m/C'_m)\,[\bar{D} - \bar{D}^o(C''_m)] \qquad (5.1\text{-}9)$$

This equation permits the estimation of $\bar{D}^{o}(C_m')$ provided both $\bar{D}^{o}(C_m'')$ and $\bar{D}$ are known.

Fortunately it turns out that a plot of $\bar{D}^{o}(C_m')$ versus $(C_m')^{\frac{1}{2}}$ lies within 1% of that of $\bar{D}$ versus $(C_1)^{\frac{1}{2}}$, and hence a solution of Equation 5.1-9 is possible by a short series of approximation.

A curve of $\bar{D}$ versus $(C_1)^{\frac{1}{2}}$ is plotted and extrapolated to the Nernst limiting value. From this a first approximation to $\bar{D}^{o}(C_m'')$ is read off and substituted in Equation 5.1-9 and $\bar{D}^{o}(C_m')$ values obtained. These values of $\bar{D}^{o}(C_m')$ are then plotted against $(C_m')^{\frac{1}{2}}$ to give a second approximation to $\bar{D}^{o}(C_m'')$ which are again substituted in Equation 5.1-9. The resulting second approximation to $\bar{D}^{o}(C_m')$ is found not to change on continuing this process. This $\bar{D}^{o}$ data is then plotted against $(C)^{\frac{1}{2}}$ and from this D values are readily obtained as follows:

Differentiating Equation 5.1-7 we get

$$\bar{D}^{o} + C\,\frac{d\bar{D}^{o}}{dC} = D$$

or

$$D = \bar{D}^{o} + \frac{(C)^{\frac{1}{2}}}{2}\,\frac{d\bar{D}^{o}}{d(C)^{\frac{1}{2}}} \qquad (5.1\text{-}10)$$

The slopes $\dfrac{d\bar{D}^{o}}{d(C)^{\frac{1}{2}}}$ are obtained graphically.

A sample calculation of the above type is shown in Section 5.1-7.

5.1.6 Volume Changes on Mixing

If there is no volume change on mixing during the diffusion process, the volume on either side of the apparatus-fixed reference plane will be unchanged. This means that the flux referred to the center of volume is the same as that referred to stationary coordinates. This condition of zero volume change is fulfilled exactly if the partial molar volume of each component is independent of concentration. Under these circumstances the experimental differential diffusion coefficient will be identical with D_{12}^{v}. For the KOH-water system, the above condition is not exactly fulfilled; however, calculations are presented below to prove that the correction due to volume changes is negligible. For these the method of Olander (87) is employed. He derived an equation from which it can be quickly ascertained whether or not the volume change corrections are necessary for a particular system. In the following calculations Olander's nomenclature is used. Subscripts: 0,1 lower and upper compartments respectively. Superscripts: i, f, m initial, final and mean conditions respectively. Olander's Equation (14) gives

$$\bar{D}\left[\frac{1 - AG}{1 - r\langle\bar{V}_s\rangle\,\delta_o}\right] = D^o + \sum_{j=1} \zeta_{\cdot}\left[\frac{1 - r\langle\bar{V}_s\rangle\,\delta_j/\zeta_j}{1 - r\langle\bar{V}_s\rangle\,\delta_o}\right] a_j \qquad (5.1\text{-}11)$$

where $\bar{D}$ = measured integral diffusion coefficient

$$\equiv \frac{1}{\beta t}\ln(\theta_i/\theta_f)$$

From Equation 5.1-11 it is only necessary to evaluate the bracketed terms for an experiment which involves the largest driving force in the region of largest r. If these differ from unity by the same order as the experimental precision, then the correction due to volume changes would be barely significant.

Akerlof and Bender (88) give the following equations for the apparent partial molal volume (ϕ) of potassium hydroxide solutions.

a) For concentrations up to m_{12}:

$$\phi = \phi_1^o + K_1(m)^{\frac{1}{2}}$$

b) For concentrations above m_{12}:

$$\phi = \phi_2^o + K_2(m)^{\frac{1}{2}} + b_2 m$$

c) Values of constants at 60°C

T^oC	ϕ_1^o	ϕ_2^o	K_1	K_2	b_2	$(m_{12})^{\frac{1}{2}}$
60°	5.2479	2.2796	3.3570	5.6131	-0.4279	2.508

From these the partial molal volumes of potassium hydroxide ($\bar{V}_{KOH}$) are calculated by using the relation

$$\bar{V}_{KOH} = \phi + \frac{1}{2} m^{\frac{1}{2}} \frac{d(\phi)}{dm^{\frac{1}{2}}} \qquad (5.1\text{-}13)$$

The partial molal volume of water is calculated using the relation

$$V = n_{KOH}\bar{V}_{KOH} + n_{H_2O}\bar{V}_{H_2O} \qquad (5.1\text{-}14)$$

where V = molal volume of the solution.

$\theta = c_o - c_1$

A = a parameter in Olander's Equation 10

$= r\bar{V}_{sb}$ when $c_1^i = 0$

and $\bar{V}_{sb}$ is defined by the relation

$$\frac{1}{\bar{V}_s} = \frac{1}{\bar{V}_{sb}} + QC \qquad c_o^i > C > c_1^i \qquad (5.1\text{-}12)$$

$\bar{V}_s$ = partial molar volume of the solvent

Q = a constant

The quantity r is given by

$$\bar{V}_{KOH}/\bar{V}_{H_2O} = K + rC \qquad c_1^i < 0 < c_o^i$$

$$G = \frac{2(c_o^i + c_1^i)(\theta_i - \theta_f) - \frac{3}{2}(\theta_i^2 - \theta_f^2) + \theta_i^2 \ln(\theta_i/\theta_f)}{4\ln(\theta_i/\theta_f)}$$

$\langle \bar{V}_s \rangle$ = average value of the solvent molar volume between upper and lower compartments.

$\delta_j = c_o^m \zeta_{j+1} = \zeta_{j+2}$

D^o = diffusivity at infinite dilution

$$\zeta_j = \frac{(c_o^m)^{j+1} - (c_1^m)^{j+1}}{(j+1)(c_o^m - c_1^m)}$$

The coefficients a_j are defined by the expansion

$$D = D^o + \sum_{j=1} a_j C^j$$

The ratio $\bar{V}_{KOH}/\bar{V}_{H_2O}$ was calculated and plotted against concentration; also $1/\bar{V}_{H_2O}$ against concentration was plotted in Figures 5.1-4 and 5.1-5. From these the largest slope of r and average value of $1/\bar{V}_{sb}$ were found to be 0.1075 liter/g.mole and 54.1 g.mole/liter, respectively. We shall use these for the following conditions for a hypothetical run.

$C_o^i = 5.532$ g.mole/liter $\qquad C_1^i = 0$

$C_o^f = 4.174$ g.mole/liter $\qquad C_1^f = 1.396$ g.mole/liter

$\theta_i = C_o^i - C_1^i = 5.532$ g.mole/liter $\qquad \beta = 0.1840$

$\theta_f = C_o^f - C_1^f = 2.778$ g.mole/liter $\qquad t = 50.5$ hours

$$\bar{D} = \frac{1}{\beta t}\ln(\theta_i/\theta_f) = \frac{1}{0.1840 \times 50.5 \times 3600}\ln\frac{5.532}{2.778} = 2.055 \times 10^{-5} \text{ cm}^2\text{sec}^{-1}$$

$$G = \frac{2(C_o^i + C_1^i)(\theta_i - \theta_f) - \frac{3}{2}(\theta_i^2 - \theta_f^2) + \theta_i^2\ln(\theta_i/\theta_f)}{4\ln(\theta_i/\theta_f)}$$

or

$$G = \frac{2(5.532)(5.532 - 2.778) - \frac{3}{2}[(5.532)^2 - (2.778)^2] + (5.532)^2\ln(5.532/2.778)}{4\ln(5.532/2.778)}$$

$$= 6.24978$$

$C_o^m = (1/2)(C_o^i + C_o^f) = 4.853$ g.mole/liter

$C_1^m = (1/2)(C_1^f + C_1^f) = 0.698$ g.mole/liter

$\zeta_1 = (1/2)(C_o^m + C_1^m) = 2.7755$

$\zeta_2 = (1/3)[(C_o^m)(C_1^m) + (C_1^m)^2] = 9.143$

$$\zeta_3 = \frac{(C_o^m)^4 - (C_1^m)^4}{4(C_o^m + C_1^m)} = 33.360$$

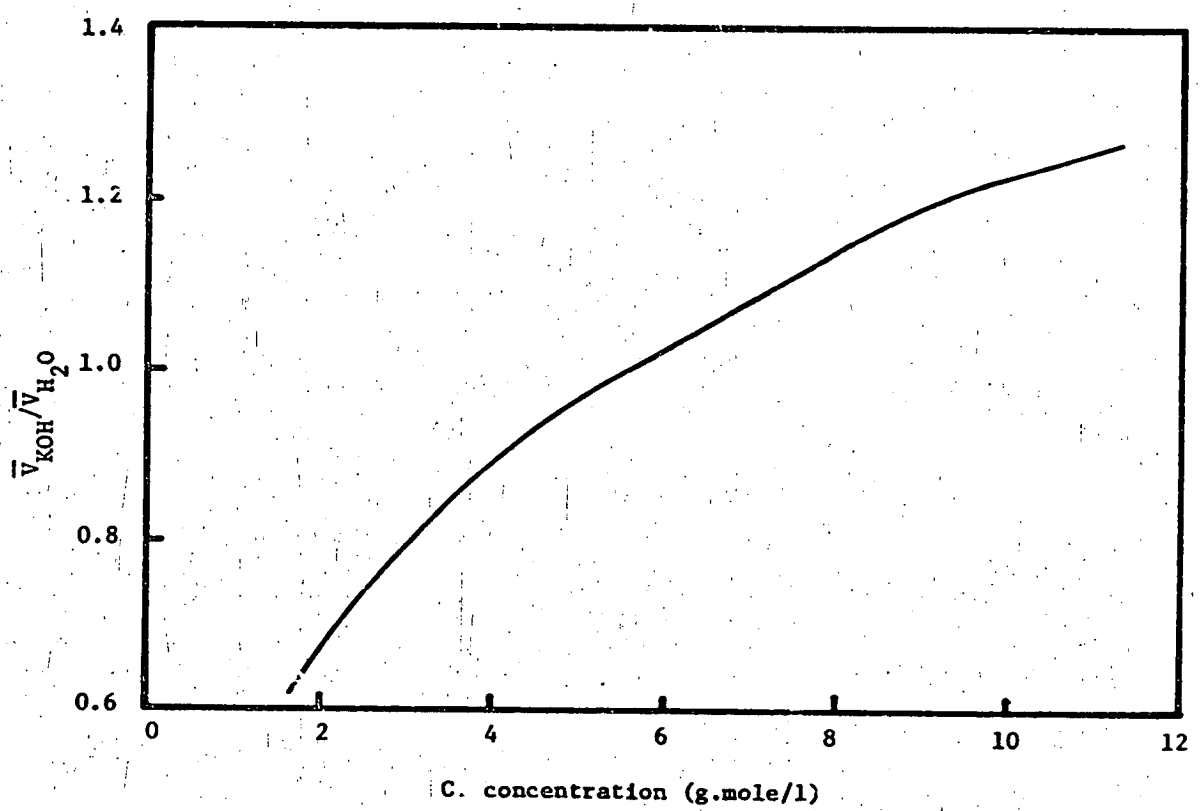

Figure 5.1-4. Partial Molal Volume Ratio for the Potassium Hydroxide-Water System at 60°C.

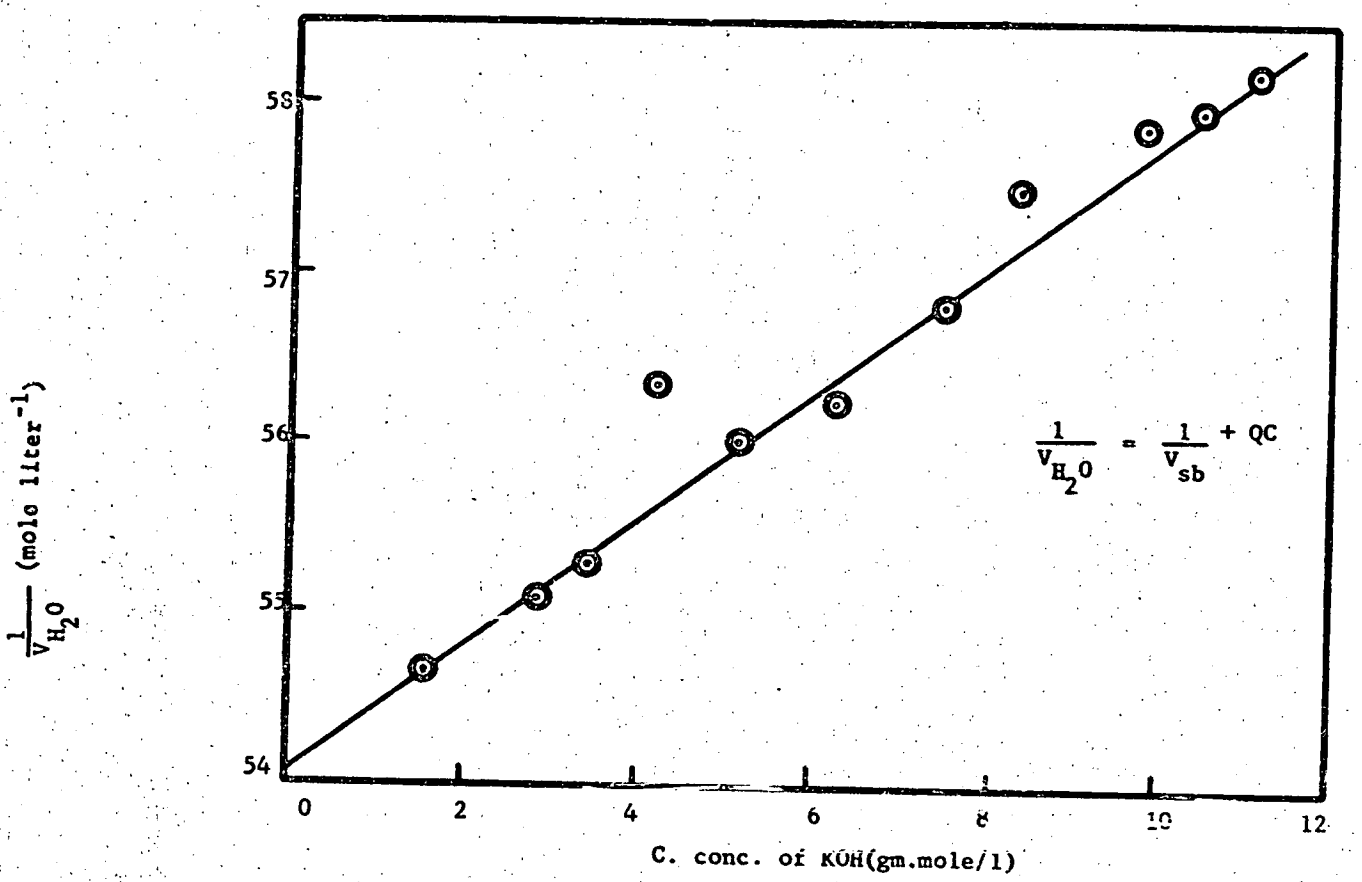

Figure 5.1-5 Reciprocal Partial Molar Volume of Water for the Potassium Hydroxide-Water System at 60°C.

$$\delta_o = c_o^m \zeta_1 - \zeta_2 = 4.3266$$

$$\delta_1 = c_o^m \zeta_2 - \zeta_3 = 14.069$$

$$\langle \bar{V}_s \rangle = \langle \bar{V}_{H_2O} \rangle = 17.8 \text{ ml} = 0.0178 \text{ liters}$$

For the case $C_1^i = 0$

$$A = r\bar{V}_{sb} = 0.001987$$

Then

$$\left[\frac{1 - AG}{1 - r \langle \bar{V}_s \rangle \delta_o} \right] = \left[\frac{1 - 0.0124183}{1 - (0.1075)(0.0178)(4.3266)} \right] = 0.99584$$

and

$$\left[\frac{1 - r \langle \bar{V}_s \rangle \delta_1/\zeta_1}{1 - r \langle \bar{V} \rangle \delta_o} \right] = \left[\frac{1 - 0.0097}{1 - 0.0083} \right] = 0.9986$$

Since both the bracketed terms differ from unity by very small factors, the correction due to volume changes is therefore insignificant. Because the above calculation was performed for the case for which volume changes should be most significant, it is concluded that in all cases the volume change effects will be negligible for potassium hydroxide solutions.

5.1.7 Calculation of Differential Diffusion Coefficients at 25°C

The method of Stokes (83) for extracting differential diffusion coefficients from diaphragm cell integral data is illustrated in Table 5.1-3 for aqueous KOH solutions at 25°C. Entries in the first two columns are the integral data which was plotted and smoothly extrapolated to the Nernst limiting value. From the initial and final concentrations entries in the third and fourth columns were computed. Corresponding to

Table 5.1-3

Mutual Diffusion Coefficients of Aqueous KOH Solutions at 25°C
(Method of Stokes)

1	2	3	4	5	6	7	8	9	10	11	12	13	14
$D \times 10^5$	$(C_l)^{\frac{1}{2}}$	$(C_m')^{\frac{1}{2}}$	$(C_m'')^{\frac{1}{2}}$	$\overline{D}^o(C_m'')$	s^*	$\overline{D}^o(C_m')$	$\overline{D}^o(C_m'')$	s^*	$\overline{D}^o(C_m')$	$(C)^{\frac{1}{2}}$	$\overline{D}^o$	$\frac{d\overline{D}^o}{d(C)^{\frac{1}{2}}}$	$D \times 10^5$
2.698	0.321	0.2921	0.1386	2.750	-0.0116	2.710	2.760	-0.0138	2.7122	0.2	2.738	0.3875	2.699
2.662	0.321	0.2863	0.1514	2.745	-0.0233	2.685	2.752	-0.0253	2.687	0.4	2.685	0.1487	2.695
2.694	0.321	0.2911	0.137	2.752	-0.0128	2.707	2.760	-0.0146	2.709	0.6	2.670	0.01	2.673
2.671	0.690	0.6300	0.2908	2.691	-0.0043	2.675	2.70	-0.0062	2.677	0.8	2.688	0.1458	2.746
2.667	0.690	0.6332	0.2877	2.692	-0.0051	2.672	2.70	-0.0067	2.674	1.0	2.730	0.275	2.867
2.740	1.025	0.9225	0.3939	2.671	0.0125	2.727	2.690	0.0091	2.731	1.2	2.800	0.3739	3.024
2.703	1.025	0.9214	0.3920	2.673	0.0054	2.698	2.689	0.0025	2.700	1.4	2.875	0.3956	3.152
2.909	1.442	1.338	0.5072	2.662	0.0354	2.873	2.668	0.0346	2.874	1.6	2.960	0.4253	3.300
2.890	1.442	1.283	0.5464	2.662	0.0413	2.848	2.668	0.04026	2.849	2.0	3.130	0.4259	3.556
3.191	2.135	1.881	0.8904	2.695	0.1111	3.080	2.698	0.1104	3.081	2.4	3.295	0.3750	3.745
3.176	2.135	1.882	0.8904	2.695	0.1076	3.068	2.698	0.1069	3.069	2.8	3.417	0.2584	3.779
3.459	2.768	2.503	1.251	2.805	0.1634	3.296	2.812	0.1617	3.298	3.2	3.500	0.100	3.660
3.502	2.768	2.500	1.254	2.803	0.1746	3.327	2.815	0.1729	3.329	3.5	3.53	0.0729	3.658
3.519	2.768	2.501	1.254	2.808	0.1789	3.341	2.815	0.1770	3.342				
3.553	3.268	2.923	1.374	2.803	0.1657	3.338	2.863	0.1525	3.400				
3.580	3.268	2.915	1.401	2.875	0.1627	3.417	2.875	0.1627	3.417				
3.602	3.268	3.025	1.186	2.780	0.1265	3.476	2.792	0.1246	3.477				
3.621	3.705	3.44	1.373	2.861	0.1212	3.500	2.854	0.1207	3.501				
3.664	3.705	3.38	1.334	2.842	0.1282	3.536	2.845	0.1277	3.537				

*S represents $\frac{C_m''}{C_m'} [\ \overline{D} - \overline{D}^o(C_m'')\ ]$

the concentrations in column four, the $\bar{D}^{\circ}(Cm'')$ values were read off as a first approximation from the plot. Using these $\bar{D}^{\circ}(Cm'')$ values, entries in column 6 were computed, and then using Equation 5.1-9 $\bar{D}^{\circ}(Cm')$ values were obtained. A second plot of $\bar{D}^{\circ}(Cm')$ versus $(Cm')^{\frac{1}{2}}$ was made and from this a second approximation to $\bar{D}^{\circ}(Cm'')$ was read off. (Column 8). Entries in columns 9 and 10 were computed as before. Finally a plot of $\bar{D}^{\circ}(Cm')$ versus $(Cm')^{\frac{1}{2}}$ was made and the smoothed data entered in columns 11 and 12. This was graphically differentiated and slopes $\frac{d\bar{D}^{\circ}}{d(C)^{\frac{1}{2}}}$ entered in column 13. Using Equation 5.1-10 the D values of column 14 were computed.

5.2 Experimental Results

Measured values of the integral diffusion coefficients at the 4 temperatures are shown in Table 5.2-1. For each condition of concentration and temperature replicate measurements were made and these are reported separately in the table. The precision of the measured $\bar{D}$ values was approximately ±0.7% in most cases. There is some artificial scatter in the data due to the different times of the diffusional runs and also due to different cells. All of the diffusion data were used in calculating $\bar{D}^{\circ}$ values. These were then smoothed by plotting and the differential values calculated as outlined in Section 5.1-7. They are given in Table 5.2-2.

The overall accuracy of the reported differential diffusivity values is estimated to be approximately ±2.5%. This value was obtained by considering the estimated errors in determining the time of the run, the concentrations, and the cell constant, errors involved in operating the cells, and errors in computing differential from integral diffusivities. More direct support for the quoted accuracy is provided by the close agreement obtained for measured integral coefficients of HCl with those available from the literature (see Table 5.1-1). Also, the data appears to agree well with the calculated Nernst limiting values, as seen from Figure 5.2-1, and also with the Onsager-Fuoss theory at low concentrations, as discussed in the next section.

TABLE 5.2-1

INTEGRAL DIFFUSION COEFFICIENTS OF AQUEOUS KOH SOLUTIONS*

(C_2 = 0)

25°C		45°		65°		75°	
C_1	$\bar{D}x10^5$	C_1	$\bar{D}x10^5$	C_1	$\bar{D}x10^5$	C_1	$\bar{D}x10^5$
0.103	2.70	0.103	3.87	0.103	5.89	0.690	6.80
0.103	2.66	0.103	3.92	0.103	5.79	0.690	6.84
0.103	2.69	0.477	3.86	0.477	5.68	0.912	7.28
0.477	2.67	0.912	3.90	0.912	5.84	0.912	7.23
0.477	2.67	0.912	3.87	0.912	5.89	1.906	7.64
1.050	2.74	1.906	4.14	1.906	6.07	1.906	7.54
1.050	2.70	1.906	4.10	1.906	6.10	4.156	8.36
2.080	2.91	4.156	4.65	4.156	6.75	4.156	8.29
2.080	2.89	4.156	4.68	4.156	6.78	7.008	8.49
4.555	3.19	7.008	5.08	7.008	7.02	7.008	8.46
4.55	3.18	7.008	5.01	9.846	7.12	9.846	8.69
7.668	3.46	9.846	5.11	9.846	7.13	9.846	8.60
7.668	3.50	9.846	5.11	12.616	7.25	12.616	8.74
7.668	3.52	11.742	5.19	12.616	7.27	12.616	8.87
10.667	3.55	12.616	5.24				
10.667	3.58	12.616	5.21				
10.667	3.60						
13.719	3.62						
13.719	3.66						

*The reported values of $\bar{D}$ are ($cm.^2 sec.^{-1}$) and the concentrations are (g.mole/l).

TABLE 5.2-2

DIFFERENTIAL DIFFUSION COEFFICIENTS OF AQUEOUS KOH SOLUTIONS

The reported values are $Dx10^5 (cm.^2 sec.^{-1})$

C(g.mole/l)	25°C	45°	65°	75°
0.040	2.70	3.89	5.76	6.70
0.160	2.66	3.83	5.68	6.89
0.360	2.67	3.86	5.73	6.94
0.640	2.75	4.05	5.96	7.29
1.000	2.87	4.15	6.22	7.72
1.440	3.02	4.36	6.49	8.11
1.960	3.15	4.61	6.74	8.45
2.560	3.30	4.85	6.91	8.64
4.000	3.56	5.21	7.17	8.98
5.760	3.75	5.29	7.30	8.89
7.840	3.78	5.26	7.30	8.74
9.925		5.15		
9.986		5.19		
10.240	3.66		7.27	8.80
12.250	3.66		7.16	
12.960				8.79

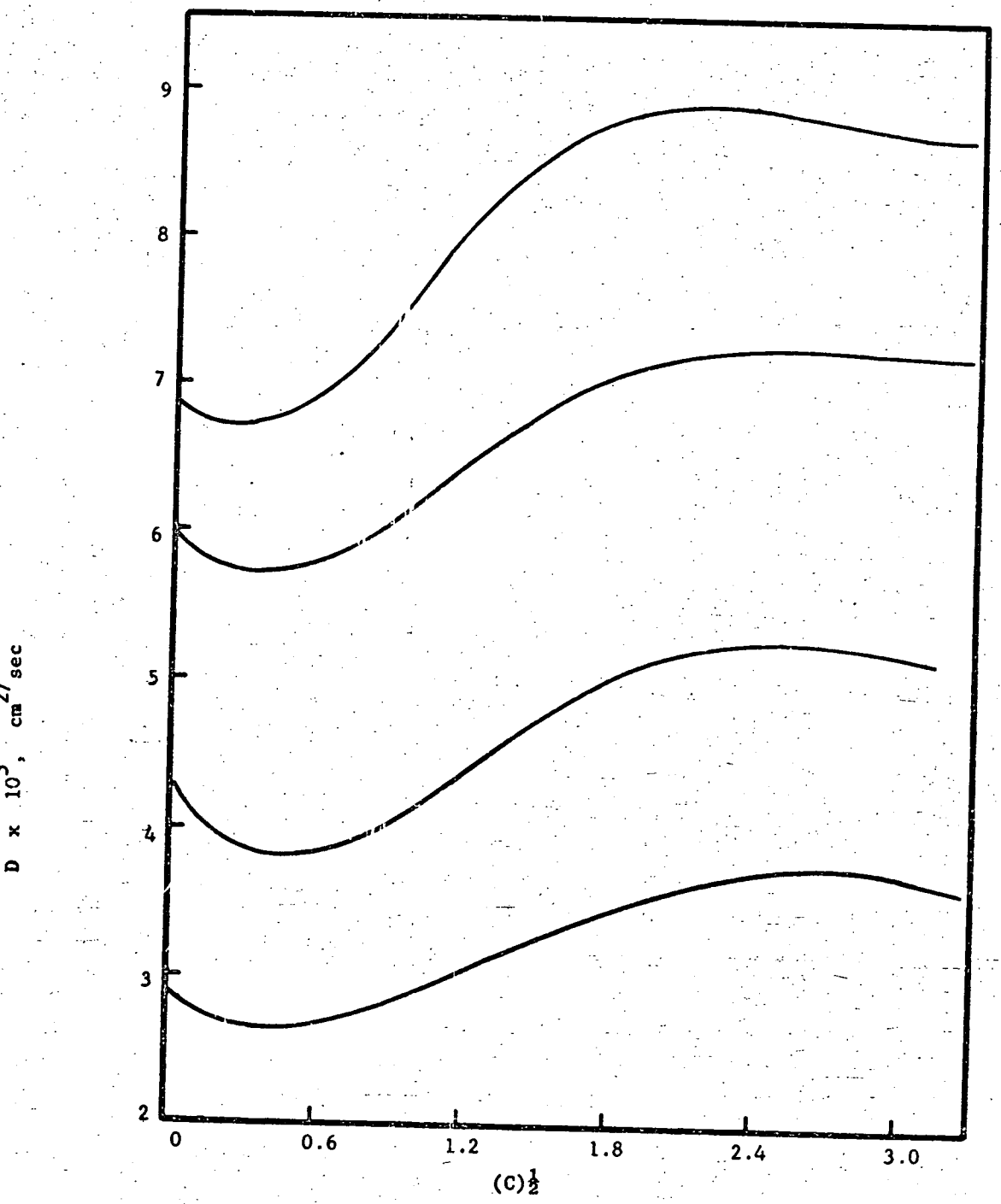

Figure 5.2-1 Diffusion Coefficients of Aqueous KOH Solutions

5.3 Discussion of Results

The concentration dependence of the diffusion coefficient at various temperatures is shown in Figure 5.2-1. In these plots the curves have been extrapolated to the calculated Nernst limiting values at C = 0. Each isotherm exhibits a minimum diffusivity at a concentration of approximately C = 0.2, and a shallow maximum at high concentrations, approximately C = 6. This complex concentration dependence is typical of diffusion in electrolyte solutions. Most electrolyte solutions show a minimum in the diffusion coefficient versus concentration curve at low concentrations but not all show the shallow maximum at higher concentrations. A similar shallow maximum is observed for concentrated solutions of sodium chloride.

The empirical relationship $D = A\exp(C/T)$, where A and C are approximately constant over moderate temperature ranges, is frequently used to describe the temperature dependence of D for a liquid of constant composition. Figure 5.3-1 shows a semilog plot of D versus T^{-1} at several compositions. The above relationship is seen to be obeyed, and may therefore be used in interpolating the data to other temperatures, and, with less confidence, in extrapolation.

The only rigorous theory of diffusion in electrolyte solutions is that of Onsager and Fuoss (89), and their approach is valid only for dilute solutions. Their final equation involves calculation of the electrophoretic correction terms and the calculation of these terms requires a choice of a suitable value for the ion diameter, $\overset{\circ}{a}$, characteristic of potassium hydroxide solutions. The value chosen was $\overset{\circ}{a} = 3.7\ \overset{\circ}{A}$. This value was obtained by comparing experimental activity coefficients for dilute

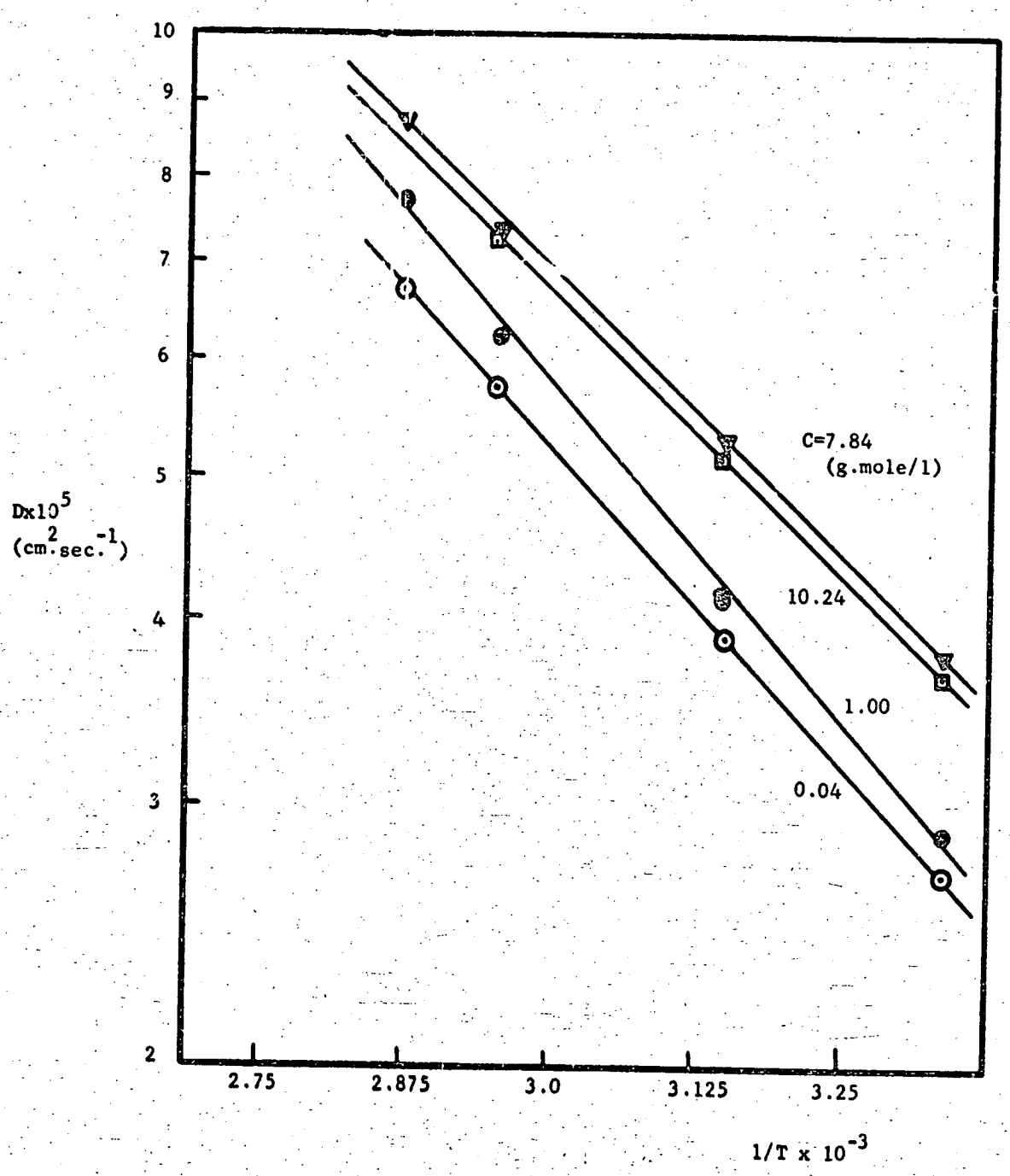

Figure 5.3-1 Log D versus 1/T for Aqueous KOH Solutions.

aqueous potassium hydroxide solutions with the theoretical expression given by the Debye-Huckel theory (90).

Table 5.3-1 shows values of the electrophoretic corrections calculated for potassium hydroxide solutions at 25°C, together with values for the thermodynamic factor and for the diffusion coefficient predicted by the Onsager-Fuoss theory. Activity coefficient data for the solutions was obtained from the e.m.f. measurements of Harned and Cook (90), and the slopes $\partial\gamma_{\pm}/\partial m$ were determined graphically. Accurate activity coefficient data at higher temperatures are not available for KOH solutions. Although vapor pressure data are available for this system up to 100°C (91), the data are not of sufficient accuracy to use the Gibbs-Duhem equation to obtain satisfactory values of the thermodynamic factor.

A comparison of the Onsager-Fuoss theory with the experimental data is included in Figure 5.3-2. The agreement is seen to be excellent at concentrations up to about 0.2 molar, but as the concentration rises above this value, the discrepancy between theory and experiment rapidly increases. The inadequacy of the theory at high concentrations is as expected, since it fails to take account of changes in the dielectric constant and viscosity with concentration, and of ionic hydration.

By using an approach similar to that followed by Ratcliff and Holdcroft (40), Bhatia derived an equation relating the diffusion coefficient to the species fraction of a particular component in an electrolytic solution (92). Thus

$$D^{id} = D_o \exp\left[-\frac{1}{RT}\,\frac{18C_n(\nu_1\delta_1 + \nu_2\delta_2)}{1000d - CM + 18C(\nu_1+\nu_2)}\right] \qquad (5.3\text{-}1)$$

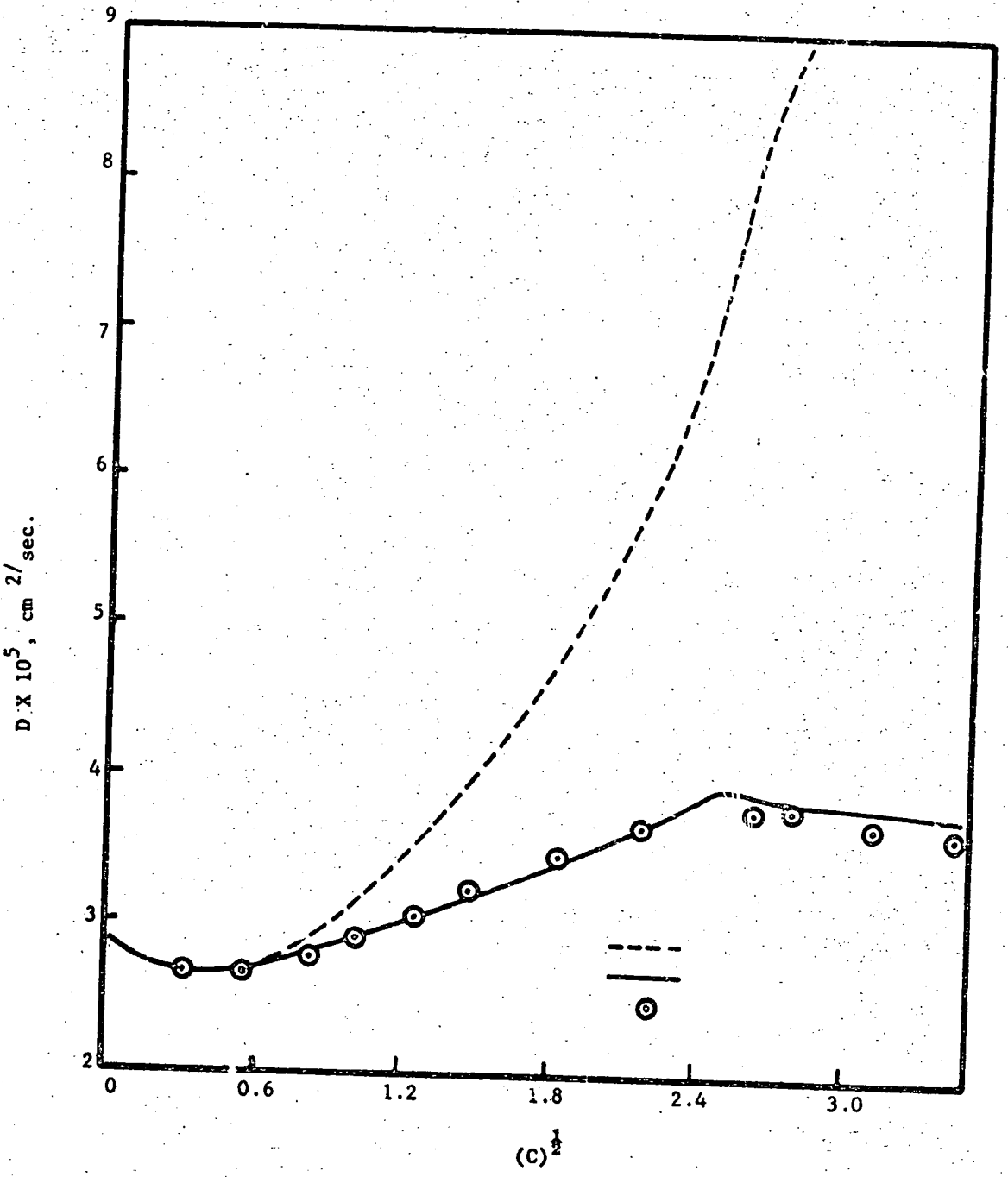

Figure 5.3-2 Diffusion Coefficients of Aqueous KOH Solutions at 25°C.

where D^{id} = diffusion coefficient corrected for non-ideality

D_o = diffusion coefficient at infinite dilution

C = concentration of the electrolyte, g.moles/l.

n = number of surrounding water molecules

ν_1 and ν_2 = number of ions of species 1 and 2 per molecule of electrolyte, respectively

δ_1 and δ_2 = activation energy perturbation parameters for species 1 and 2, respectively

d = density, g./cm.^{3}

M = molecular weight, g./g.mole.

A plot of $\ln(D^{id}/D_o)$ versus $C/[1000d - CM + 18C(\nu_1 + \nu_2)]$ should be approximately linear if the relation is obeyed. Values of D^{id} were calculated at 25°C using the experimental D values, together with values of the thermodynamic factor given in Table 5.3-1 and are plotted in Figure 5.3-3. Equation (5.3-1) is seen to be obeyed within experimental error for potassium hydroxide for concentrations up to about 8 molar. For higher concentrations there is some discrepancy between theory and experiment. It is estimated that the procedure used to determine slopes in evaluating the thermodynamic term may lead to errors of ±1%, and this may contribute to the scatter of experimental points in Figure 5.3-3.

The slope of the line in Figure 5.3-3 is $-18n(\delta_{K_+} + \delta_{OH_-})/RT$, and was found to have a value of +70.6. The value of $n(\delta_1 + \delta_2)$ for KOH at 25°C is then

$$n(\delta_{K_+} + \delta_{OH_-}) = 2{,}325 \text{ cal.(g.mole)}^{-1} \qquad (5.3\text{-}2)$$

Using this value for the perturbation parameter, theoretical values of the mutual diffusion coefficient were calculated using Equation (5.3-1),

TABLE 5.3-1

TEST OF ONSAGER-FUOSS THEORY

($\mathring{a}$ = 3.7 $\mathring{A}$ngstrom units)

(g.mole/l)	$-\Delta_1 x10^6$	$\Delta_2 x10^7$	$1+m\frac{d\ln\gamma}{dm}$	$(Dx10^5)_{calc}$ $cm.^2 sec.^{-1}$
0.101	0.3578	0.4192	0.93271	2.6465
0.298	0.5122	0.4377	0.94946	2.6803
0.694	0.6461	0.4625	1.02549	2.8815
1.087	0.7175	0.4740	1.13956	3.1939
1.572	0.7753	0.5103	1.27086	3.5545
2.195	0.8256	0.5351	1.42580	3.9805
3.360	0.8861	0.5745	1.78930	4.9837
4.693	0.9307	0.5955	2.08721	5.8037
6.961	0.9787	0.6006	2.97493	8.2567
7.727	0.9907	0.5936	3.21922	8.9305
9.847	1.0173	0.5637	4.05825	11.2463
11.876	1.0367	0.4689	4.71706	13.0620

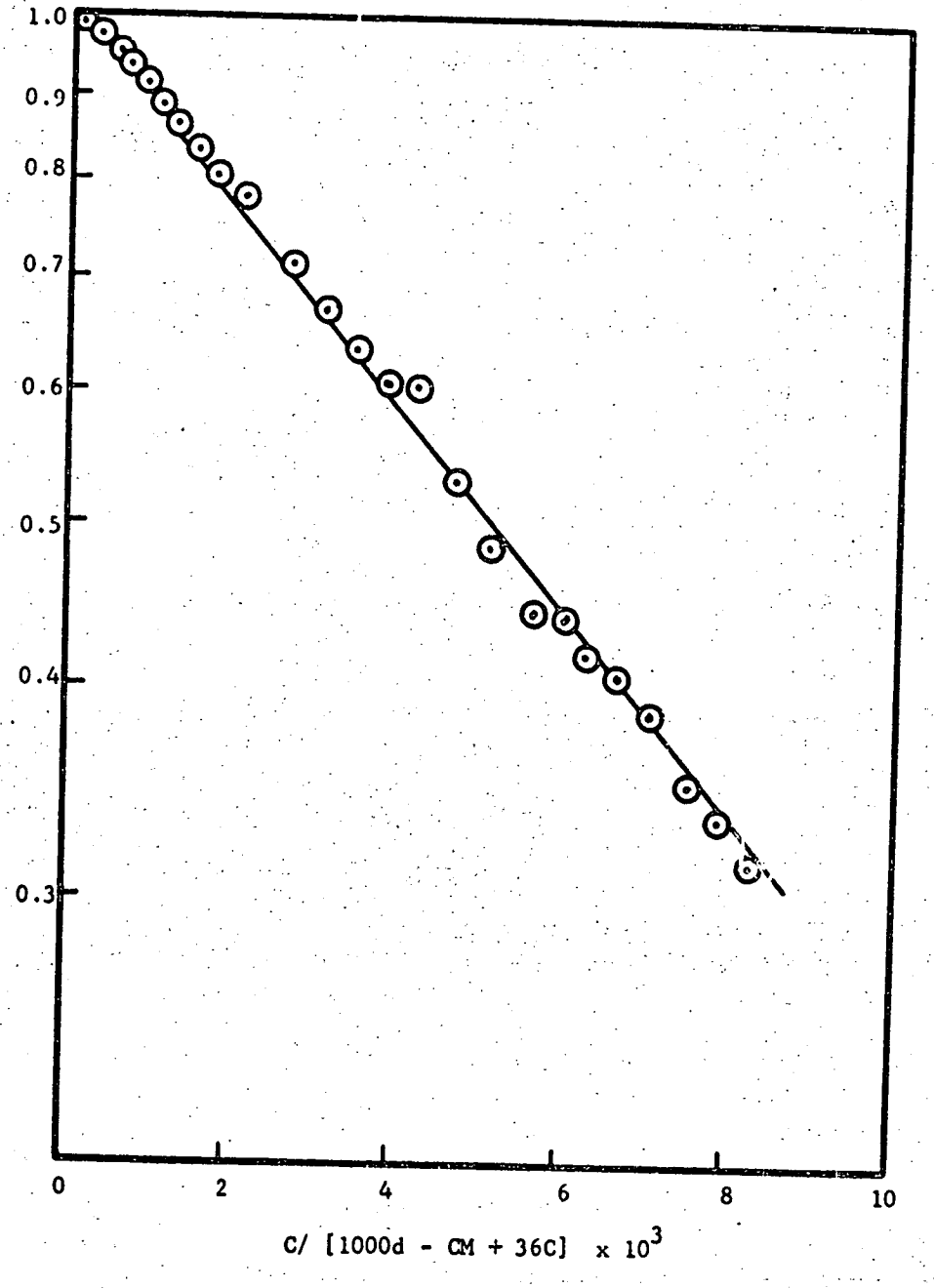

Figure 5.3-3 Relative Diffusion Coefficients $\frac{D^{id}}{D^o}$ for Aqueous KOH Solutions at 25°C.

and are compared with experiment in Figure 5.3-2. The proposed model is seen to provide a much better fit than the Onsager-Fuoss theory at high concentrations. For the concentration range 0-10 g.mole/l, the average percent deviation between theory and experiment is 1.31%.

There is no unambiguous way to obtain the individual ionic perturbation parameters from the experimental data. However, it is possible to obtain values for δ_{K_+} and δ_{OH_-} if same arbitrary zero is assumed for a particular ion, or some other assumption is made. The limiting ionic mobilities of K^+ and Cl^- ions are very nearly equal at 25°C; moreover the effect of KCl concentration on viscosity or diffusion coefficient is small. It seems reasonable, therefore, to assume that the perturbation parameters δ_{K_+} and δ_{Cl_-} are approximately the same. This assumption has been previously used to obtain ionic perturbation parameters for the diffusion of gases in electrolytic solutions (93), and is adopted here.

Diffusion coefficients and activity coefficients for aqueous potassium chloride solutions at 25°C were obtained from Conway (29), and values of D^{id}/D_o are plotted in Figure 5.3-4. From the straight line region it is found that

$$n(\delta_{K_+} + \delta_{Cl^-}) = -940 \text{ cal(g.mole)}^{-1}$$

so that

$$n\delta_{K^+} = n\delta_{Cl^-} = -470 \text{ cal.(g.mole)}^{-1}$$

From Equation (5.3-2),

$$n\delta_{OH^-} = 2795 \text{ cal.(g.mole)}^{-1}$$

It would be of interest to obtain values of $n\delta_i$ for the ions at

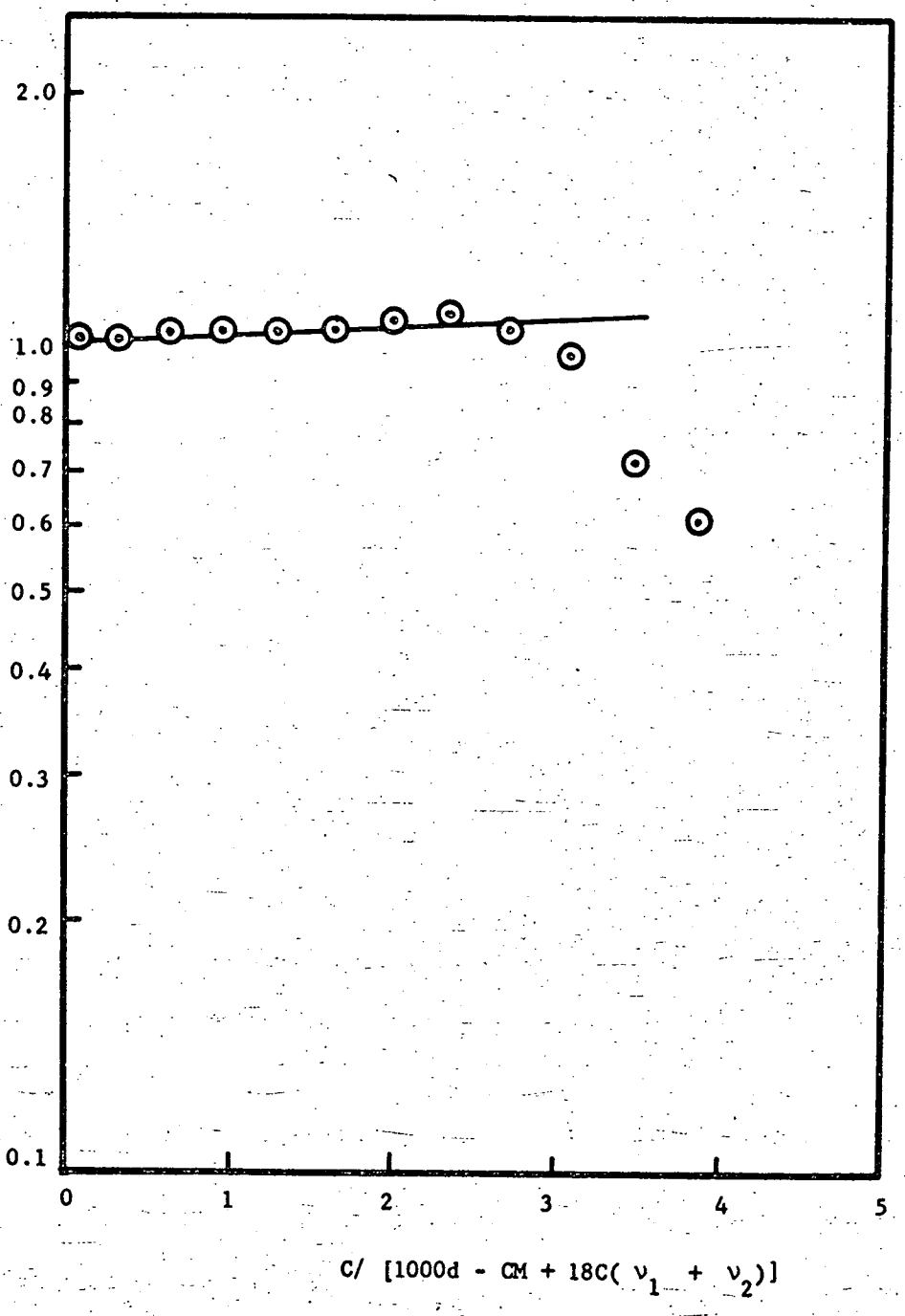

Figure 5.3-4 Relative Diffusion Coefficients for Aqueous KCl Solutions at 25°C.

other temperatures. As pointed out above, accurate activity coefficient data for this system are not available at the higher temperatures; in addition diffusion coefficients for potassium chloride solutions at high temperatures are unavailable. The temperature dependence of the corresponding perturbation parameters for gases diffusing in electrolytes is known to be small (93).

It is of interest to compare the concentration dependence of the mutual diffusion coefficient for potassium hydroxide solutions with the behavior of other transport coefficients for this system. It is possible to develop a theory along the lines of that proposed here for fluidity (ϕ), self-diffusion coefficient of water (D_w) and diffusion coefficient of gases in the electrolyte (D_g). The theory predicts linear relationships when a semilog plot of ϕ/ϕ^o, D_w/D_w^o and D_g/D_g^o against electrolyte species fraction is made. Such plots are shown for fluidity and for the diffusion of oxygen in potassium hydroxide solutions in Figures 5.3-5 and 5.3-6. An approximately linear relationship is found in each case. McCall and Douglass (94) have presented data for the self-diffusion coefficient of water in KOH solutions at 25°C, and find that this transport coefficient also gives a linear relationship. The values of the ionic perturbation parameter are different for each of the transport coefficients considered, since different intermolecular forces and friction factors are involved.

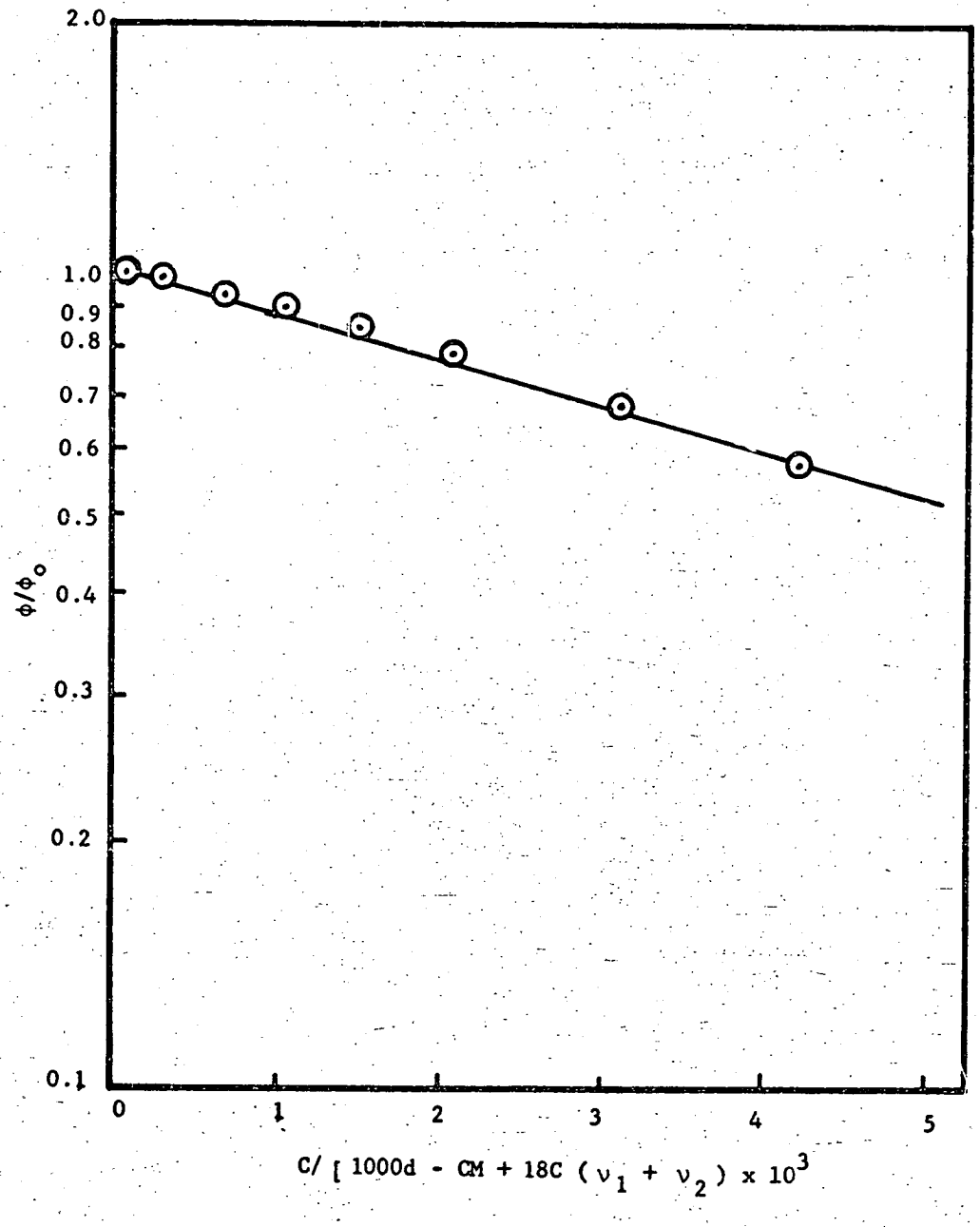

Figure 5.3-5 Relative Fluidity for Aqueous KOH Solutions at 25°C.

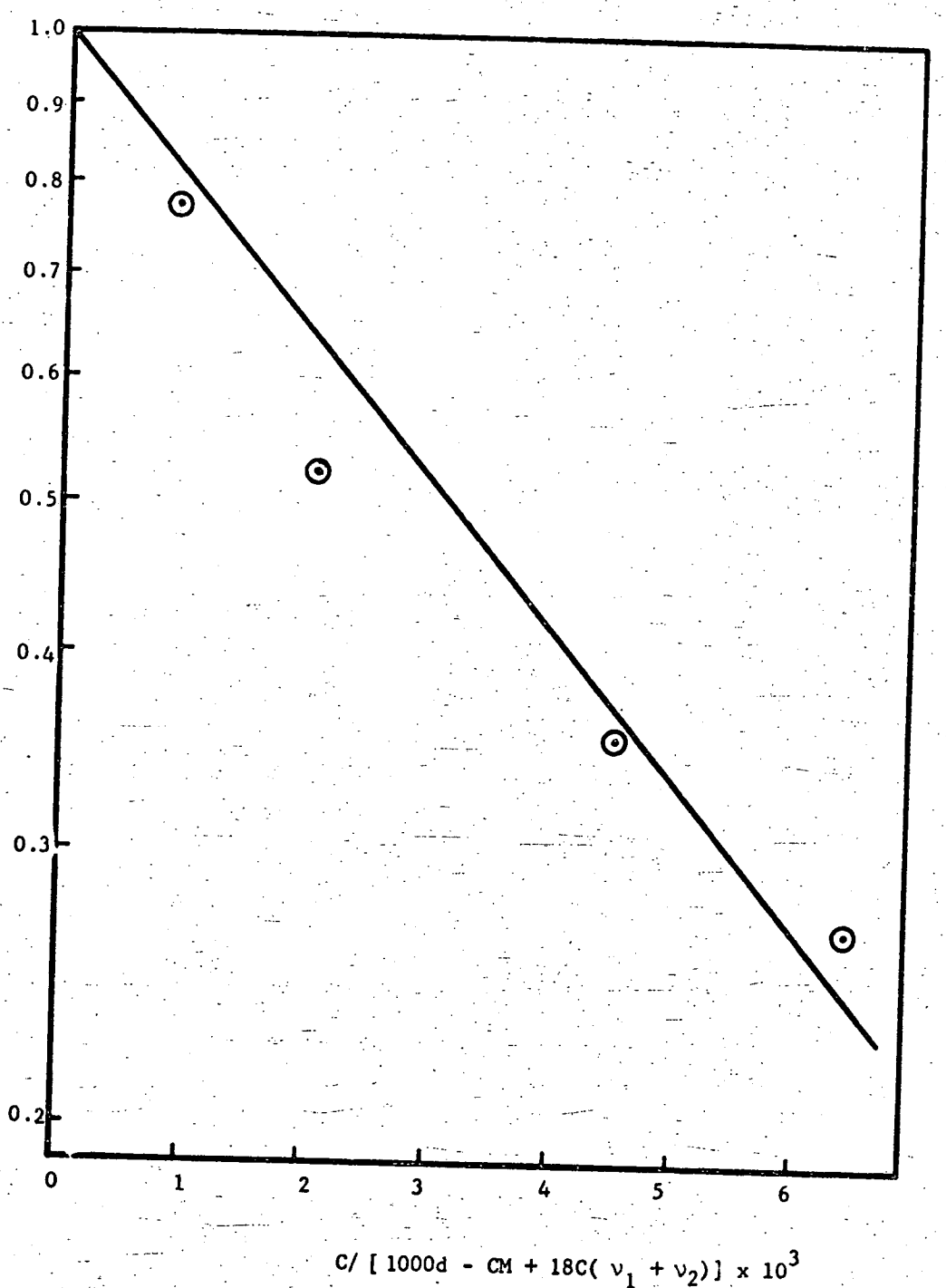

Figure 5.3-6 Relative Diffusivity of O_2 in Aqueous KOH Solutions at 25°C.

6. Vapor Pressures of KOH and LiOH Solutions - J. Jolly

A knowledge of the vapor pressures of water over KOH and LiOH solutions is of value in itself, and is also necessary in order to carry out the gas solubility experiments. For KOH solutions, measurements have been reported over a wide range of concentrations and temperatures. Thus, International Critical Tables (91) contains data for the temperature range 0 to 100°C and the concentration range 0 to saturation. Duhring line and boiling point data are available (95,96) for temperatures to 144°C, and KOH concentrations to 80% (wt.). Recently, Vogel et al. (97) have reported data for the temperature and concentration ranges 140-200°C and 55-80 wt. %. The vapor pressure data for KOH available in the literature were considered sufficient for the present purposes, and further measurements were not pursued in this work. However, data available in the literature were fitted to the Antoine equation, the constants being evaluated for various KOH concentrations.

For LiOH solutions, vapor pressure data have been reported for 25°C and a concentration range of zero to saturation by Walter and Groeneveld (98). Measurements are also available for the temperature range 100 to 350°C for three concentrations (99,100). No data have been reported for the temperature range 25-100°C. Measurements in this range were therefore undertaken in this study.

6.1 Correlation of Data for KOH Solutions

To correlate existing vapor pressure data for potassium hydroxide solutions the Antoine equation was used:

$$\log_{10} P = A - \frac{B}{C+t} \qquad (6.1\text{-}1)$$

where P is vapor pressure in millimeters of mercury, t is temperature in ^{o}C, and A, B and C are constants which vary with the KOH concentration. The experimental data consisted of vapor pressure measurements at temperatures up to 100°C (91), and those based on Duhring lines and boiling temperature data ( ) at higher temperatures. The vapor pressure values of Vogel et al. (97) are somewhat lower than those of Gerlach (96) at high temperatures. In obtaining Antoine constants for high temperatures, only the data of Gerlach were used. In determining the constants A, B and C for each KOH concentration, the following procedure recommended by Thomson (101) was used:

1) The data were plotted as log P vs. 1/(273+t), and inspected for linearity and scatter in the data points. It was found that the data could be best represented by two straight lines, corresponding to a low and high temperature range for each KOH concentration. The transition temperature from the low to the high temperature region varied somewhat with concentration, being approximately 60°C for water and rising to about 120°C at higher KOH concentrations. Two sets of Antoine constants were subsequently obtained, corresponding to these two regions.

On examining the experimental data a few points were found which departed somewhat from the straight line in a random fashion. Where such deviations appeared to be due to experimental error, these points were not subsequently used in obtaining the constants.

2) For each KOH concentration, values of the constant C were found for each temperature region from the equation:

$$\frac{\log P - \log P_1}{t - t_1} = \frac{A}{t_1+C} - \frac{\log P}{t_1+C} \qquad (6.1\text{-}2)$$

where t_1 is some reference temperature and P_1 is the vapor pressure at that temperature. C was evaluated by plotting the left-hand side of this equation against log P, and determining the slope. Values of C found in this way showed an increase with increasing KOH concentration. Before calculating A and B, the C values were rounded to the nearest degree.

3) Having found values of C for each KOH concentration, the best straight line relating log P to 1/(C+t) was determined for both the high and low temperature regions, and hence values of A and B were found by the method of least squares. These calculations were performed on a digital computer.

Values for the constants A, B and C for various KOH concentrations are shown in Table 6.1-1 for the low temperature region, and in Table 6.1-2 for higher temperatures. The values of C obtained show a continuous variation with KOH concentration, but the variations in A and B with concentration are less well-defined. It seems reasonable to attribute these variations to small errors in the experimental vapor pressure data. Several sets of A, B and C values appear suitable for each concentration, each set giving almost as good a fit of the experimental data as the others; a meaningful choice between these various sets would require vapor pressure data of very high accuracy.

The Antoine equation with the constants shown in Tables 6.1-1 and 6.1-2 gave good agreement with experimental data over the whole range of temperatures and KOH concentrations, the agreement between predicted and experimental vapor pressures being within 1% for all points. A comparison of predicted and experimental values for a number of KOH concentrations and temperatures chosen at random is shown in Table 6.1-3.

Table 6.1-1

Antoine Constants for Correlation of Vapor Pressures of KOH Solutions
Low Temperature Range

Wt. % KOH( )	Temperature Range	A	B	C
0	0-80°C	8.0928	1746.1	235
4.72	0-80	8.0757	1745.3	235
9.09	0-80	8.0646	1747.1	235
16.66	0-80	8.1052	1768.1	235
23.07	0-80	7.9800	1751.7	235
28.57	0-100	7.9603	1772.2	236
33.33	0-100	7.9782	1818.7	239
37.50	0-120	8.0529	1891.5	243
44.45	0-120	8.3770	2118.9	254
50.00	0-140	9.5007	2907.8	300
54.55	0-140	9.8749	3239.3	320

Table 6.1-2

Antoine Constants for Correlation of Vapor Pressures of KOH Solutions
High Temperature Range

Wt. % KOH( )	Temperature Range	A	B	C
0	80-180°C	7.9668	1668.2	228
10	80-180	7.9564	1676.4	228
20	90-180	7.9221	1685.9	228
30	100-200	7.8321	1696.6	230
40	120-200	7.9805	1818.2	232
50	140-220	7.8007	1840.4	234
60	140-250	7.8496	2090.3	243
70	150-310	7.5914	2305.3	264
80	220-440	7.5886	2814.0	303

Table 6.1-3

Comparison of Predicted and Experimental Vapor Pressures

Wt. % KOH	Temperature Range	Temperature °C	P_{predic} mm.Hg	$P_{expt.}$ mm.Hg
23.07	0-100	20	12.9	12.9
		40	40.7	40.7
		60	110.1	110.1
		80	262.4	263
		100	563.6	563
33.33	0-100	40	28.8	28.6
		60	78.6	78.6
		80	189.3	190
		100	410.6	413
44.45	0-100	20	4.40	4.40
		60	42.6	42.6
		80	107.9	108
		100	246.3	246
20.0	100-180	100	606	600
		120	1195	1200
		140	2192	2200
		160	3775	3800
		180	6165	6140
60.0	178-284	178	766	760
		206	1527	1520
		222	2261	2280
		246	3758	3800
		284	7642	7600
80.0	223-444	223	198.6	200
		328	1543	1520
		354	2316	2280
		387	3712	3800
		444	7600	7600

Since the agreement in most cases is better than 1%, it is concluded that the Antoine equation provides estimates of the vapor pressure of KOH solutions that are sufficiently accurate for the purposes of the work under this grant.

It should be emphasized that this close agreement is not found when comparing with the data of Vogel et al. (97) because of discrepancies between their data and those of Gerlach (96).

When one examines the values of the Antoine constants in Tables 6.1-1 and 6.1-2, it is clear that constants A and B do not vary smoothly as the concentration of KOH changes. This situation results from the experimental data which were used in the computer calculation of the constants; the computer gives equal weight to all data irrespective of their accuracy. It is not surprising, therefore, that the concentration dependence of the Antoine constants is not a smooth one.[1] It is possible, of course, to smooth the Antoine constants empirically at some sacrifice in agreement between calculated vapor pressures and the experimental values (which, it should be noted, were used for evaluating the original Antoine constants of Tables 6.1-1 and 6.1-2). To check this point the several values of the Antoine constants were plotted versus the KOH concentration and smooth curves drawn through the points. New values of the Antoine constants were read from the curves and used in recalculating vapor pressures for several KOH concentrations and temperatures. Whereas the agreement between experimental vapor pressures and those calculated with the computer-derived Antoine constants is excellent, discrepancies of 15 to about 50% are noted when the smoothed Antoine constants are used for the calculation. These calculations are summarized in Table 6.1-4.

Table 6.1-4

Comparison of Experimental and Computed Vapor Pressures of KOH Solutions

KOH Concentration wt %	Temperature °C	Expt	Computer Constants	Smoothed Constants
20	100	600	606	912
	180	6140	6165	9100
60	178	760	766	684
	284	7600	7642	6650
80	223	200	199	243
	444	7600	7600	8800

The significant discrepancies between the data of Gerlach and those of Vogel et al. suggest that additional study of the vapor pressures of aqueous alkali solutions is needed; moreover, better correlations are required to permit interpolation for other alkali concentrations and temperatures.

6.2 Measurement of Vapor Pressure of LiOH Solutions

Several methods were studied to determine vapor pressure of lithium hydroxide solutions, and it was decided to adopt Cumming's dew-point method (103) suitably modified. This method is believed to give an accuracy of about 0.01°C in the determination of the dewpoint, and measurements can be extended to high vapor pressures. One of the chief advantages of this method over tensimetric methods generally is the fact that the measurements may be made in the presence of air. The accuracy of tensimetric methods on the other hand is seriously affected in the presence of even traces of air. The method is also suitable for measurements over a large range of electrolyte concentration. It is a matter of indifference when using this method whether the system studied is liquid or solid, viscous or liquid, one phase or several.

6.2.1 Apparatus for Measuring Vapor Pressures

The apparatus consisted of a highly polished silver tube with silver base, which was silver-soldered to a stainless steel sleeve, the latter being closed at the top by a stainless steel cap as shown in Figure 6.2-1. A thermometer (0.01°C graduations) and tubes through which water could be circulated to and from a constant temperature bath were inverted through the cap. The silver tube was fitted into a glass vessel which contained the LiOH solution. The top of the glass vessel rose half an inch or so above the silver tube and its sleeve so that the closed space was completely immersed in a constant temperature bath controlled to 0.05°C. One of the outlets of the glass container was connected by means of a vacuum glass stopcock to a vacuum pump so that air could be evacuat

from the system. The other outlet could be connected to a manometer. The silver tube was kept very highly polished in all the experiments.

6.2.2 Experimental Techniques for Measuring Vapor Pressures

Approximately 20-30 ml. of LiBr solution was placed in the glass container, the silver tube affixed, and the apparatus evacuated. Although the presence of air does not measurably affect the vapor pressure, the formation and disappearance of dew is much sharper and more readily observed when air is absent. Sharpness of dewpoint is governed by the speed with which equilibrium is again established after dew has been deposited or evaporated from the silver tube. At no time was difficulty experienced in making measurements through sluggishness in the re-establishment of equilibrium. After evacuation the vacuum pump was shut off and the evacuated apparatus was placed in a constant temperature bath, where it was allowed to remain until equilibrium had been reached. A period of 20-30 minutes was found to be sufficient for this purpose. The bath temperature was controlled to 0.05°C.

Hot water was circulated in and out of the silver tube from another constant temperature bath. This constant temperature bath was fitted with both heating and cooling arrangements which facilitated raising or lowering the temperature within a very short time. The bath was equipped with a controller to maintain the temperature within 0.05°C. After attaining equilibrium, the temperature of water circulating in the silver tube was slowly reduced with the help of the thermostat of the water circulating bath. The temperature was noted when the first traces of dew were formed on the silver tube.

It was noticed in such preliminary observations that supercooling occured before deposition of dew, the first dew-point observed being lower than the following ones; consequently in all experiments a clearly observable deposit of dew was produced, and allowed to disappear, before taking observations of temperature.

The determination was then begun by very gradually lowering the temperature of the water running through the silver tube, carfully noting the temperature. At the first sign of dew formation (slight discontinuity of the polished surface, the boundary line becoming faintly visible under bright and carefully adjusted illumination) the temperature was read. The supply of heat to the adjustable thermostat was then altered so as to slowly raise the temperature of the running water. The temperature was again read when dew disappeared from the silver surface. This process was repeated several times.

The point of appearance of dew with falling temperature was found to agree within $0.05^{\circ}C$ with the point of disappearance of dew with rising temperatures. Reported values are the mean of these two readings. In every determination the observation of dew-point was carried out at least three times, allowing a period of 15 minutes to elapse between each observation for equilibrium to be re-established. Determinations were not accepted unless the three results agreed within $0.05^{\circ}C$. The lithium hydroxide solution was standardized before and after the experiment with standard hydrochloric acid. These dew-point temperatures were used to determine the vapor pressure from standard tables of vapor pressure of water in the literature.

Up to 40°C, the thermometers used were high precision with 0.05°C graduations; for higher temperatures, the thermometers used had 0.01°C graduations. These thermometers were standardized against National Bureau of Standard corrected thermometers.

In all static methods for the measurement of vapor pressure there is the possibility of formation of a surface layer on the solution through condensation or evaporation. Thus, if condensation occurs from the vapor space to the solution (e.g., during disappearance of dew from the silver tube) a more dilute surface layer will be formed, specifically lighter than the bulk of the solution, and the concentration will only be equalized by the relatively slow process of liquid diffusion. To avoid this error the solution was shaken throughout each observation.

McBain and Salmon (104) recommended a preliminary immersion of the lower portion of the silver surface in boiling water; no dew subsequently deposits upon this portion, and the appearance of a line of division upon the bright surface is claimed to facilitate the observation of dew point. However such preliminary treatment was judged to be unnecessary, and was therefore omitted.

6.2.3 Experimental Vapor Pressures of Lithium Hydroxide Solutions

The experimental data for vapor pressure of lithium hydroxide solutions at various temperatures and concentrations are given in Table 6.2-1 and shown in Figure 6.2-2. Vapor pressure readings were interpolated from the water vapor pressure table taken from Chemical Engineers' Handbook (105).

The dew-point method is believed to give an accuracy of about 0.01°C. In every determination the observation of dew-point was

carried out at least three times and the mean was taken to calculate the vapor pressure shown in Table 6.2-1. The precision of the experiments was approximately $\pm$0.5% of the vapor pressure; the absolute accuracy of the reported values depends upon the sharpness of formation and disappearance of dew and on the accuracy of the water vapor pressure table. Considering all of these, the overall accuracy of the measurements is estimated to be $\pm$ 1.5%. The data reported here are in excellent agreement (within 0.1 mm.Hg) with those obtained by Walter and Groenveld (97) at 25°C. No data were available for comparison in the range 25°C to 100°C. The agreement between values of vapor pressure at 100°C reported here and those given in the literature (91) is of the order of 1.5%.

To check the accuracy of the method, a further independent comparison was made by noting the dew points and vapor pressures of potassium hydroxide solutions, and comparing these with the literature values. These values together with literature values have been tabulated in Table 6.2-2. The agreement is quite satisfactory and is within 1.0%. This comparison lends further confidence to the method used.

Table 6.2-1

Dew-Point and Vapor Pressure of LiOH Solutions

Temperature of Solution	Wt.% LiOH	Dewpoint °C	Vapor Pressure mm Hg
25°C	0	25.00	23.75
	1.90	24.56	23.14
	3.85	24.14	22.57
	6.45	23.37	21.54
	8.05	23.04	21.12
	10.10	22.39	20.30
40°C	0	40.00	55.32
	1.90	39.51	53.88
	3.85	38.90	52.16
	6.45	38.35	50.42
	8.05	37.76	49.02
	10.10	36.81	46.58
60°C	0	60.00	149.38
	2.40	59.23	144.11
	4.82	58.57	139.79
	6.45	57.98	136.90
	8.52	57.48	132.82
	10.20	56.89	129.13
80°C	0	80.00	355.10
	1.90	79.36	346.08
	3.85	78.54	334.70
	6.45	77.72	323.63
	8.05	77.25	317.40
	10.10	76.83	311.87
100°C	0	100.00	760.00
	1.90	98.95	731.92
	3.85	97.51	694.82
	6.45	95.19	638.36
	8.05	93.60	601.89
	10.10	91.18	549.71

(Values of vapor pressure for pure water were taken from the literature (105))

Table 6.2-2

Vapor Pressure of Potassium hydroxide Solutions

Temperature of Solution	Wt.% KOH	Vapor Pressure mm.Hg	
		This Work	Literature ( )
25°C	10.10	21.76	21.80
	25.45	16.85	16.90
	30.05	14.12	14.10
40°C	16.50	47.32	47.00
	21.60	41.95	41.80
	24.95	38.80	38.75
	40.01	20.12	20.00
60°C	31.50	85.30	84.00

7. DENSITY MEASUREMENT

Considerable difficulties were experienced with the pycometer procedure described in the previous report when making measurements at high temperature. These difficulties arose primarily from rapid corrosion of the glass capillary. In view of these problems a modified Westphal balance procedure (Hydrostatic Weighing Method of Kohlrausch) has been adopted and is described below.

Theory. This method is based on the Archimedes Principle, in which a plummet is weighed in air, water, and the solution whose density is to be determined, respectively. The density of the solution at the temperature t_i, at which this measurement is conducted is given by

$$\rho_{soln} = \frac{W_S - W_A}{W_W - W_A} \times \rho_{water \text{ at } t_i} \qquad (7.0\text{-}1)$$

where W_S = weight of the plummet in the solution

W_A = weight of the plummet in air

W_W = weight of the plummet in water.

Using this method Doddlich and Bigeleisen (106), who used a plummet having a volume of 300cc, claimed that under optimum conditions, the reproducibility of density measurement can be as high as $\pm 2.0 \times 10^{-6}$ gm/cc.

7.1 Description of Apparatus

An analytical balance with one pan replaced by a coin silver plummet (approximately 5 cc in volume) suspended by a fine Platinum-Rhodium wire was used. The wire passed through a hole (about 3/8" in diameter) in the platform of the balance so that the plummet could be immersed in thermostated potassium hydroxide solution placed below the balance case.

To prevent corrosion of the plummet it was electroplated with pure silver.

To prevent evaporation from the KOH solution being tested a flow of nitrogen equilibrated with KOH of the same concentration and at the same temperature as the sample under test was directed over the surface of the solution. To accomplish this two groups of saturators were used as shown in Figure 7.0-1. The first group consisted of two saturators containing distilled water kept at a temperature such that the vapor pressure of water is the same as that of the KOH solution. The second group consisted of two more saturators at the same temperature and KOH concentration as that of the sample.

7.2 Procedure

The plummet was weighed first in air and then in the KOH solution which was maintained at a fixed temperature. The plummet was immersed to such a depth that the surface of the solution always came to the same mark on the wire, so that the same volume of liquid was displaced at all times. Then the weight of the plummet was determined at intervals of 5 minutes, to ensure that an equilibrium condition was reached and to guard against accidental errors in weighing. The temperature of the solution was determined at the beginning and the end of each experiment. The experiment was repeated three to five times with fresh samples of the same composition to ensure reproducibility.

The plummet volume for temperatures up to 80°C was determined by weighing the plummet in water in the same manner as stated above. For temperatures above 80°C, the volume of the plummet was obtained by extrapolating that obtained at lower temperature to the desired temperature, assuming that the thermal expansion coefficient of silver remains constant

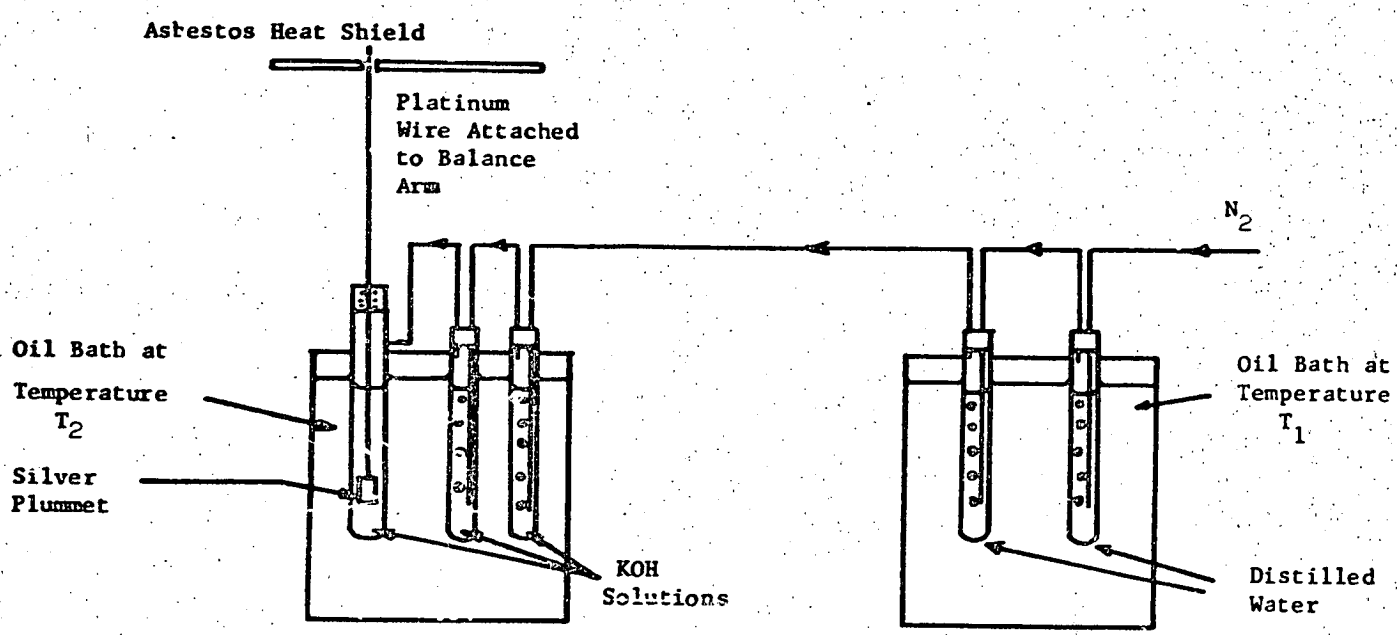

Figure 7.2-1

SATURATORS FOR DENSITY MEASUREMENTS

over the interval of 80°C to 160°C. At 80°C the volumetric expansion coefficient was approximately $0.00006(^{\circ}C)^{-1}$.

At high temperature, the solution tended to vaporize quite rapidly, thus affecting the temperature and concentration of the solution. To minimize this effect, an atmosphere of nitrogen saturated with water vapor was maintained by passing presaturated nitrogen over the surface.

In experimenting with dilute solutions, dissolved gas in the solution tended to form small bubbles and adhere to the surface of the plummet, and had to be removed before taking readings.

Concentrated solutions, whose saturation temperatures are above room temperature, were prepared and stored in an oven maintained at temperatures higher than the saturation temperature, and the concentration was determined at the time of density measurement by titration.

Note: In these experiments, no attempt was made to free the potassium hydroxide solution of carbonate, but the carbonate content for each concentration was determined and was found to be less than one per cent of the potassium hydroxide content. Also, no attempt was made to eliminate the effect of surface tension by coating the wire with platinum black.

7.3 Discussion of Results.

The densities of potassium hydroxide solutions at various temperatures and concentrations are tabulated in Table 7.3-1 and are shown in Figures 7.3-1 and 7.3-2. These results agree closely with the data from Table 5 of Solvay Technical Bulletin No. 15 for 60°C and 80°C. The deviations shown are standard deviation from the arithmetic means. The error in the concentration determination is estimated to be about 0.1% of the total KOH concentration. No measurements were made of a solution whose

Table 7.3-1

DENSITIES OF KOH SOLUTIONS

Wt. percent KOH	59.9 ± 0.1°C Exptl. Data	59.9 ± 0.1°C Solvay Data	79.9 ± 0.1°C Exptl. Data	79.9 ± 0.1°C Solvay Data
6.17	1.0381 ± 0.0001	1.0375	1.0269 ± 0.0001	1.0279
11.50	1.0863 ± 0.0002	1.0857	1.0746 ± 0.0001	1.0767
20.90	1.1758 ± 0.0002	1.1750	1.1652 ± 0.0001	1.1650
27.80	1.2448 ± 0.0001	1.2441	1.2329 ± 0.0001	1.2336
36.00	1.3294 ± 0.0002	1.3299	1.3973 ± 0.0001	1.3955
43.00	1.4080 ± 0.0001	1.4072	1.3180 ± 0.0001	1.3186
47.20	1.4560 ± 0.0001	1.4554	1.4442 ± 0.0008	1.4435
50.37	1.4957 ± 0.0001	1.4925*	1.4848 ± 0.0001	1.4803*

*Extrapolated Value

Temp	Wt. percent	Exptl. Value	Temp	Wt. percent	Exptl. Value
99.2 ± 0.1°C	36.0	1.3073 ± 0.0001	141 ± 0.2°C	53.9	1.4901 ± 0.0001
	43.0	1.3858 ± 0.0001		55.72	1.5160 ± 0.0001
	43.97	1.3969 ± 0.0001		59.71	1.5622 ± 0.0001
	55.4	1.5324 ± 0.0001		65.1	1.6268 ± 0.0001
	59.46	1.5809 ± 0.0001			
120.5±0.1°C	55.4	1.5205 ± 0.0001	161.4±0.1°C	64.68	1.6086 ± 0.0001
	59.46	1.5683 ± 0.0001		72.25	1.7046 ± 0.0001
	65.1	1.6342 ± 0.0001		77.1	1.7652 ± 0.0001

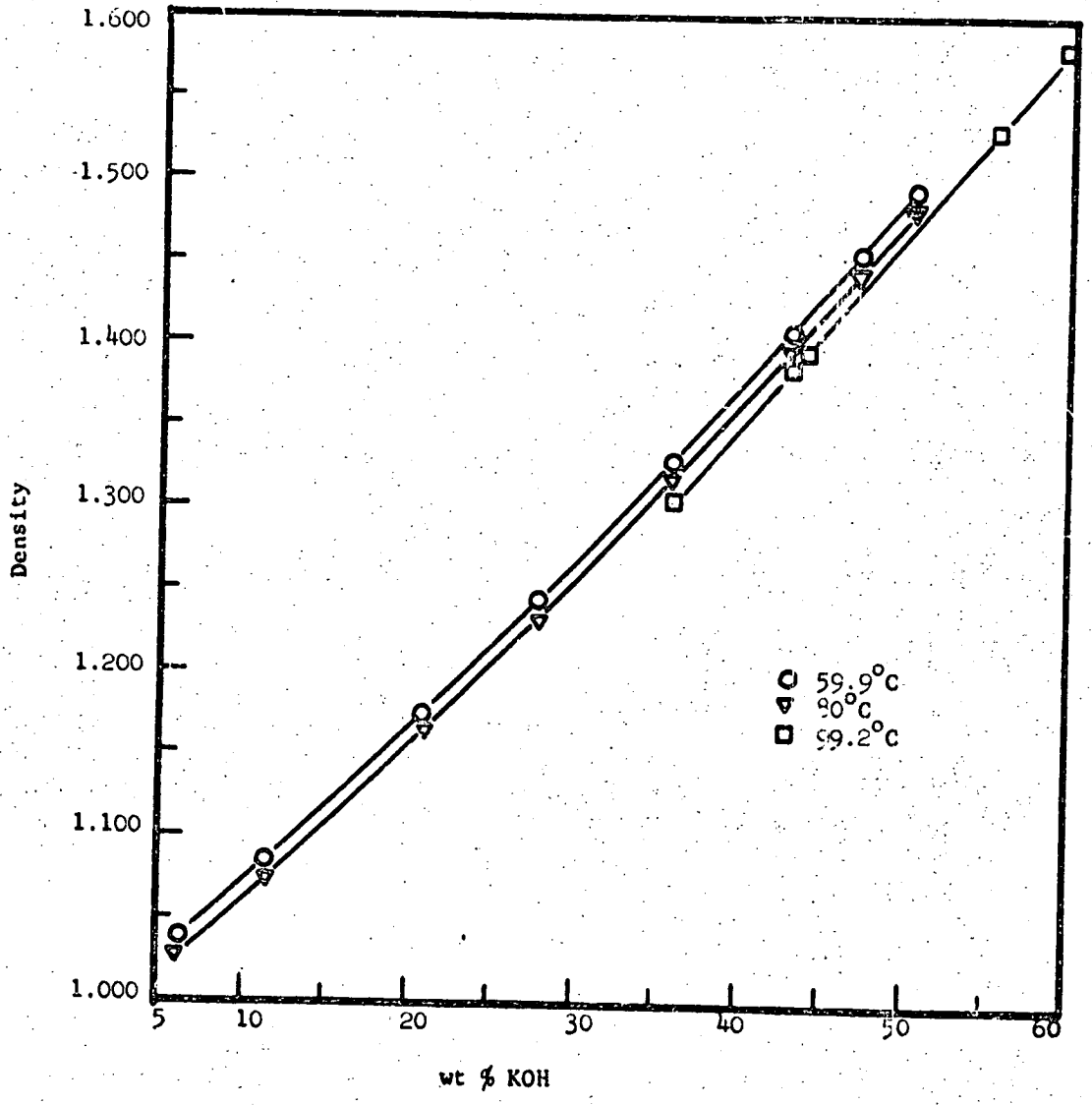

Figure 7.3-1

CONCENTRATION DEPENDENCE OF DENSITY OF AQUEOUS KOH SOLUTIONS

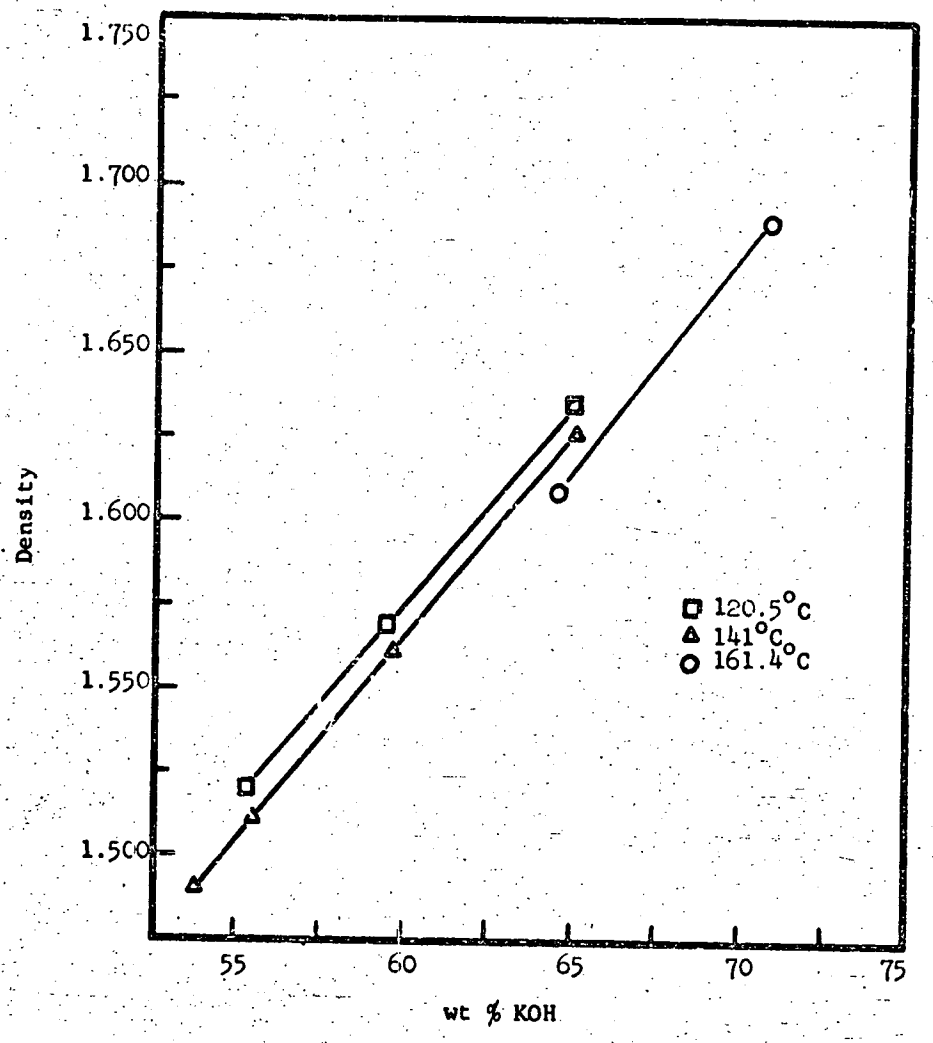

Figure 7.3-2

CONCENTRATION DEPENDENCE OF DENSITY OF AQUEOUS KOH SOLUTIONS

vapor pressure were greater than 400mm Hg at a given temperature because it was felt that uncertainty in the measured values that would arise due to rapid vaporization would be too great, and extrapolation from values at low vapor pressure may give better results. The deviations in the temperatures shown in the table represent errors in temperature determination rather than fluctuation in temperature during an experiment.

APPENDIX 1

Sample Calculation of $\ln(\gamma_1 K_1^c)$

Solubility of oxygen in 2% LiOH solution at 25°C

Parameters needed

Density of 2% LiOH Solution = 1.0203 gm/cc. of solution

$a_1 = 3.46$ Å $\quad \frac{\epsilon_1}{k} = 118°K \quad \alpha_1 = 1.57$

$a_2 = 2.75$ Å $\quad \frac{\epsilon_2}{k} = 85.3°K \quad \mu_2 = 1.84$ debye

$a_3 = 1.20$ Å $\quad \frac{\epsilon_3}{k} =$ unknown $\quad \alpha_3 = .0313 \times 10^{-24}$ cm^3

$a_4 = 3.30$ Å $\quad \frac{\epsilon_4}{k} = 137.2°K$

Evaluation of $\bar{g}_1^h/kT$

$$\frac{\bar{g}_1^h}{kT} = -\ln(1-\zeta_3) + \frac{6\zeta_2}{1-\zeta_3}\frac{a_1}{2} + \frac{12\zeta_1}{1-\zeta_3} + \frac{18\zeta_2^2}{(1-\zeta_3)^2}\left(\frac{a_1}{2}\right)^2 + \frac{4}{3}\pi\frac{P}{kT}\left(\frac{a_1}{2}\right)^3$$

where

$$\zeta_k = \frac{1}{6}\pi \sum_{j=1}^{m} \rho_j (a_j)^k$$

Density of 2% LiOH solution = 1.00203 gm/cc.

No. of Li^+ ions per cc. of solution $= \frac{2}{23.94} \times \frac{1.0203}{100} \times \tilde{N}$

$= .0008523\ \tilde{N}$

No. of OH^- ions per cc. of solution = $.0008523\ \tilde{N}$

No. of water molecules/cc. of solution = $\frac{98}{18} \times \frac{1.0203}{100} \times \tilde{N}$

$= .05554\ \tilde{N}$

$$\zeta_1 = \frac{1}{6}\pi \times 10^{-8} \times 6.023 \times 10^{23} \left[.0554 \times 2.75 + .008523 \times 1.2 + .008523 \times 3.3\right]$$

$$= 0.4939 \times 10^{15}$$

$$\zeta_2 = \frac{1}{6}\pi \times 10^{-16} \times 6.023 \times 10^{23} \left[.05554 \times 2.75^2 + .0008523 \times 1.2^2 + .0008523 \times 3.3^2\right]$$

$$= 1.3578 \times 10^{7}$$

$$\zeta_3 = \frac{1}{6}\pi \times 10^{-24} \times 6.023 \times 10^{23} \left[.05554 \times 2.75^3 + .0008523 \times 1.2^3 + .0008523 \times 3.3^3\right]$$

$$= 0.3744$$

$$1 - \zeta_3 = 1 - 0.3744 = 0.0255$$

$$\ln(1-\zeta_3) = -0.47004$$

$$\frac{\bar{g}_1^h}{kT} = 0.47 + \frac{6 \times 1.3578 \times 10^7}{0.6255}\left(\frac{a_1}{2}\right) + \left[\frac{12 \times 0.4939 \times 10^{15}}{0.6255} + \frac{18 \times (1.3578)^2 \times 10^{14}}{(0.6255)^2}\right]\left(\frac{a_1}{2}\right)^2 + \frac{4}{3}\pi \frac{6.023 \times 10^{23}}{82.03 \times 290} \times \left(\frac{a_1}{2}\right)^3$$

$$\frac{\bar{g}_1^h}{kT} = 0.47 + 1.3024\times10^{8}\left(\frac{a_1}{2}\right) + 1.778\times10^{16}\left(\frac{a_1}{2}\right)^2$$

But for oxygen $\frac{a_1}{2} = 1.73\ \text{Å}$

$$\frac{\bar{g}_1^h}{kT} = 0.47 + 1.3024\times10^{8} \times 1.73\times10^{-8} + 1.778\times10^{-16} \times (1.73)^2\times10^{16} = 8.0445$$

Evaluation of $\ln(kT\Sigma\rho_j)$

$$\ln(kT\Sigma\rho_j) = \ln\,[82.03\times298\times(.0008823+.05554+.0008823)]$$

$$= \ln\,[1385.6] = 7.2347$$

Evaluation of $\frac{\bar{g}_1^s}{kT}$

$$\bar{g}_1^s = -\frac{32\pi}{9}\sum_{j=1}^{4}\rho_j\,\sigma_{1j}^3\,\epsilon_{1j} - \frac{4\pi\rho_2\alpha_2\mu_2^2}{3\sigma_{12}^3}$$

We have got all the other parameters except ϵ_3 which can be evaluated as follows:

$$\frac{\epsilon_3}{k} = \frac{3.146\times10^{-12}\alpha_3^{3/2}(z)^{1/2}}{(\sigma_3)^3\,k}$$

$$= \frac{3.146\times10^{-12}\times(0.0313\times10^{-24})^{3/2}(2)^{1/2}}{(1.2)^6\,(10^{-8})^6\times1.38\times10^{-16}}$$

$$= 59.37\ ^{o}K$$

Using the sub $\epsilon_{12} = \sqrt{\epsilon_1\epsilon_2}$ $\qquad \sigma_{12} = \frac{\sigma_1+\sigma_2}{2}$

$$\frac{\epsilon_{12}}{k} = 100.3 \qquad\qquad \sigma_{12} = 3.105$$

$\frac{\epsilon_{13}}{k} = 83.7$ $\qquad$ $\sigma_{13} = 2.33$

$\frac{\epsilon_{14}}{k} = 127.25$ $\qquad$ $\sigma_{14} = 3.38$

For 2% LiOH

$$\frac{\bar{g}_1^s}{kT} = -\frac{32\pi}{9}\left(\frac{6.023\times10^{23}}{298}\right)\times10^{-24}\,[.05554\times(3.105)^3\times100.3$$

$$+ .0008523\times(2.3)^3\times83.7 + .0008523\times(3.38)^3\times127.25]$$

$$- \left[\frac{4\pi\times.05554\times6.023\times10^{23}\times1.57\times10^{-24}(1.87)^2\times10^{-36}}{298\times3\times(3.105)^3\times1.38\times10^{-16}\times10^{-24}}\right]$$

$$= -[3.76+.020+.095] - 0.60$$

$$= -3.875 - 0.60$$

$$= -4.475$$

$$\therefore \ln(\gamma_1 k_1^o) = \frac{\bar{g}_1^h}{kT} + \frac{\bar{g}_1^s}{kT} + \ln(kT\Sigma\rho_j)$$

$$= 8.0445 - 4.475 + 7.2347$$

$$\ln(\gamma_1 k_1^o) = 10.8042$$

APPENDIX 2

Sample Calculation of Diffusivity for an Experimental Run

Basic Data: Temperature 60°C

Concentration of KOH solutions 5%

Vapor pressure of 5% KOH at 60°C[1] = 145 mm.Hg.

Area of electrode A = 0.0489 cm^2

At 8 minute $i_t = 0.695 \times 10^{-6}$ ampere (See Figure 1)

Voltage applied = -0.45 volts

C_o = solubility of O_2 in 5% KOH solution

At 60°C[2] = 0.605×10^{-6} g-mol/centimeter^3

Calculation: Substituting the above data into Equation 4.1-4

$$D^o = \left(\frac{i_t}{nFAC_o \frac{P-p^o}{P}} \right)^2 \times \pi t$$

The factor $\frac{P-p^o}{P}$ was introduced to account for the water vapor present in the vapor phase.

$$D^o = \left(\frac{0.695 \times 10^{-6} \text{ ampere}}{2 \frac{\text{Faraday}}{\text{g-mole}} \times 96.5 \times 10^3 \frac{\text{ampere-sec}}{\text{Faraday}} \times 0.0489 \text{cm}^2 \times 0.605 \times 10^{-6} \frac{\text{g-mole}}{\text{cm}^2}} \right)^2$$

$$\times \left(\frac{1}{\frac{760-145}{760} \times \pi \times 6 \times 8 \text{ sec.}} \right)^2 \times \pi \times 8 \times 60 \text{ sec.}$$

$$D^o = 3.418 \times 10^{-5} \text{ cm}^2/\text{sec.}$$

Literature Cited

1. Long, F. A., and McDevit, W. F., Chem. Rev., 51, 119 (1952).
2. Conway, B. E., Ann. Rev. Phys. Chem., 17, 481 (1966).
3. Shoor, S. K., Ph.D. Dissertation, Univ. of Florida (1968).
4. Debye, V. P., and McAulay, J., Physik. Z., 26, 22 (1925).
5. Kirkwood, J. G., Chem. Rev., 24, 233 (1939).
6. Conway, B. E., Desnoyers, J. E., and Smith, A. C., Phil. Trans. Roy. Soc. London, A256, 389 (1964).
7. Pierotti, R. A., J. Phys, Chem. 67, 1840 (1963), 69, 281 (1965).
8. Reiss, H., Frisch, H. L., Helfand, E., and Lebowitz, J. L., J. Chem. Phys., 32, 119 (1960).
9. Pierotti, R. A., J. Phys. Chem. 71, 2366 (1967).
10. Davidson, N., Statistical Mechanics, McGraw-Hill Book Co., Inc., New York, N.Y. (1962), p.481.
11. Hill, T.L., Statistical Mechanics, McGraw-Hill Book Co., Inc., New York, N. Y. (1956), p.180.
12. Reiss, H. Frisch, H. L., and Lebowitz, J. L., J. Chem. Phys., 31, 369 (1959).
13. Lebowitz, J. L. Helfand, E., and Praestgaard, E., J. Chem. Phys., 43, 774 (1965).
14. Starling, S. G., and Woodall, A. J., Physics, Longmans, London, (1961).
15. Geffcken, G., Z. Physik. Chem., 49, 257 (1904).
16. Knaster, M. B., and Apel'baum, L. A., Russ. J. Phys. Chem. 38, 120 (1964).
17. Ruetschi, P., and Amlie, R. F., J. Phys. Chem., 70, 718 (1966).
18. Davis, R. E., Horvath, G. L., and Tobias, C. W., Electrochim. Acta, 12, 287 (1967).
19. Cook, M. W., and Hanson, D. N. Rev. Sci. Inst., 28, 370 (1957).
20. Clever, H. L., Battino, R., Saylor, J. H., and Gross, P. M. J. Phys. Chem. 61, 1078 (1957).
21. Gubbins, K. E., Carden, S. N., and Walker, R. D., J. Gas Chromatography, 3, 98 (1965).
22. Lange, N. A., Ed., Handbook of Chemistry, 10th Ed., McGraw-Hill Book Co., Inc., New York, N. Y. (1961).

23. Hischfelder , J. O., Curtiss, C. F., and Bird, R. B., Molecular Theory of Gases and Liquids, John Wiley & Sons, Inc., New York, N. Y. (1954).

24. Margenau, H., Philosophy of Science, 8, 630 (1941).

25. Mavroyannis, C., and Stephen, M. J., Mol. Phys. 5, 629 (1962).

26. Pauling, L., and Wilson, E. B., Introduction To Quantum Mechanics, McGraw-Hill Book Co., Inc., New York, N. Y., (1935), p.277.

27. Landolt-Bornstein, Zahlenwerte and Funktion aus Physik-Chemie-Astronomie - Geophysik-Technik. Vol. I, Part 1 (1950).

28. Nightingale, E. R., J. Phys. Chem. 63, 138 (1959).

29. Conway, B. E., Electrochemical Data, Elsevier Publishing Co., New York, N.Y., (1952).

30. Ben-Naim, A., and Friedman, H. L., J. Phys. Chem., 71, 448 (1967).

31. Ulich, H., Z. Elektrochem., 36, 497 (1930).

32. Himmelblau, D. M., Chem. Rev., 64, 527 (1964).

33. Kamal, M. R., and Canjar, L. N., Chem. Eng. Prog., 62(1), 82 (1966).

34. Bearman, R. J., J. Phys. Chem., 65, 1961 (1961).

35. Kirkwood, J. G., Baldwin, R. L., Dunlop, P. J., Gosting, L. J., and Kegeles, G., J. Chem. Phys., 33, 1505 (1960).

36. Glasstone, S., Laidler, K. J., and Eyring, H., "Theory of Rate Processes," McGraw-Hill Book Co., New York (1941).

37. Ree, H. R., Taikyne, R., and Eyring, H., Ind. Eng. Chem., 50, 1036 (1958).

38. Bernel, L. R., and Fowler, R. H., J. Chem. Phys., 1, 515 (1933).

39. Podolsky, R. J., J. Am. Chem. Soc., 80, 4442 (1958).

40. Ratcliff, G. A., and Holcroft, J. G., Trans. Inst. Chem. Engrs. (London), 41, 315 (1963).

41. Bhatia, R. N., Gubbins, K. E., and Walker, R. D., Trans. Faraday Soc. 64, 2091 (1968).

42. Arnold, J. H., J. Am. Chem. Soc., 52, 3937 (1937).

43. Davies, A. B., Ponter, A. B., and Craine, K., Can. J. of Chem. Engr., 45, 372 (1967).

44. Einstein, A., Ann. Phys., 17, 549 (1905).

45. Sutherland, C. B. B. M., Phil. Mag., 9, 781 (1905).

46. Li, J. C. and Chang, P., J. Chem. Phys., 23, 518 (1955).

48. Wilke, C. R., and Chang, P., A.I.Ch.E. J., 1, 264 (1955).

49. Scheibel, E. G., Ind. Eng. Chem., 46, 2007 (1954).

50 Wise, D. L. and Houghton, G., Chem. Eng. Sci., 21, 999 (1966).

51. Johnson, P. A., and Babb, A. L., Chem. Rev., 387 (1956).

52. Gubbins, K. E. and Bhatia, R. N., Tech. Paper No. 390, Florida Eng. and Industrial Experiment Station (1967).

53. Walker, R. D., Second Semi-Annual Report, October, 1966, NASA Research Grant NGR 10-005-022.

54. Gubbins, K. E., and Walker, R. D., J. Electrochem. Soc., 112, 469 (1965)

55. Guoy, G. L., Compt. rend., 90, 307 (1880).

56. Wiener, O., Wied. Ann., 49, 105 (1893).

57. Kolthoff, I. M. and Lingane, J. J., "Polarography," Vol. I, Interscience, New York (1952).

58. Latinen, H. A., and Kolthoff, I. M., J. Am. Chem. Soc., 61, 3344 (1939).

59. von Stackelberg, H., Pilgrim, M., and Toome, V., Z. Electrochem., 57, 342 (1953).

60. Lingane, J. J., Electroanalytical Chemistry, Chap. 22, Interscience, New York (1958).

61. Bockris, J. O'M., Damjanovic, A. and Gemshaw, M. A., J. Electrochem. Soc., 114, 1107 (1967).

62. Tamman, G., and Jessen, V., Z. Anorg. Allgem. Chem., 179, 125 (1929).

63. Exner, F., Pogg. Ann., 94, 59 (1855).

64. Hufner, G., Z. Physik. Chem., 27, 227 (1898).

65. Hagenbach, A., Wied. Ann., 65, 673 (1898)

66. Ipatev, V. V., and Drushina-Artemovich, S. I., Z. Anorg. Alleg. Chem., 216, 66 (1933).

67. Davison, J. F., and Cullen, E. T., Trans. Brit. Inst. Chem. Eng., 33, 51 (1957).

68. Bhatia, K. K., M. S. Thesis, University of Florida (1965).

69. Baird, M. H. I., and Davidson, J. F., Chem. Eng. Sci., 17, 473 (1962).

70. Carlson, T., J. Am. Chem. Soc., 33, 1027 (1911).

71. Chiang, S. H., and Toor, H. L., A.I.Ch.E.J., 5, 165 (1959).

72. Brdicka, R., and Wiesner, K., Collection Czech. Chem. Commun., 12, 39 (1947).

73. Semerano, G., Riccoboni, L., and Foffani, A., Gazz. Chim. Ital., 79, 395 (1949).

74. Kolthoff, I. M., and Miller, C. S., J. Am. Chem. Soc., 63, 1013 (1941).

75. Kramers, H., Douglas, R. A., and Ulmann, R. M., Chem. Eng. Sci., 8, 190 (1959).

76. Harned, H. S., and Nuttall, R. L., J. Am. Chem. Soc., 71, 1460 (1949).

77. Harned, H. S., and Owen, B. B., The Physical Chemistry of Electrolytic Solutions, Reinhold, New York (1959)

78. Robinson, R. A., and Stokes, R. H., Electrolyte Solutions, Academic Press, Inc., New York (1955).

79. Geddes, A. L., and Pontius, R. B., Technique of Organic Chemistry, Vol. I, Part II, Interscience Publishers, Inc., New York (1959).

80. Gordon, A. R., Ann. N.Y. Acad. Sci., 46, 235 (1945).

81. Garner, C., Physics, 5, 4 (1934).

82. Northrup, J. N., and Anson, M. L., J. Gen. Physiol., 12, 543 (1928).

83. Stokes, R. H., J. Am. Chem. Soc. 72, 2243 (1950).

84. Chang, P., and Wilke, C. R., J. Phys. Chem., 59, 592 (1955).

85. Dullien, F. A. L., and Shemilt, L. W., Trans. Farad. Soc., 58, 244 (1961).

86. Robinson, R. L., Edmister, W. C., and Dullien, F. A. L., J. Phys. Chem., 69, 258 (1965).

87. Olander, D. R., J. Phys. Chem., 67, 1011 (1963).

88. Akerlof, G., and Bender, P., J. Phys. Chem., 50, 2366 (1948).

89. Onsaga, L., and Fuoss, R. M., J. Phys. Chem., 36, 2689 (1932).

90. Harned, H. S., and Cook, M. A., J. Phys. Chem., 59, 496 (1937).

91. International Critical Tables, Vol. 4, McGraw-Hill Book Co., New York, N.Y. (1928).

92. Bhatia, R. N., M.S.E. Thesis, University of Florida (1967).

93. Gubbins, K. E., Bhatia, K. K., and Walker, R. D., A.I.Ch.E. Journal 5, 548 (1966).

95. "Caustic Potash", Solvay Technical and Engineering Science Bulletin No. 15, Solvay Process Division, Allied Chemical Corp., 1960.

96. Gerlach, G. T., Zeit, Anal. Chemie, 26, 413 (1887).

97. Vogel, W. M., Routsis, K. J., Kehrer, V. J., Landsman, D. A., and Tschinkel, J. G., J. Chem. Eng. Data, 12, 465 (1967).

98. Walter, K., and Groeneveld, A., Zeitscrift fur Physikahsche, Chemie Neve Folge, 32, S (110-126) (1962).

99. Foote Mineral Co., Technical Bulletin.

100. Stephan, E. F., and Miller, P. D., J. Chem. Eng. Data, 1, 501 (1962).

101. Thomson, G. W.,"Determination of Vapor Pressure" in "Technique of Organic Chemistry", Vol. 1, Part 1, ed. A. Weissbeger, 1959.

102. Cumming, A. C., J. Chem. Soc., 95, 1772 (1909).

103. McBain, J. W., and Salmon, C. S., Proc. Roy. Soc., 97, A44 (1920).

104. Perry, R. H., Ed., Chemical Engineers Handbook, McGraw-Hill Book Co., New York, N.Y., 1963.

105. Reddlich, D., and Pigelelsen, J., J. Am. Chem. Soc., 64, 758 (1942).

106. DeGroot, S. R., and Mazen, P., Non-Equilibrium Thermodynamics, North-Holland Publishing Co., Amsterdam, 1962.

107. Morrison, T. J., and Johnstone, N. B., J. Chem. Soc., 76, 3441 (1954).

108. Lannung, A., J. Am. Chem. Soc., 52, 68 (1930).

109. Friedman, H. L., J. Am. Chem. Soc., 76, 3294 (1954).